NAVAL POSTGRADUATE SCHOOL

MONTEREY, CALIFORNIA

THESIS

LINEAR FREQUENCY MODULATED SIGNALS VS ORTHOGONAL FREQUENCY DIVISION MULTIPLEXING SIGNALS FOR SYNTHETIC APERTURE RADAR SYSTEMS

by

Sade A. Holder

June 2014

Thesis Co-Advisors: Frank Kragh
Ric Romero

Approved for public release; distribution is unlimited

THIS PAGE INTENTIONALLY LEFT BLANK

REPORT DOCUMENTATION PAGE			*Form Approved OMB No. 0704-0188*
Public reporting burden for this collection of information is estimated to average 1 hour per response, including the time for reviewing instruction, searching existing data sources, gathering and maintaining the data needed, and completing and reviewing the collection of information. Send comments regarding this burden estimate or any other aspect of this collection of information, including suggestions for reducing this burden, to Washington headquarters Services, Directorate for Information Operations and Reports, 1215 Jefferson Davis Highway, Suite 1204, Arlington, VA 22202-4302, and to the Office of Management and Budget, Paperwork Reduction Project (0704-0188) Washington DC 20503.			
1. AGENCY USE ONLY *(Leave blank)*	**2. REPORT DATE** June 2014	**3. REPORT TYPE AND DATES COVERED** Master's Thesis	
4. TITLE AND SUBTITLE LINEAR FREQUENCY MODULATED SIGNALS VS ORTHOGONAL FREQUENCY DIVISION MULTIPLEXING SIGNALS FOR SYNTHETIC APERTURE RADAR SYSTEMS			**5. FUNDING NUMBERS**
6. AUTHOR(S) Sade A. Holder			
7. PERFORMING ORGANIZATION NAME(S) AND ADDRESS(ES) Naval Postgraduate School Monterey, CA 93943-5000			**8. PERFORMING ORGANIZATION REPORT NUMBER**
9. SPONSORING /MONITORING AGENCY NAME(S) AND ADDRESS(ES) N/A			**10. SPONSORING/MONITORING AGENCY REPORT NUMBER**
11. SUPPLEMENTARY NOTES The views expressed in this thesis are those of the author and do not reflect the official policy or position of the Department of Defense or the U.S. Government. IRB protocol number ____N/A____.			
12a. DISTRIBUTION / AVAILABILITY STATEMENT Approved for public release; distribution is unlimited			**12b. DISTRIBUTION CODE** A

13. ABSTRACT (maximum 200 words)

The goal of this thesis is to investigate the effects of an orthogonal frequency-division multiplexing (OFDM) signal versus a linear frequency modulated or chirp signal on simulated synthetic aperture radar (SAR) imagery. Various parameters of the transmitted signal, such as pulse duration, transmitted signal energy, bandwidth, and (specifically for the OFDM signal) number of subcarriers and transmission scheme were examined to determine which parameters are most important to reconstructing a SAR image. Matched filtering and interpolation are two techniques used to reconstruct the SAR image. SAR systems are used in various military and civilian sector applications. Some SAR application examples include ground surveillance, reconnaissance and remote sensing. These applications demand high resolution imagery; therefore, knowledge of exactly which parameters of the transmitted radar signal are more important in producing fine resolution imagery is worth investigating. This research will also aid in providing flexibility in terms of what type of signal and signal parameters are best suited for a particular SAR application and associated military missions. In addition to improving the method attaining high resolution images, SAR process improvement can potentially reduce military SAR system design cost.

14. SUBJECT TERMS Synthetic aperture radar (SAR), orthogonal frequency division multiplexing (OFDM), linear frequency modulation (LFM), communications radar			**15. NUMBER OF PAGES** 161
			16. PRICE CODE
17. SECURITY CLASSIFICATION OF REPORT Unclassified	**18. SECURITY CLASSIFICATION OF THIS PAGE** Unclassified	**19. SECURITY CLASSIFICATION OF ABSTRACT** Unclassified	**20. LIMITATION OF ABSTRACT** UU

NSN 7540-01-280-5500 Standard Form 298 (Rev. 2-89)
Prescribed by ANSI Std. 239-18

THIS PAGE INTENTIONALLY LEFT BLANK

Approved for public release; distribution is unlimited

LINEAR FREQUENCY MODULATED SIGNALS VS ORTHOGONAL FREQUENCY DIVISION MULTIPLEXING SIGNALS FOR SYNTHETIC APERTURE RADAR SYSTEMS

Sade A. Holder
Lieutenant, United States Navy
B.S., United States Naval Academy, 2009

Submitted in partial fulfillment of the
requirements for the degree of

MASTER OF SCIENCE IN ELECTRICAL ENGINEERING

from the

NAVAL POSTGRADUATE SCHOOL
June 2014

Author: Sade A. Holder

Approved by: Frank Kragh
Thesis Co-Advisor

Ric Romero
Thesis Co-Advisor

R. Clark Robertson
Chair, Department of Electrical and Computer Engineering

THIS PAGE INTENTIONALLY LEFT BLANK

ABSTRACT

The goal of this thesis is to investigate the effects of an orthogonal frequency-division multiplexing (OFDM) signal versus a linear frequency modulated or chirp signal on simulated synthetic aperture radar (SAR) imagery. Various parameters of the transmitted signal, such as pulse duration, transmitted signal energy, bandwidth, and (specifically for the OFDM signal) number of subcarriers and transmission scheme were examined to determine which parameters are most important to reconstructing a SAR image. Matched filtering and interpolation are two techniques used to reconstruct the SAR image. SAR systems are used in various military and civilian sector applications. Some SAR application examples include ground surveillance, reconnaissance and remote sensing. These applications demand high resolution imagery; therefore, knowledge of exactly which parameters of the transmitted radar signal are more important in producing fine resolution imagery is worth investigating. This research will also aid in providing flexibility in terms of what type of signal and signal parameters are best suited for a particular SAR application and associated military missions. In addition to improving the method attaining high resolution images, SAR process improvement can potentially reduce military SAR system design cost.

THIS PAGE INTENTIONALLY LEFT BLANK

TABLE OF CONTENTS

I. INTRODUCTION....1
- **A. PREVIOUS WORK....3**
- **B. PURPOSE OF THESIS....3**
- **C. THESIS ORGANIZATION....3**

II. SIGNAL PROCESSING FUNDAMENTALS....5
- **A. SIGNALS....5**
- **B. FOURIER TRANSFORMS....5**
- **C. SIGNAL REPRESENTATION....7**

III. SAR MATHEMATICAL MODEL....11
- **A. RADAR PRELIMINARIES....11**
  - **1. Basic Radar Concept....11**
  - **2. Radar Range-Resolution....12**
- **B. SAR RANGE-IMAGING....12**
  - **1. SAR Range-Imaging Concept....12**
  - **2. SAR Range Resolution....15**
- **C. SAR CROSS-RANGE IMAGING....15**
  - **1. SAR Cross-Range Imaging Concept....15**
  - **2. SAR Cross-Range Resolution....18**
- **D. TWO-DIMENSIONAL SAR....21**
  - **1. SAR Spotlight Mode....21**
  - **2. SAR Stripmap Mode....22**
  - **3. Stripmap SAR Model....23**
    - ***a. Radar Antenna....23***
    - ***b. Stripmap SAR geometry....24***
    - ***c. Stripmap SAR Data Collection....28***
    - ***d. Fast-Time....29***
    - ***e. Slow-Time....29***

IV. SAR RECONSTRUCTION....31
- **A. RANGE RECONSTRUCTION....31**
- **B. CROSS-RANGE RECONSTRUCTION....33**
  - **1. Cross-range Matched Filtering....33**
  - **2. Wavenumber Domain....34**
- **C. TWO-DIMENSIONAL RECONSTRUCTION....35**
  - **1. Stripmap SAR Reconstruction....35**
    - ***a. Fast-Time Matched Filter....36***
    - ***b. Slow-Time Fast Fourier Transform....37***
    - ***c. Two-Dimensional Matched Filtering....38***
    - ***d. Interpolation....38***
    - ***e. Inverse Fast Fourier Transform....39***
- **D. SAMPLING REQUIREMENTS....39**
  - **1. Nyquist Sampling Theorem....40**

a. Fast-time Domain Sampling Requirements 40
b. Slow-Time Domain Sampling Requirements 41
c. Frequency-Domain Sampling Requirements 41
d. Spatial Frequency-Domain Sampling Requirements 42
2. Resampling via Ideal Low Pass Filter 42

V. RADAR SIGNALS 45
A. PULSE COMPRESSION BASICS 45
B. OFDM BASICS 47
1. Modulation Scheme 47
a. Binary Phase-Shift Keying 48
b. Quadrature Phase-Shift Keying 48
2. OFDM Transmitted Radar Signal 48

VI. SIMULATION IMPLEMENTATION AND RESULTS 53
A. ONE-DIMENSIONAL RANGE RECONSTRUCTION 53
1. Range MATLAB Implementation 53
2. Range-Imaging Simulation Results 54
a. Linear Frequency Modulated Signal 55
b. Orthogonal Frequency Division Multiplexing 59
B. TWO-DIMENSIONAL IMAGE RECONSTRUCTION 72
1. Two-dimensional SAR with MATLAB Implementation 72
2. Two-Dimensional Results 76
a. LFM 81
b. BPSK-OFDM 85
c. QPSK-OFDM 95

VII. CONCLUSION AND FUTURE WORK 115
A. CONCLUSION 115
B. FUTURE WORK 116

APPENDIX MATLAB CODES 117

LIST OF REFERENCES 135

INITIAL DISTRIBUTION LIST 137

LIST OF FIGURES

Figure 1. Signal in time and frequency domain. 6
Figure 2. Bandpass signal spectrum $S(\omega)$, after [12]....8
Figure 3. Analytic representation $S_+(\omega)$, after [12]....9
Figure 4. Baseband representation $S_c(\omega)$, after [12]....9
Figure 5. Basic radar concept, from [3]....11
Figure 6. SAR range-imaging scene, from [14]. 13
Figure 7. Range target function after [15]. 14
Figure 8. SAR cross-range geometry from [14]. 16
Figure 9. Depiction of slant range distance using Pythagorean theorem. 17
Figure 10. Synthetic aperture aspect angle, after [13]. 18
Figure 11. Real aperture radar cross-range resolution, after [16]. 19
Figure 12. Geometry of single point target within synthetic aperture beamwidth, after [1]. 20
Figure 13. Spotlight SAR mode, from [15]. 22
Figure 14. Stripmap SAR mode, from [15]. 23
Figure 15. Stripmap SAR geometry, from [14]. 25
Figure 16. Received echoed signal $s(t,u)$ for a single point target, after [14]. 26
Figure 17. Aspect angle of target located at (x_i, y_i), after [14]. 27
Figure 18. Synthetic aperture $M \times N$ array. 28
Figure 19. Illustration of matched filter via FFT processing, from [4]. 33
Figure 20. Reconstruction flow chart via spatial frequency interpolation for two-dimensional SAR images. 36
Figure 21. Depiction of interpolation of k_x data, from [4]. 39
Figure 22. Linear frequency modulated signal with $T_p = 4$ ms, $\alpha = 3\times10^9$ Hz/s. 47
Figure 23. OFDM waveform generation. 49
Figure 24. OFDM Signal modulated using BPSK scheme where $T_p = 6.4\ \mu s$, $N = 128$ and $B = 20$ MHz. 51
Figure 25. Range imaging simulation flow chart. 53
Figure 26. LFM reconstructed range target function at chirp rate, $\alpha = 1\times10^{13}$ Hz/s, 2×10^{13} Hz/s, 5×10^{13} Hz/s, 10×10^{13} Hz/s. 57
Figure 27. LFM reconstructed range target function at pulse duration, $T_p = 0.2\,\mu s,\ 0.4\,\mu s,\ 1.0\,\mu s,$ and $1.4\,\mu s$. 59
Figure 28. BPSK-OFDM reconstructed range target function with $N = 64$, $B = 10$ MHz, 20 MHz, 50 MHz, and 70 MHz. 61
Figure 29. BPSK-OFDM reconstructed range target function: $N = 8$, $B = 10$ MHz, 20 MHz, 50 MHz, and 70 MHz. 63

Figure 30. BPSK-OFDM reconstructed range target function with $T_p = 0.2$ μs, 0.4 μs, 0.6 μs, and 0.8 μs. 65
Figure 31. QPSK-OFDM reconstructed range target function with $N = 64$, $B = 10$ MHz, 20 MHz, 50 MHz, and 70 MHz. 67
Figure 32. QPSK-OFDM reconstructed range target function with $N = 8$, $B = 10$ MHz, 20 MHz, 50 MHz, and 70 MHz. 69
Figure 33. QPSK-OFDM reconstructed range target function with $T_p = 0.2$ μs, 0.4 μs, 0.6 μs, and 0.8 μs. 71
Figure 34. Two-dimensional initial parameters flow charts....72
Figure 35. Two-dimensional image reconstruction flow chart. 74
Figure 36. Measured echoed signal $s(t,u)$ for single point target located at center of target scene....80
Figure 37. Fast-time matched filtered signal $s_{MF}(t,u)$ for single point target located at center of target scene....80
Figure 38. Reconstructed target function $f(x,y)$ for single point target located at center of target scene. 81
Figure 39. Simulation 2: Reconstructed target function for LFM signal with varying chirp rate. 83
Figure 40. Simulation 3. Reconstructed target function for LFM signal with varying pulse duration. 84
Figure 41. Reconstructed target function for simulation four, set one for BPSK-OFDM signal with $N = 4$ 86
Figure 42. Reconstructed target function for simulation four, set two for BPSK-OFDM signal with $N = 16$. 87
Figure 43. Reconstructed target function for simulation five, set one for BPSK-OFDM signal with $B = 50$ MHz. 90
Figure 44. Reconstructed target function for simulation five, set two for BPSK-OFDM signal with $B = 60$ MHz. 91
Figure 45. Reconstructed target function for simulation five, set three for BPSK-OFDM signal with $B = 70$ MHz. 92
Figure 46. Reconstructed target function for simulation five, set four for BPSK-OFDM signal with $B = 80$ MHz. 93
Figure 47. Reconstructed target function for simulation six, set one for QPSK-OFDM with $N = 4$. 96
Figure 48. Reconstructed target function for simulation six, set two for QPSK-OFDM with $N = 16$. 97
Figure 49. Reconstructed target function for simulation seven, set one with QPSK-OFDM signal with $B = 50$ MHz. 100
Figure 50. Reconstructed target function for simulation seven, set two for QPSK-OFDM with $B = 60$ MHz 101

Figure 51. Reconstructed target function for simulation seven, set three for QPSK-OFDM with $B = 70$ MHz 102
Figure 52. Reconstructed target function for simulation seven, set four for QPSK-OFDM with $B = 80$ MHz 103
Figure 53. Reconstructed target function for simulation eight with $T_p = 0.06667$ μs 106
Figure 54. Reconstructed target function for simulation eight with $T_p = 0.13334$ μs 106
Figure 55. Reconstructed target function for simulation eight with $T_p = 0.2$ μs. 107
Figure 56. Reconstructed target function for simulation eight with $T_p = 0.26667$ μs 107
Figure 57. Reconstructed target function for simulation nine with $B = 50$ MHz. 110
Figure 58. Reconstructed target function for simulation nine with $B = 60$ MHz. 110
Figure 59. Reconstructed target function for simulation nine with $B = 70$ MHz. 111
Figure 60. Reconstructed target function for simulation nine with $B = 80$ MHz. 111
Figure 61. Reconstructed target function for BPSK OFDM and QPSK-OFDM signals generated with $B = 70$ MHz, $N = 2$, and $T_p = 0.02857$ μs, and T_p =0.05714 μs, respectively. 113
Figure 62. Reconstructed target function for BPSK OFDM and QPSK-OFDM signals generated with $B = 80$ MHz, $N = 2$, and $T_p = 0.025$ μs, and T_p = 0.05 μs, respectively. 114

THIS PAGE INTENTIONALLY LEFT BLANK

LIST OF TABLES

Table 1. Range imaging target scene parameters. 55
Table 2. LFM signal parameters for range simulation one. 56
Table 3. LFM signal parameters for range simulation two. 58
Table 4. BPSK-OFDM signal parameters for range simulation three. 60
Table 5. BPSK-OFDM signal parameters for range simulation four. 62
Table 6. BPSK-OFDM signal parameters for range simulation five. 64
Table 7. QPSK-OFDM signal parameters for range simulation six. 66
Table 8. QPSK-OFDM signal parameters for range simulation seven. 68
Table 9. QPSK-OFDM signal parameters for simulation eight. 70
Table 10. Stripmap SAR target scene parameters. 77
Table 11. Stripmap SAR planar array antenna parameters. 78
Table 12. Stripmap SAR simulation one signal parameters. 79
Table 13. LFM signal parameters for simulations two and three. 82
Table 14. BPSK-OFDM signal parameters for simulation four. 85
Table 15. BPSK-OFDM signal parameters for simulation five. 89
Table 16. QPSK-OFDM signal paramters for simulation six. 95
Table 17. QPSK-OFDM signal parameters simulation seven. 99
Table 18. Signal parameters for simulation eight. 105
Table 19. Signal parameters for simulation nine. 109

THIS PAGE INTENTIONALLY LEFT BLANK

LIST OF ACRONYMS AND ABBREVIATIONS

BPSK	binary phase-shift keying
DFT	discrete Fourier transform
FFT	fast Fourier transform
IDFT	inverse discrete Fourier transform
IFFT	inverse fast Fourier transform
LFM	linear frequency modulated
OFDM	orthogonal frequency-division multiplexing
QAM	quadrature amplitude modulation
QPSK	quadruple phase-shift keying
RADAR	radio detection and ranging
RAR	real aperture radar
SAR	synthetic aperture radar
SFIA	spatial frequency interpolation algorithm

THIS PAGE INTENTIONALLY LEFT BLANK

EXECUTIVE SUMMARY

Synthetic aperture radar (SAR) is a well-known, advanced radar technique used for producing two-dimensional images of a target area or the Earth's surface. The concept of SAR was established by Wiley in 1951, where he found that the radar's motion, or more precisely, the relative motion between a radar and a target-of-interest could be used to obtain fine image resolution [1]. SAR systems, employed on airborne or spaceborne platforms, provide high resolution imagery, allowing for various applications in both the military and civilian sectors.

Unlike the traditional radar, which only measures range to a target in one-dimension, SAR systems have the ability to measure range via a second dimension. This second-dimension, referred to as cross-range, is what sets SAR apart from other radars that only provide range information [2].

There are two main modes of SAR: spotlight mode and stripmap mode. In spotlight mode, the SAR system focuses its antenna on the same target area while the aircraft moves along the synthetic aperture. Conversely, in stripmap mode, the SAR antenna forms an image by maintaining its beam on a strip as it moves along the synthetic aperture [2]. This work focuses on the stripmap SAR mode.

An important consideration with any radar system is the transmitted radar signal it uses to detect the target. Most radar systems use linearly frequency modulated signals to achieve the performance of a shorter pulse while transmitting a long pulse [3]. In this thesis, the orthogonal frequency-division multiplexed (OFDM) communication signal is investigated for potential use in SAR systems. Various parameters of both the LFM and OFDM signals, such as pulse duration, signal bandwidth, transmitted signal energy, and, specifically for the OFDM signal, number of subcarriers and transmission scheme are examined to determine which parameters are most important in creating the best SAR images.

A SAR target scene is an area of interest containing several point targets in the two-dimensional (x_i, y_i) plane. The mathematical expression of the targets within the target scene, also referred to as the two-dimensional target function, is expressed as

$$f_0(x,y) = \sum_{i=1}^{n} \sigma_i \delta(x - x_i, y - y_i)$$

where each term in the sum represents one point target, $\delta()$ is the Dirac delta function, x_i and y_i are the range and cross-range position of each point target, respectively, and the magnitude of each target in the image depends on its reflectivity σ_i [2].

SAR works by transmitting radar pulses $p(t)$ onto a two-dimensional target area as it flies along a flight path. The flight path is referred to as the synthetic aperture or u. A two-dimensional array stores the reflected signals, where one array dimension is associated with fast-time t as it relates to the radar signal, which is propagated at the speed of light. The second dimensional variable is slow-time u, which pertains to the radar's time due to displacement that is much slower than the speed of light. [2].

The mathematical representation of the two-dimensional reflected signal is

$$s(t,u) = \sum_{i=1}^{n} \sigma_i p\left[t - \frac{2\sqrt{x_i^2 - (y_i - u)^2}}{c} \right],$$

where u is the position of the radar along its flight path and

$$\frac{2\sqrt{x_i^2 - (y_i - u)^2}}{c}$$

is the round trip time for the radar signal to travel to each point target and back to the radar receiver [2].

A series of signal processing steps are performed on the reflected data before the final image is produced. These steps, outlined in Figure 1, involve fast-time matched filtering, or a correlation of the received data and reference signal. The fast-time matched filter is applied to one of two array dimensions. Next, a slow-time variable Fourier transform is performed on the array second dimension. A two-dimensional matched filter

is then applied to transform the data into the wavenumber domain. Next, an interpolation method is utilized to ensure the equal spacing of data in the wavenumber domain. Finally, an inverse Fourier transform is performed to produce the final image. These steps require the SAR data to undergo transformation in several domains. Specifically, the fast-time, slow-time, frequency and wavenumber domains are exploited; therefore, careful consideration is paid to the sampling requirement for each domain [2].

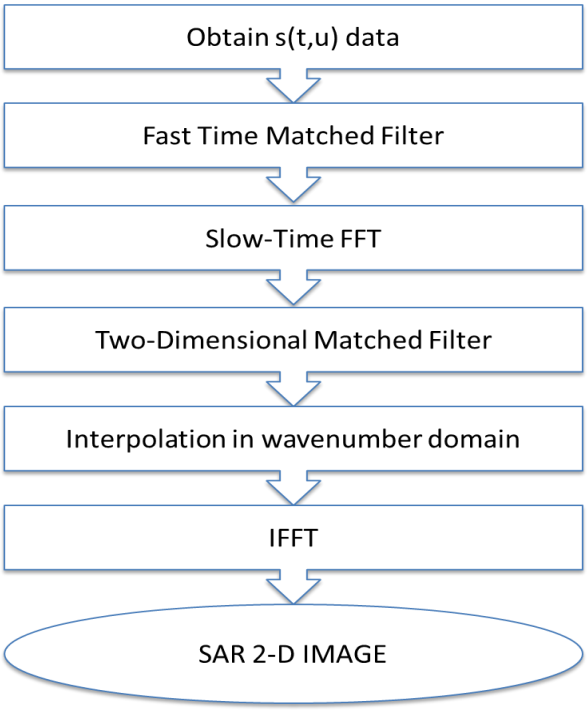

Figure 1. Steps for two-dimensional SAR reconstruction algorithm.

The reconstruction algorithm implementation occurs in MATLAB, where the user can vary the parameters of either the LFM or OFDM transmitted signals. The algorithm output displays the received SAR signal, the fast-time matched filtered signal and the two-dimensional SAR image.

We conducted several simulations with varying pulse width, chirp rate and bandwidth of the LFM signal. Similarly, we varied the bandwidth and pulse width of the BPSK-OFDM and QPSK-OFDM signals by changing the number of subcarriers or OFDM symbols per signal and sampling times either individually or concurrently. The

resulting transmitted signal energy of each signal was also taken into consideration. For each simulation, we investigated how the three signals and their parameters affect the SAR image quality.

The simulation results indicated that bandwidth and pulse duration are the two most important parameters, aside from signal energy, for achieving the highest quality SAR image for both the LFM and OFDM signals. The most influential factor for the LFM signals is the sampling interval. That is to say, we can elongate the pulse duration, which directly increases the bandwidth of the LFM signal and still attain fine resolution provided that the sampling interval is adjusted accordingly. This method for attaining better resolution does not hold true for OFDM signals. Specifically, we found that increasing the pulse width for lower bandwidth OFDM signals directly improves image resolution. However, implementing wider OFDM signal with elongated pulse duration results in images that are smeared and ambiguous. Therefore, we concluded that a shorter duration OFDM signal is sufficient for achieving fine resolution when the signal is generated with wider bandwidth.

Overall the results obtained in this work show that finer resolution SAR imagery can result from use of an OFDM communication signal with the right parameters. Further, the OFDM signal offers much flexibility in relation to usable bandwidth and duration of the signal.

LIST OF REFERENCES

[1] I. G. Cumming and F. H. Wong, *Digital Processing of Synthetic Aperture Radar Data, Algorithms and Implementation*. Norwood, MA: Artech House, Inc, 2005.

[2] M. Soumekh, *Synthetic Aperture Radar Signal Processing with MATLAB Algorithms.* New York: Wiley-Interscience, 1999.

[3] B. R. Mahafza, *Radar Signal Analysis and Processing Using MATLAB.* Boca Raton, FL: CRC Press, 2009.

ACKNOWLEDGMENTS

I would like to thank my thesis advisor, Professor Kragh for his continual guidance throughout my time in graduate school but especially for his help in conducting this research project. This work would not have been possible without his advice on the subject matter.

I would also like to express my gratitude to all the Electrical Engineering professors, particularly, Professor Romero, Professor Fargues and Professor Ha for their advice and support throughout my academic career.

Finally, I would like to thank my family, friends and my boyfriend, Sean, for being by my side along the way.

THIS PAGE INTENTIONALLY LEFT BLANK

I. INTRODUCTION

Radar imaging is the concept of utilizing a radar antenna mounted onto an airborne platform to form images of an object space [1] or target-of-interest. This technique is valuable in a number of military applications such as remote sensing, navigation and guidance, reconnaissance and various other purposes. In fact, dating back to the WWII, the military has utilized high quality radar images for useful information and feature extractions from target areas [2].

Unlike traditional radar whose primary purpose is to determine the *range* to an object in one-dimension, imaging radars use a second dimension for image production. That second dimension is *cross-range*. High cross-range resolution is what allows for high quality images. Antenna theory tells us that a large radar antenna is needed to achieve fine cross-range resolution [3]. However, antenna size is limited in payload and mounting restrictions on an airborne platform. This inherent size limitation is where the concept of synthetic aperture radar (SAR) becomes useful [4].

SAR was developed in 1951 by Wiley; he found that the echoed signals obtained from a target area can be used to synthesize a much larger antenna [1], [4]. SAR utilizes the flight path of an airborne or spaceborne vehicle to overcome the limitations of regular radar in the sense that a much smaller antenna is used to produce high-resolution images that normally require a very large antenna [4].

A SAR system relies on the relative motion between the target area and the radar antenna to produce images [4]. While the aircraft transits, the SAR system illuminates an area of interest with multiple microwave signal pulses from its antenna. The returns of these pulses, or echoes, are collected and stored. The system then creates an image by combining the individual returns from each point target. Through signal processing techniques, the SAR system utilizes the combination of these reflected signals to synthesize a much larger antenna that generates a higher resolution image than a smaller antenna is capable of producing [4].

Several characteristics and features of SAR systems make them valuable to both military and civilian sectors. As mentioned earlier, the SAR system’s relative size is

small in relation to its performance, making it valuable in applications where platform weight is a concern. In addition, SAR images are valuable in areas of target detection. This detection advantage is specifically useful for military combat operations where detailed information about a target is needed [2]. These systems also enable users to distinguish terrain features such as coastlines, mountain ridges and urban areas [5]. These listed examples are just a small number of applications where the addition of SAR systems greatly benefits both the military and civilian sectors.

The most commonly used signal type for producing SAR images is the linear frequency modulating (LFM) signal, also known as a chirp signal [2], [5]. LFM signals allow for pulse compression techniques that achieves the performance associated with shorter pulses while using a longer pulse [2]. These signals employ a sinusoidal pulse, where the instantaneous frequency of the signal increases or decreases linearly over time [6]. The frequency modulation of the signal widens its bandwidth. Since bandwidth is directly proportional to resolution, LFM signal use is desirable in SAR systems to enable attainment of high resolution imagery. [2].

The use of orthogonal frequency-division multiplexing (OFDM) signals for SAR imaging is investigated in this thesis. OFDM is a signal modulation technique used in wireless and commercial communication. An OFDM signal consists of many orthogonal subcarriers, where each subcarrier occupies a portion of the overall signal's bandwidth. Several characteristics of OFDM, such as bandwidth and spectral efficiency, make the signal worth investigating for potential use in SAR systems. The OFDM signal's duration is easily varied by varying the number of OFDM symbols and/or the duration of each symbol, where that duration is controlled by the number of subcarriers and the sampling rate. Furthermore, OFDM allows for controlling the bandwidth by changing the sampling interval [7].

The focus of this thesis is to compare and contrast the traditional LFM radar signal parameters with those of an OFDM signal. We examine the effects of pulse duration of each signal, which, for OFDM, is primarily determined by the number of subcarriers as well as the number of symbols per OFDM signal [7]. We also investigate

how signal bandwidth affects SAR imagery. The signal's transmitted energy is another important parameter consideration used in assessing overall performance.

A. PREVIOUS WORK

This thesis builds on the prior work done by Fason, who explored the effects of different input signals on one-dimensional range and cross-range SAR imaging [8]. The author also examined the performance of the same radar signal's application in two-dimensional SAR imaging. The investigated transmitted signals include the sinusoidal pulse signal, white Gaussian noise, and LFM signal. Of these three signals, Fason found that the LFM signal is more appropriate for use in SAR systems because it provides a larger usable bandwidth. Fason was successful in testing the performance of these signals up to a certain point in his proposed SAR reconstruction algorithm. Specifically, he was able to generate the fast-time matched filtered signal but not the final two-dimensional image. This research uses Fason's work as a starting point to reconstruct the two-dimensional image and examine the effects on different radar signals and parameters for two-dimensional SAR imaging [8].

B. PURPOSE OF THESIS

The primary focus of this thesis is to analyze the potential improvements of SAR imagery using OFDM signals. We first developed a SAR simulation tool in MATLAB, where signals can be easily interchanged to allow for signal performance comparison and analysis. Specifically, the effects of OFDM signals of different modulation schemes and number of sub-carriers are compared against LFM signals. We also investigated how OFDM signal parameters such as transmitted signal energy, bandwidth, and duration affect the SAR imagery.

C. THESIS ORGANIZATION

A brief overview of the thesis chapter content is provided in this paragraph. General signal processing and signal representation are included in Chapter II, which includes discussion on the relevant signal fundamentals. A brief review on how the traditional radar determines range is given in Chapter III. Also included in Chapter III is a

detailed discussion of the one-dimensional SAR range and cross-range imaging concepts, followed by a transition into the two-dimensional stripmap SAR imaging concept. In Chapter IV, we discuss the reconstruction process for all three imaging concepts. In Chapter V, we introduce the radar signals studied in this work, to include the theory and motivation for using OFDM as a radar signal. A detailed discussion on the SAR model MATLAB implementation, the range imaging simulation results and the two-dimensional stripmap SAR results are provided in Chapter VI. Finally, the research results are summarized in Chapter VIII, and conclusion and recommendations for future related work are provided.

II. SIGNAL PROCESSING FUNDAMENTALS

Many signal processing methods and terms, which are required to explain and analyze SAR processing as well as the steps to understand SAR image reconstruction are presented in this thesis. This chapter is provided to equip the reader with signal processing and representation fundamentals, which are needed to understand the mathematical details of the radar signals used later in this thesis.

A. SIGNALS

Signals are used to represent information in formats such as video, images, speech, radio communications, radar, and may others [2]. Signals can either have a continuous or discrete-time variable representation [4]. A continuous-time signal, often referred to as an analog signal, is defined along a continuous real-valued time variable. Conversely, a discrete-time signal is defined at integer-valued discrete times [4].

In an actual radar system, the antenna transmits a continuous-time signal. The signal must be converted to discrete-time in order to perform signal processing and analysis. Throughout this thesis, the signals referenced are discrete-time, which can be obtained by periodically sampling a continuous time signal [9], [10].

The two most common ways to represent a signal are via the time-domain and the frequency-domain. Throughout our analysis, we frequently transition between the two domains. In terms of computer analysis, the frequency domain is sometimes preferred since it usually allows for more computationally efficient signal processing. Although many mathematical computations required for this thesis are accomplished via software, it is necessary and useful to show the mathematical steps before implementation in MATLAB. This chapter is presented to show the conversion between the two domains [9].

B. FOURIER TRANSFORMS

The discrete Fourier transform (DFT) is an important mathematical tool used in signal and image processing. Much of the SAR processing techniques such as range and

cross-range matched filtering and image reconstruction are carried out in the frequency domain. The DFT is a technique used to convert a discrete-time signal from a function of time into a function of frequency [9]. Illustrated in Figure 1 is an example of a waveform in the time-domain versus its spectrum in the frequency domain.

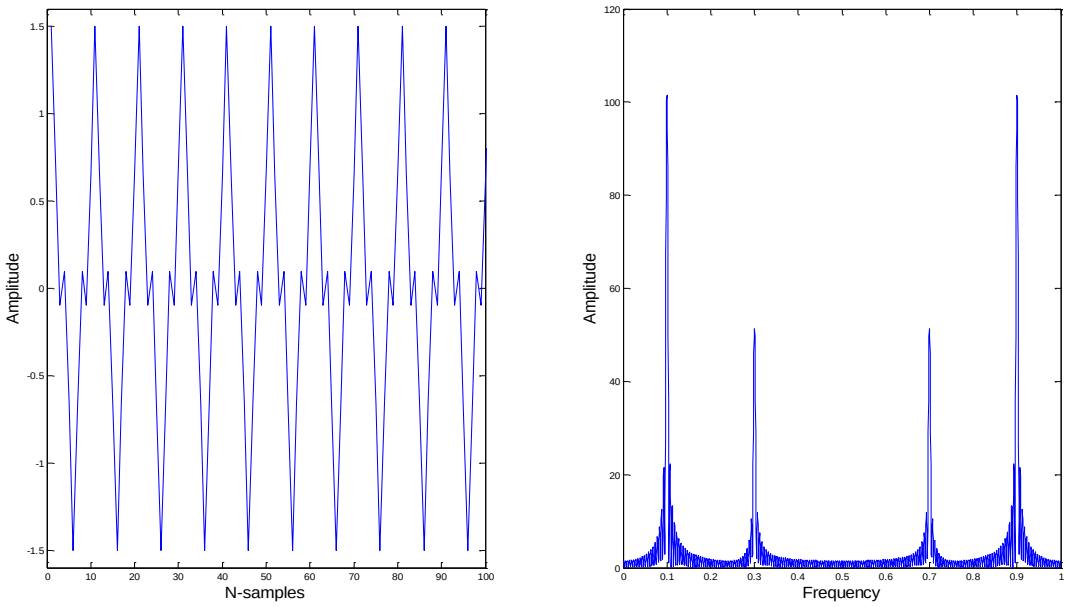

Figure 1. Signal in time and frequency domain.

Consider a discrete-time signal $x[n]$ consisting of N samples. The DFT is a summation equation over the N samples, $n = 0,1,\ldots,N-1,$ where each sample $x[n]$ is multiplied by a complex exponential. The DFT is

$$X[k] = \sum_{n=0}^{N-1} x[n] \exp(-j2\pi kn / N), \tag{1}$$

for $k = 0,1,...,N-1,$ where $X[k]$ is the frequency domain representation of the signal and N is the number of time samples [9].

The values of the frequency domain signal $X[k]$ indicate a set of sinusoids with different amplitudes and phases at each frequency [9]. In Figure 1, it can be seen that most of the signal's energy is contained near normalized frequencies 0.1, and 0.3.

An in-depth discussion of the DFT's use in the eventual two-dimensional SAR image reconstruction is provided in Chapter IV. In the simulations for this work, the DFT is applied using the fast Fourier transform (FFT) in MATLAB. The FFT is an efficient computer algorithm used in communications and signal processing to compute the DFT [9].

Though it is computationally efficient to carry out signal processing in the frequency domain, the final step of recovering a SAR image is a transformation of the frequency domain signal to the time domain. The inverse discrete Fourier transform (IDFT) is a mathematical operation used to convert the signal back to the time domain. The IDFT equation is

$$x[n] = \frac{1}{N}\sum_{k=0}^{N-1} X[k]\exp\left(j2\pi kn/N\right), \tag{2}$$

for $n = 0,1,...,N-1$. The inverse fast Fourier transform (IFFT) is a computer algorithm used to compute the IDFT [9].

The DFT and IDFT are important mathematical tools used for this analysis. In the succeeding chapters, we further examine how the mathematical tools explained above are essential in determining which signal type produces the best SAR image.

C. SIGNAL REPRESENTATION

The radar signals referenced in this thesis take on two forms: the analytic representation and complex envelope representation. This section is provided to introduce the difference in the signal representations and the reasons for choosing between the available options.

An important equation used to interpret different signals is Euler's identity, which is defined as

$$e^{j2\pi f_c t} = \cos\left(2\pi f_c t\right) + j\sin\left(2\pi f_c t\right). \tag{3}$$

Euler's identity provides a mathematical framework that aids in explaining the different representations of signals. The cosine component of Euler's identity is real, while the sine component is imaginary [10].

A bandpass signal is a signal whose carrier frequency is significantly greater than its bandwidth [11]. Consider a bandpass signal $s(t)$ expressed as

$$s(t) = a(t)\cos\left(2\pi f_c t + \varphi(t)\right), \tag{4}$$

where $a(t)$ represents the amplitude modulation information, $\varphi(t)$ represents the phase modulation information and f_c represents the carrier frequency.

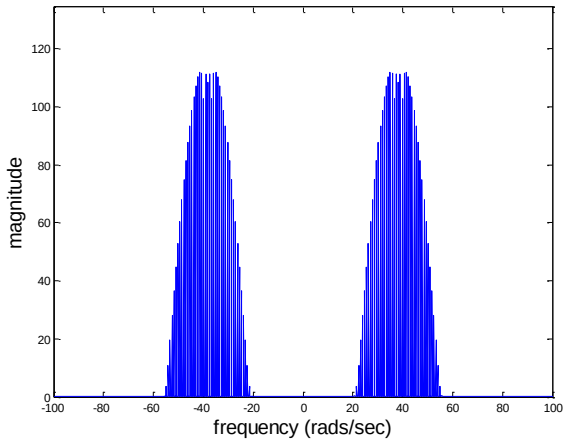

Figure 2. Bandpass signal spectrum $S(\omega)$, after [12].

The spectrum $S(\omega)$ of a bandpass signal $s(t)$ is obtained by carrying out the FFT. A spectrum $S(\omega)$ of a typical bandpass signal is shown in Figure 2. It can be seen that the spectrum is an even function. The spectrum concentration is located around the carrier frequency.

Since the bandpass signal is a real function, all the information contained in the positive half of the spectrum is also in the negative half. An alternate way of representing a signal is via its analytic form, where the negative frequencies are discarded [11].

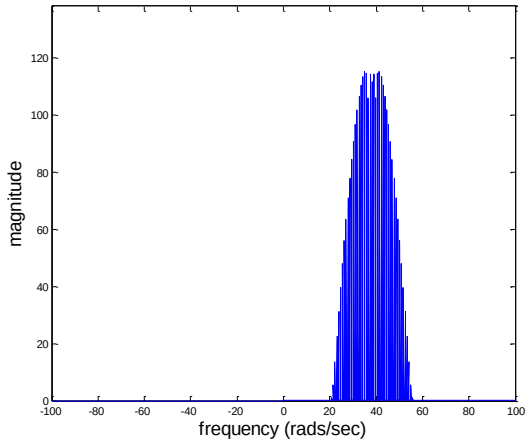

Figure 3. Analytic representation $S_+(\omega)$, after [12].

An analytic signal can be expressed as

$$\hat{s}(t) = a(t)\exp\left[j2\pi f_c t + \varphi(t)\right], \tag{5}$$

where the amplitude, phase, and carrier frequency are the same as in the bandpass representation in (4). The spectrum $S_+(\omega)$ of the analytic signal is illustrated in Figure 3, where it can be seen that only the positive frequencies, $\omega > 0,$ are meaningful [11].

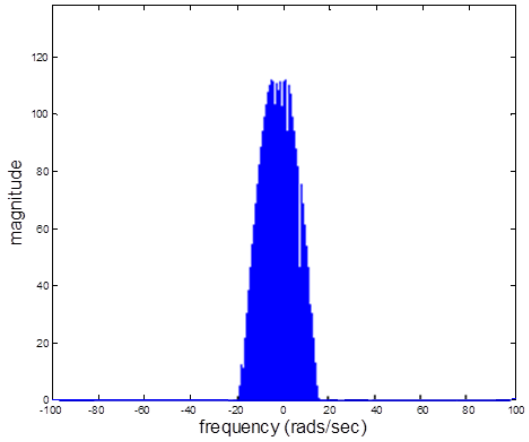

Figure 4. Baseband representation $S_c(\omega)$, after [12].

A third of way of representing a bandpass signal $s(t)$ is via its complex envelope form. The complex envelope signal $\tilde{s}(t)$ is obtained by shifting the analytic spectrum $S_+(\omega)$ down to the origin or DC. The complex envelope signal $\tilde{s}(t)$ is expressed as

$$\tilde{s}(t) = a(t)\exp(j\varphi(t)). \tag{6}$$

An illustration of the spectrum $S_c(\omega)$ of the complex envelope signal is illustrated in Figure 4. The spectrum is now centered around the origin at $\omega = 0$ [11].

The motive behind converting a bandpass signal to its complex envelope form is to avoid sampling at the high frequencies, which allows for reducing the sampling frequency per the sampling theorem [10], [11].

III. SAR MATHEMATICAL MODEL

A. RADAR PRELIMINARIES

1. Basic Radar Concept

Radar stands for radio detection and ranging. As indicated in its name, radar is an instrument used for detecting and locating targets. As illustrated in Figure 5, pulsed radar works by transmitting a sequence of electromagnetic waves as short pulses that reflect off a target-of-interest. A receiver records the reflected signals, which are much weaker versions of the transmitted pulse. The system calculates the distance to the target by using the measured time delay of the echoed signal. Signal processing techniques are performed to extract target-related information from the reflected signals [6].

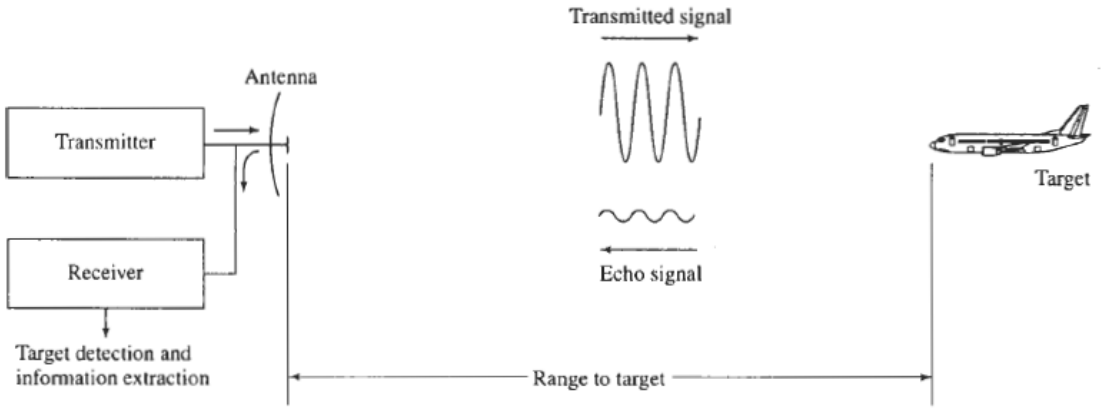

Figure 5. Basic radar concept, from [3].

Radar signal processors are designed to interpret the property that signals reflected from a target, or "scatterers," are time-shifted versions of the original transmitted signal. The radar range is given by

$$R = \frac{cT_r}{2}, \tag{7}$$

where c is the speed of electromagnetic wave propagation and T_r is the radar signal round-trip time from the target to the radar receiver [6].

2. Radar Range-Resolution

Range resolution is an important characteristic of any radar system. It is defined as a radar system's ability to distinguish between two or more separate reflectors that are very close in range [6]. Range resolution is

$$\Delta R = c\frac{\tau}{2}\ , \tag{8}$$

where τ is the duration of the transmitted radar pulse. Reflected targets must have a separation distance greater than ΔR to prevent overlapping of their images on a radar display.

B. SAR RANGE-IMAGING

1. SAR Range-Imaging Concept

This section is provided to develop the mathematical models for the SAR range imaging scene as well as the SAR range-imaging equations used throughout this thesis. In terms of SAR, range is the radar target distance perpendicular to the radar's flight path. SAR range-imaging is the process used to determine the range location of targets within a target scene through the transmission of the radar signal [4], [13].

It is important to call attention to a few assumptions made to derive the SAR equations used throughout the remainder of this thesis. First, SAR is monostatic (i.e., the transmitter and receiver are collocated). The radar does not transmit and receive at the same time. When the radar is not transmitting, it is receiving echoed signals. The second assumption is that the *target scene* is a target area on the ground. It can be thought of as comprised by n points. In the following simplified illustrative example, the target scene consists of four points. Collectively, these four points comprise a target or area on the ground. Although a target's reflectivity depends on several parameters, such as size and angle of incidence, these parameters are ignored throughout this thesis. Therefore, a third assumption is that the target's reflectivity equates to that of an ideal point reflector, which we define as a constant between 0 and 1 [14].

The range processing of a SAR system is identical to that of a conventional radar system [2]. An illustration for the case of n point targets is shown in Figure 6. In the one-dimensional target scene, $x_1, x_2, x_3, ..., x_n$ are the ranges of the point targets and $\sigma_1, \sigma_2, \sigma_3, ..., \sigma_n$, respectively, are the corresponding reflection coefficients of the targets. For the SAR range-imaging analysis and simplicity, we assume that all point targets have equal cross-range position, denoted as Y_c. SAR works by transmitting a signal $p(t)$ at periodic intervals to the target scene. The total target area is $2X_0$ wide, and the center of the target scene is denoted as X_c; therefore, the n targets exist within the interval $x \in [X_c - X_0, X_c + X_0]$ [14].

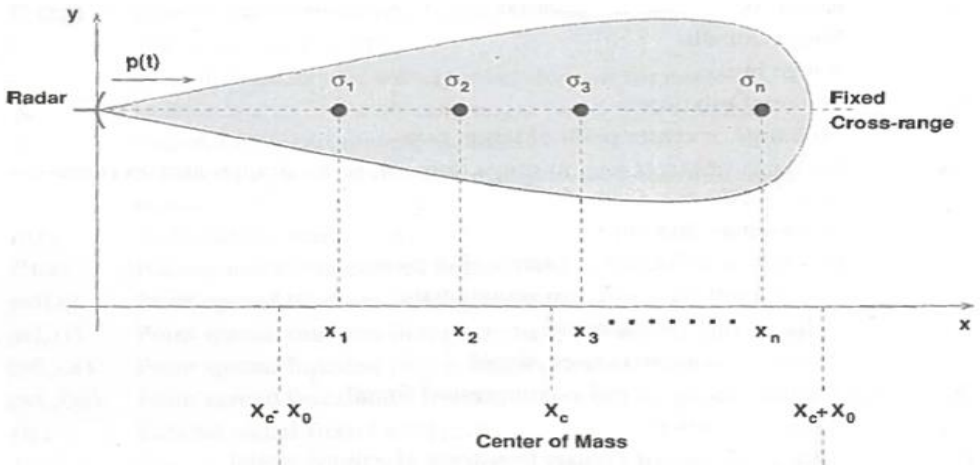

Figure 6. SAR range-imaging scene, from [14].

Now that we have developed a geometric model for the SAR range-imaging concept, we can present a mathematical representation of the target area, which again is made up of the n point targets shown in Figure 6. We represent the range domain target function that identifies a group of point targets along the x-axis as

$$f(x) = \sum_{i=1}^{n} \sigma_i \delta(x - x_i), \tag{9}$$

where $\delta()$ is the Dirac delta function and each term in the sum represents one point target. The magnitude of each target in the image depends on its reflectivity σ_i [14]. Figure 7 is an illustration of the range target function.

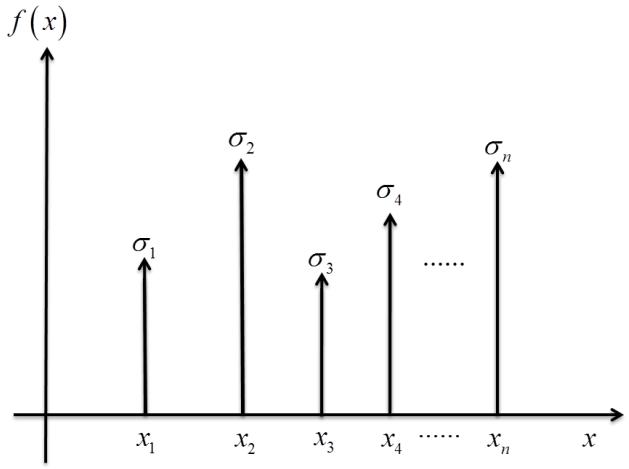

Figure 7. Range target function after [15].

Suppose radar signal $p(t)$ illuminates the target area in the range direction as shown in Figure 6. The reflected signals, or echoes, are delayed and attenuated versions of transmitted signal. Each echo is an indication of the presence of a point target and, therefore, vital to reconstructing the image. The received echo signal $s(t)$ is the convolution of the target function with the transmitted radar signal. It is expressed as

$$\begin{aligned} s(t) &= p(t) \otimes f\left(\frac{ct}{2}\right) \\ s(t) &= \sum_{i=1}^{n} \sigma_i p\left(t - \frac{2x_i}{c}\right), \end{aligned} \tag{10}$$

where $\otimes$ is the convolution operation and t is the time it takes the signal to propagate distance $ct/2$ and back.

2. SAR Range Resolution

As previously mentioned, SAR range processing is the same as traditional radar range processing; therefore, determining range resolution is also identical [4]. The bandwidth of a radar signal is inversely proportional to its duration. An alternate form of the range-resolution formula in Equation (8) is

$$\Delta R \approx \frac{c}{2B} \tag{11}$$

where B is the bandwidth of the transmitted signal and c is the speed of light. As seen from Equation (11), the range resolution of a SAR image is limited by the transmitted signal's bandwidth. Consequently, it is desirable to use a wide bandwidth signal to obtain fine range resolution.

C. SAR CROSS-RANGE IMAGING

1. SAR Cross-Range Imaging Concept

Cross-range is the radar-target distance parallel to the radar's flight path. Therefore, cross-range imaging depends on the motion of the platform and not only the transmitted signal. For SAR images, it is equally as important to locate a target in the cross-range direction as in the range direction.

Similar to the range-imaging geometry where we assume all targets have a common cross-range, we assume all targets are located at a fixed range position, denoted as X_c for the cross-range imaging case. The radar-carrying aircraft travels in the same direction as the cross-range axis. We refer to the flight path the radar travels as the synthetic aperture u axis. The radar's instantaneous location is denoted as $(0,u)$. The radar moves along the synthetic aperture axis, which has a support band of $u \in [-L,L]$; therefore, the total synthetic aperture length is $2L$ [14].

An illustration of the cross-range geometry is shown in Figure 8. A group of n point targets are located in the target scene and at $(X_c, y_1), (X_c, y_2), (X_c, y_3), \cdots,$

(X_c, y_n). The total target area scene is $2Y_0$ long, and the center of the target scene is a known cross-range Y_c. All targets in the cross-range imaging scene reside within $y \in [Y_c - Y_0, Y_c + Y_0]$ [14].

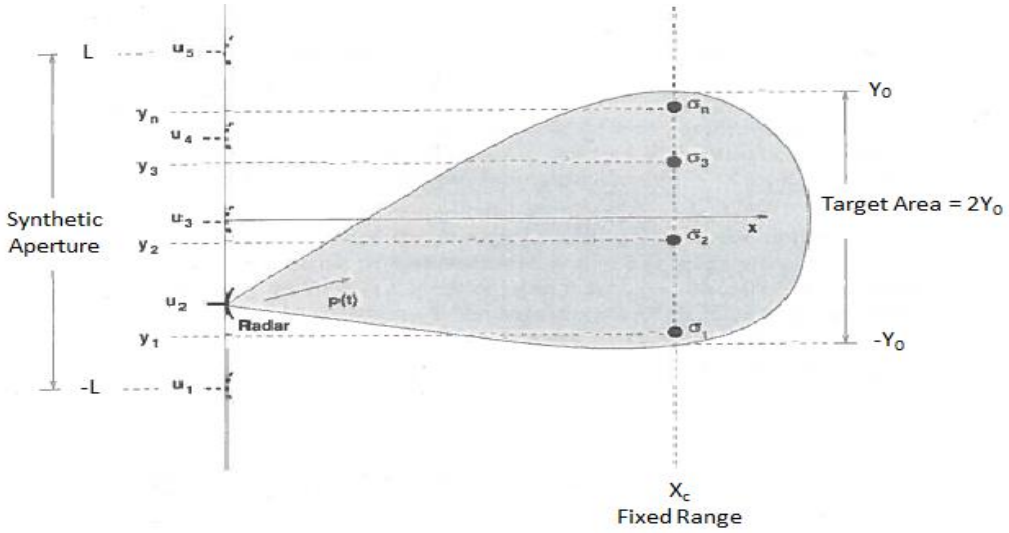

Figure 8. SAR cross-range geometry from [14].

The target function for the SAR cross-range case is similar to that of the SAR range case, in other words,

$$f(y) = \sum_{i=1}^{n} \sigma_i \delta(y - y_i). \tag{12}$$

The cross-range target function is also a group of impulses, where the area of each impulse is the target's reflectivity [14].

The distance between each point target and the radar is needed to later determine the echoed signal. This distance varies with the position of the radar as the aircraft moves along the cross-range *y*-axis as well as the position of each i^{th} target (i.e., (x_i, y_i) [14]). Distance *d* calculated using Figure 9 and the Pythagorean theorem, is expressed as

$$d = \sqrt{x_i^2 + (y_i - u)^2} \tag{13}$$

where x_i and y_i are the range distance and the cross-range distance to the i^{th} target, respectively, and u is the instantaneous cross-range location of the SAR platform.

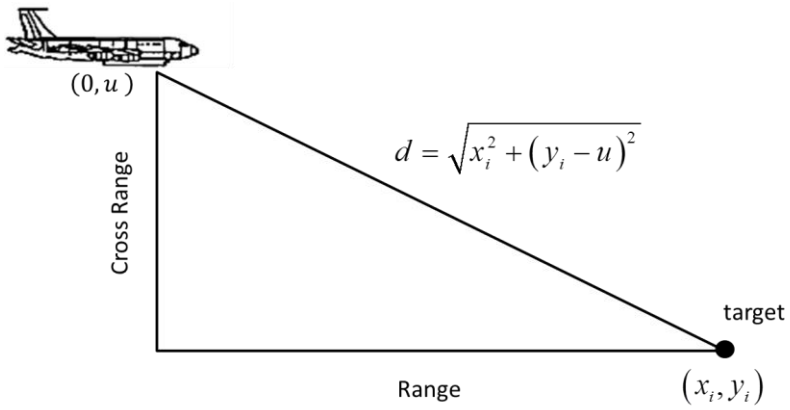

Figure 9. Depiction of slant range distance using Pythagorean theorem.

The motion of the SAR-carrying aircraft also influences the position of the target with respect to the radar or aspect angle [14]. The aspect angle of the radar, which is formed between each target and the radar's position located at $(0,u)$, is

$$\theta_i(u) = \arctan\left(\frac{y_i - u}{X_c}\right), \tag{14}$$

where X_c is a the center of the target scene in the range direction.

An example of the aspect angles of the radar with respect to a single point target located at (X_c, y_i) is illustrated in Figure 10.

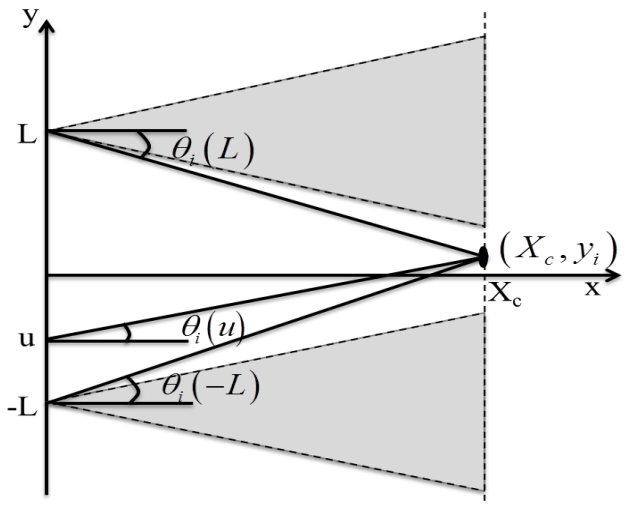

Figure 10. Synthetic aperture aspect angle, after [13].

Now consider that a SAR sensor transmits a radar signal $p(t)$ as it moves along the $y = u$ axis. The echoed signal is a sum of the individual returns from each point target and is expressed by

$$s(t,u) = \sum_{i=1}^{n} \sigma_i p\left[t - \frac{2\sqrt{x_i^2 - (y_i - u)^2}}{c} \right], \tag{15}$$

where

$$\frac{2\sqrt{x_i^2 - (y_i - u)^2}}{c} \tag{16}$$

is the round trip time for the radar signal to travel to each point target and back to the radar receiver [14].

2. SAR Cross-Range Resolution

In this section, we will see that cross-range resolution is independent of the radar's transmitted bandwidth but instead is governed by the total length of the synthetic aperture.

Cross-range resolution is defined as the ability to separate targets at similar ranges in the direction parallel to the motion of the radar sensor [4]. To explain SAR cross-range resolution, we first explain cross-range resolution for a real aperture radar (RAR).

Resolution in the cross-range direction is dependent on the spread of the beam across a particular target as well as the real aperture radar size [1]. The cross-range resolution for real aperture radar is

$$\Delta CR \approx \theta R, \tag{17}$$

where θ is the antenna beamwidth and R is the range distance. Antenna beam width θ is proportional to the real aperture size and is given as

$$\theta = \frac{\lambda}{L_{antenna}}, \tag{18}$$

where λ is the wavelength and $L_{antenna}$ is the physical length of the radar antenna; therefore, cross-range resolution for a real aperture radar is

$$\Delta CR \approx \frac{\lambda R}{L_{antenna}}, \tag{19}$$

which is also illustrated in Figure 11 [16].

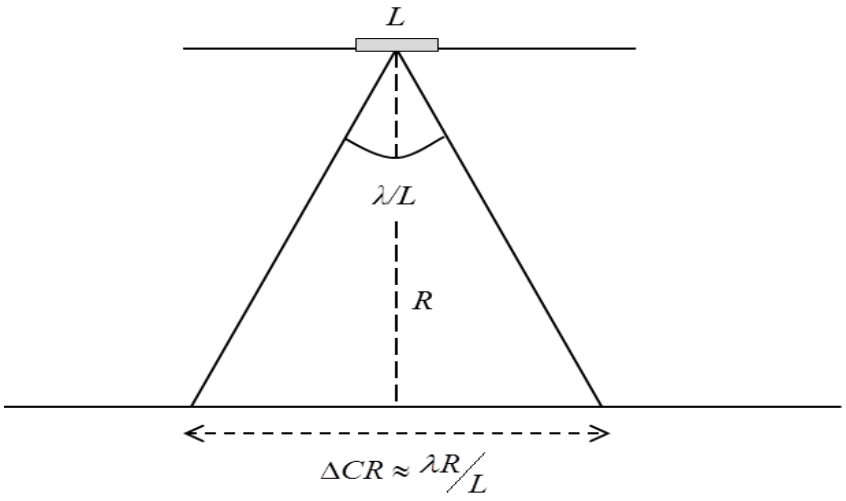

Figure 11. Real aperture radar cross-range resolution, after [16].

Consider a simple example where $R = 5000$ meters, $\lambda = 0.1$ meter and $L_{antenna} = 10$ meters. The cross-range resolution for a RAR is

$$\frac{R\lambda}{L_{antenna}} = 500 \text{ m.} \tag{20}$$

A value of 50 meters for cross-range resolution is rather high and signifies poor resolution. Under these conditions, obtaining a cross-range resolution of 10 meters requires a 500 meter antenna length.

Equation (20) reveals the cross-range resolution limitation of a RAR, which is that improving cross-range resolution for a fixed range distance and signal wavelength can only be achieved by employing a large antenna. SAR overcomes the physical limitations of a RAR by utilizing the flight path of the radar to synthesize a much larger aperture length [1], [13].

Now that we have examined cross-range resolution for real aperture radars, we continue our analysis to show how SAR cross-range resolution is different. Consider Figure 12 where it can be seen that a reflector is illuminated by a beam with full beamwidth θ. The combination of the two beamwidths results in a maximum *synthetic* antenna length of L, which is the synthetic aperture.

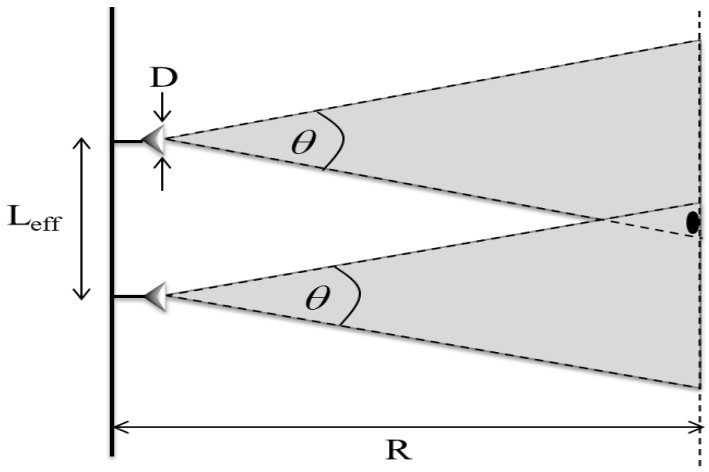

Figure 12. Geometry of single point target within synthetic aperture beamwidth, after [1].

The beamwidth of the synthetic aperture is,

$$\theta = \frac{\lambda}{L_{eff}}, \tag{21}$$

where L_{eff} is the synthetic aperture the radar forms via multiple transmitted and received signals during its flight path. As a result, the cross-range resolution for a SAR is

$$\Delta CR = \frac{\lambda R}{L_{eff}}. \tag{22}$$

We now compare the cross-range resolution value of a SAR system by using the same values for λ and R that were used in the RAR example; however, unlike a RAR where the physical length of the antenna determines cross-range resolution, we use the synthetic aperture length or L_{eff} = 1000 meters. Then the cross resolution becomes

$$\frac{\lambda R}{D_{eff}} = 5\,\text{meters}. \tag{23}$$

The cross-range resolution of the SAR system far surpasses that of the RAR's. Furthermore, increasing the length of D_{eff} to obtain finer resolution is as simple as increasing the length of time or distance that the aircraft flies over a target-of-interest at range R [13].

D. TWO-DIMENSIONAL SAR

Now that we have developed the equations and mathematical models for SAR range and cross-range imaging, we further expand the traditional SAR concept analysis. For this analysis, we first discuss the two main operational modes of SAR. The spotlight and stripmap techniques represent the two modes of SAR image collection.

1. SAR Spotlight Mode

In spotlight mode, the SAR sensor acts like a spotlight that continuously illuminates a single location or target as the aircraft continues along its flight path.

Operating the SAR in spotlight mode increases the cross-range resolution as the same target or target area is kept within the radar's beam for a longer time. Figure 13 is a simple illustration of how SAR operates in spotlight mode [14], [15] .

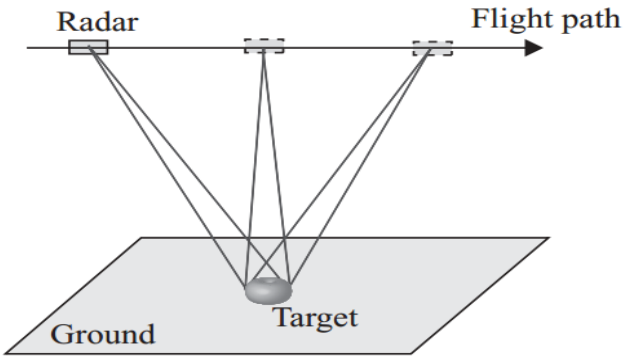

Figure 13. Spotlight SAR mode, from [15].

2. SAR Stripmap Mode

In stripmap mode, the SAR sensor illuminates a larger area perpendicular to the aircraft's flight path. This technique can be thought of as a scan mode, where the radar is not necessarily interested in a specific target. Rather, the radar scans a particular "strip" on the ground for an overall awareness of what is around. This mode's primary use is surveillance and reconnaissance. Fine cross-range resolution in stripmap mode is achieved since the SAR effectively forms a larger antenna while attaining a longer view of the area-of-interest [15]. An example of how SAR operates in stripmap mode is shown in Figure 14 [14], [15].

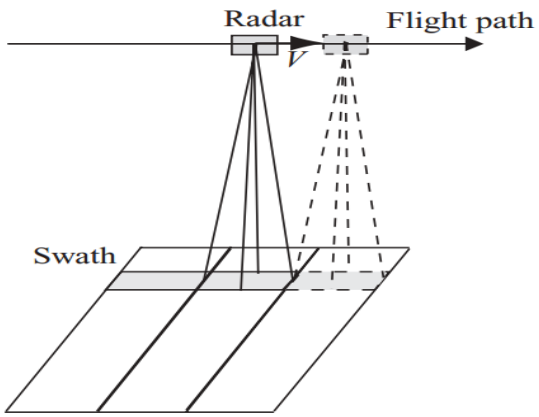

Figure 14. Stripmap SAR mode, from [15].

The stripmap SAR operational mode is the focus of this thesis.

3. Stripmap SAR Model

a. Radar Antenna

An important element of any radar system is its antenna. The antenna type determines how the radiated signal energy is directed. Further, the antenna's physical structure and design determine its radiation pattern [3], [14].

The radiation pattern refers to the transmitted radar signal's direction and spread from the antenna to the target area [3]. The SAR radiation pattern is a measure of relative phase and magnitude of the echoed signal. Factors that affect the radiation pattern are the radar's transmitted signal frequency and physical properties. For stripmap SAR, the radiation pattern is perpendicular to the aircraft's motion [14].

The type of antenna referenced in this research is a planar radar antenna. Soumekh defines a planar radar antenna as an antenna that corresponds to a flat two-dimensional spatial aperture in the three-dimensional spatial domain [14]. A planar antenna concentrates its energy or beam in a cone-shaped pattern. The half-beamwidth distance for a planar antenna is

$$B = r\sin\left(\phi_d\right), \tag{24}$$

where r is the radial distance to the target scene from the aperture from which the beam originates and ϕ_d is the radar's beam divergence or angular spread, given by

$$\phi_d = \arcsin\left(\frac{\lambda}{D}\right), \tag{25}$$

where λ is the *transmitted signal's* wavelength and D is the antenna diameter. From Equations (24) and (25) we determine that the radiation pattern of a planar radar depends on the radar frequency as well as the diameter of the radar [3], [14].

b. Stripmap SAR geometry

The stripmap SAR geometry is similar to the cross-range geometry. The main difference is that targets now reside within a two-dimensional target area.

The SAR operation in stripmap mode is illustrated in Figure 15. It can be seen that the radar illuminates a target area whose dimensions are $\left[-Y_0, Y_0\right]$ in the cross-range direction and $\left[X_c - X_0, X_c + X_0\right]$ in the range direction. The target area length is defined by the SAR platform's displacement. The aircraft travels in a straight line along the y-axis, which is the same as the synthetic aperture u-axis. In stripmap SAR, the target's range remains constant; however, the cross-range coordinates change as the radar beam is swept across a strip on the ground [14].

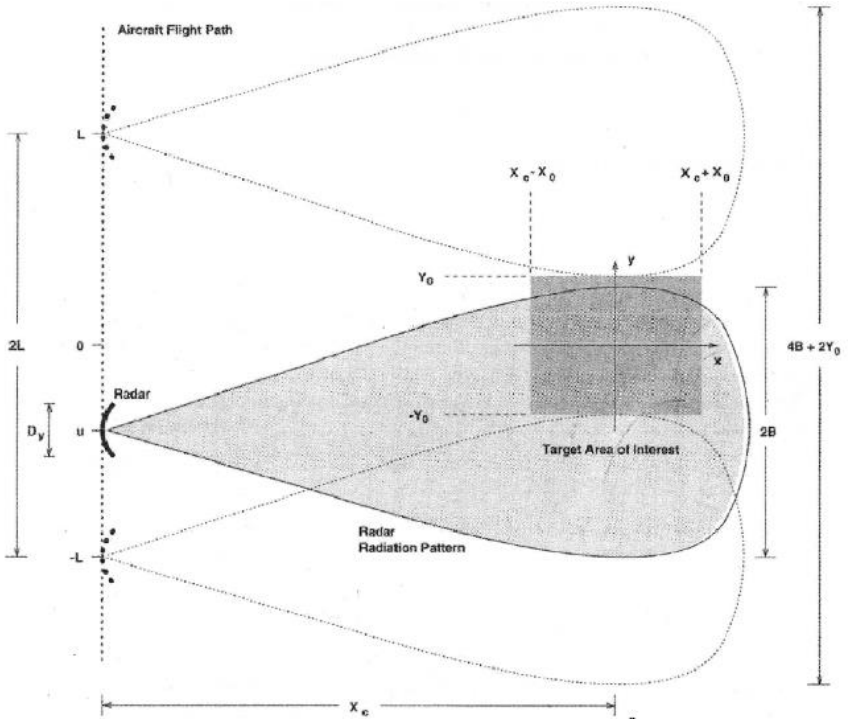

Figure 15. Stripmap SAR geometry, from [14].

The radiation pattern is the cone extending from the antenna to the target area. The radar's half-beamwidth is determined by the antenna type and the divergence angle as indicated in Equations (24) and (25) [14].

The received echo signal for the stripmap SAR case is

$$s(t,u) = \sum_{i=1}^{n} \sigma_i p\left[t - \frac{2\sqrt{x_i^2 + (y_i - u)^2}}{c} \right]. \tag{26}$$

where $2\sqrt{x_i^2 + (y_i - u)^2}\,/c$ is the time it takes the transmitted radar signal to travel to each point target, located at (x_i, y_i), and back to the radar receiver.

A graphical representation of the round trip propagation time as a function of radar position for a single point target is illustrated in Figure 16. The sum of the returns at time t forms a half-hyperbolic shape due to the equation for the round-trip delay.

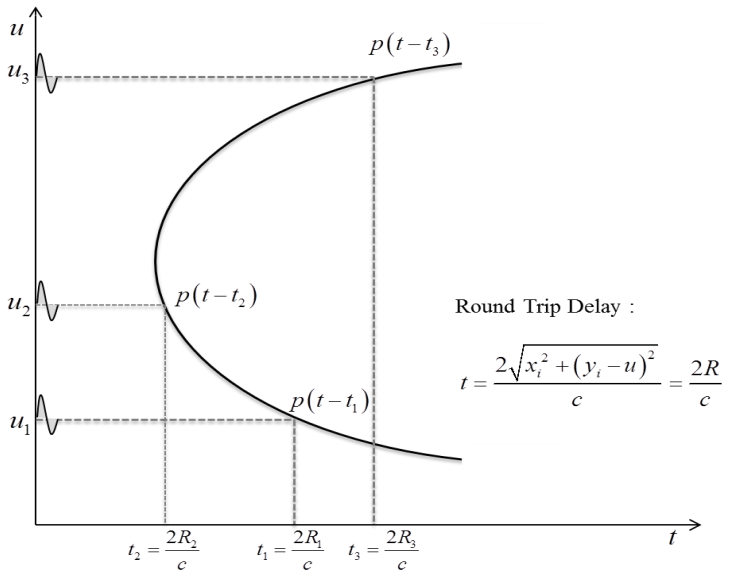

Figure 16. Received echoed signal $s(t,u)$ for a single point target, after [14].

The radar transmits several pulses where the total beamwidth of each pulse is $2B$. The synthetic aperture's total length $2L$ is the distance traveled while the target area is illuminated by the transmitted radar signal $p(t)$. The synthetic aperture interval $[-L, L]$ is dependent on the radar's half-beamwidth as well as the target's cross-range distance. The length of the synthetic aperture is

$$L = B + Y_0, \tag{27}$$

where half-beamwidth B is defined in Equation (24) and Y_0 is half the target area length in the cross-range direction. Substituting Equation (24) into Equation (27), we get

$$\begin{aligned} L &= r\sin\phi_d + Y_0 \\ &= x\tan\phi_d + Y_0, \end{aligned} \tag{28}$$

where we see that the synthetic aperture interval varies with the radar's half-beamwidth, which also depends on the antenna's divergence angle [14].

Similar to the range and cross-range case, we assume that the targets located in the target scene are stationary. However, it is important to note that the observability of each target depends not only on each target's reflectivity but also on the radar's radiation

pattern and each target's angular position with respect to the radar. The observability of a reflector located at (x_i, y_i) for stripmap mode is illustrated in Figure 17.

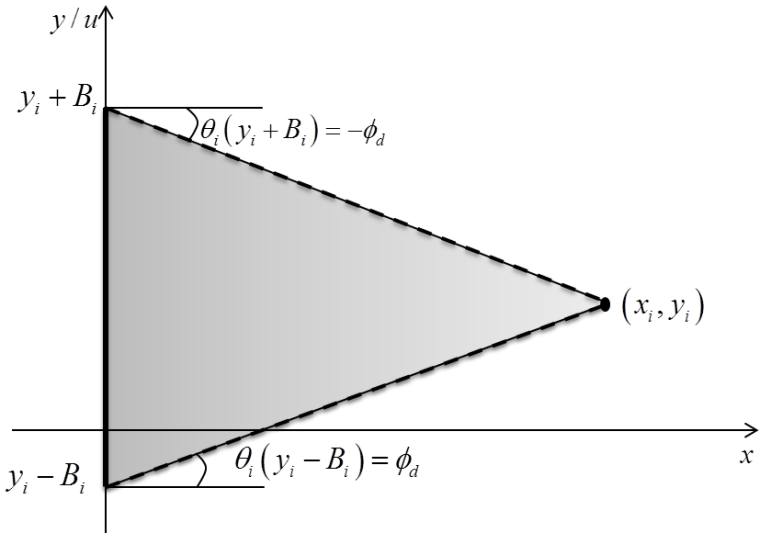

Figure 17. Aspect angle of target located at (x_i, y_i), after [14].

Although we are assuming that the target area does not change for the stripmap SAR case, the antenna's location constantly changes due to aircraft motion. Therefore, the antenna's aspect angle with respect to each point target also varies along the aircraft's flight path. This aspect angle, which is also introduced in the cross-range analysis, is given by

$$\theta_i(u) = \arctan\left(\frac{y_i - u}{x_i}\right). \tag{29}$$

A reflector is observable to the radar when the radar is within the synthetic aperture u interval

$$u \in [y_i - B_i : y_i + B_i], \tag{30}$$

where half-beamwidth B_i was presented in Equation (24) [14].

Substituting Equation (30) into Equation (29), we get

$$\left[\theta_i\left(y_i - B_i\right) : \theta_i\left(y_i + B_i\right)\right] = \left[-\arctan\left(\frac{B_i}{x_i}\right) : \arctan\left(\frac{B_i}{x_i}\right)\right]. \tag{31}$$

From Equation (31), we determine that the aspect angle of each target is exactly equal to the divergence angle of the radar [14].

c. Stripmap SAR Data Collection

This section is provided to illustrate how SAR data is collected and stored into a two-dimensional array. Figure 18 is a simplified matrix diagram that contains data for a single point target.

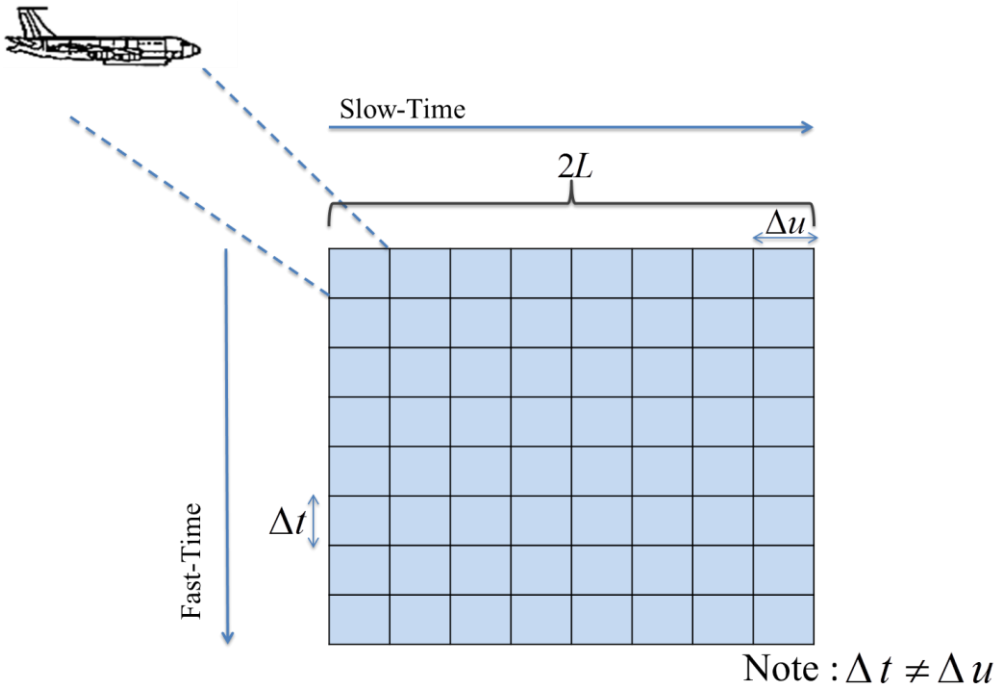

Figure 18. Synthetic aperture $M \times N$ array.

Consider that a SAR sensor transmits pulses as it travels over a single point target. The $M \times N$ matrix is populated with reflected signal returns that are indexed by two different time variables: fast-time *t* and slow-time *u*. Each column corresponds to the fast-time samples received from transmitting a single radar signal from a distinct position. Each row of data corresponds to slow-time samples received from successive reflective

radar pulses across the entire synthetic aperture $2L$ [15]. Collectively, time, range and radar position information is stored in each index of the array.

d. Fast-Time

The fast-time index values are obtained by periodically emitting signals at a predetermined rate. We refer to this index as fast-time because the transmitted radar signal propagates at the speed of light, which is much faster than the platform speed. The fast-time delay of the received echoed signal is proportional to range [14], [16].

e. Slow-Time

The slow-time index is due to the radar platform's position at the time it transmits a radar signal. Since the SAR aircraft travels much slower than the speed of light, this index is referred to as slow-time. Since slow-time corresponds to the motion of the aircraft, it is used to measure cross-range [14], [16].

THIS PAGE INTENTIONALLY LEFT BLANK

IV. SAR RECONSTRUCTION

The purpose of this chapter is to discuss the algorithms utilized to reconstruct the SAR target function for the range, cross-range and two-dimensional cases. Since the main goal of this work is to examine the effects of signal parameters on the stripmap two-dimensional SAR case, more emphasis is placed on the two-dimensional reconstruction algorithm. Nonetheless, we first offer an analysis of the range and cross-range reconstruction algorithms as they are both necessary to understand the complete two-dimensional SAR concept.

A. RANGE RECONSTRUCTION

Matched filters are commonly used in radar systems to detect the presence of an echoed signal that corresponds to the existence of a target. The arrival time of the echo is used to determine the target location. The filter is matched to the echo signal that is returned from a unit reflectivity point target located at $(x, y) = (X_c, 0)$. The echoed signal due to the assumed target, located at $(X_c, 0),$ is expressed as

$$\begin{aligned} s_0(t) &= p(t) \otimes \delta\left(t - \frac{2X_c}{c}\right) \\ &= p\left(t - \frac{2X_c}{c}\right), \end{aligned} \tag{32}$$

where $p(t)$ is the transmitted radar signal and $t_{X_c} = 2X_c/c$ is the round trip time or the time it takes the transmitted radar signal to propagate to center of the target scene and back. This hypothetical echoed signal, or more precisely $s_0^*(-t),$ is used as the impulse response of the matched filter [14].

The process of matched filtering involves the correlation or comparison of an unknown received signal with the reference signal $s_o(t),$ which is equivalent to convolving the unknown or reflected signals with the matched filter's impulse response. The output of the matched filter is

$$s_{MF}(t) = s(t) \otimes s_0^*(-t), \tag{33}$$

where $s(t)$ is the received echoed signal, $s_0^*(-t)$ is the matched filter's impulse response, and $(^*)$ denotes the complex conjugate [14].

The mathematical operation explained in Equation (33) is computationally expensive. Thus, matched filtering is carried out more efficiently in the frequency domain.

Convolution in the time-domain is equivalent to multiplication in the frequency-domain [10]. Therefore, we first convert both the received and referenced signals to their frequency-domain equivalents. The Fourier transform with respect to fast-time *t* of the received echo signal in Equation (10) and the ideal signal in Equation (32) is

$$S(\omega) = P(\omega) \sum_{i=1}^{n} \sigma_i \exp\left[-j2\omega \frac{x_i}{c} \right] \tag{34}$$

and

$$S_0(\omega) = P(\omega) \exp\left(-j\omega t_{X_c} \right), \tag{35}$$

respectively, where ω represents the frequency-domain variable in radians per second, and $P(\omega)$ is the Fourier transform of radar signal $p(t)$. The frequencies of interest are

$$\omega = \left[\omega_c - \omega_0, \omega_c + \omega_0 \right],$$

where $\omega_c = 2\pi f_c$ is the angular carrier frequency and $\omega_0 = 2\pi f_0$ is the radar signal angular baseband bandwidth [14].

Matched filtering can now be carried out in the frequency-domain via

$$S_{MF}(\omega) = S(\omega) S_0^*(\omega), \tag{36}$$

where $S_0^*(\omega)$ is the complex conjugate of the reference signal [14].

The reconstructed range target function is obtained by performing the inverse Fourier transform operation with respect to time t on $S_{MF}(\omega)$, which is expressed as

$$f(x) = F^{-1}\left[S_{MF}(\omega) \right], \tag{37}$$

where F^{-1} denotes the inverse Fourier transform operation.

A summary of matched filtering steps are in Figure 19 [4], [14].

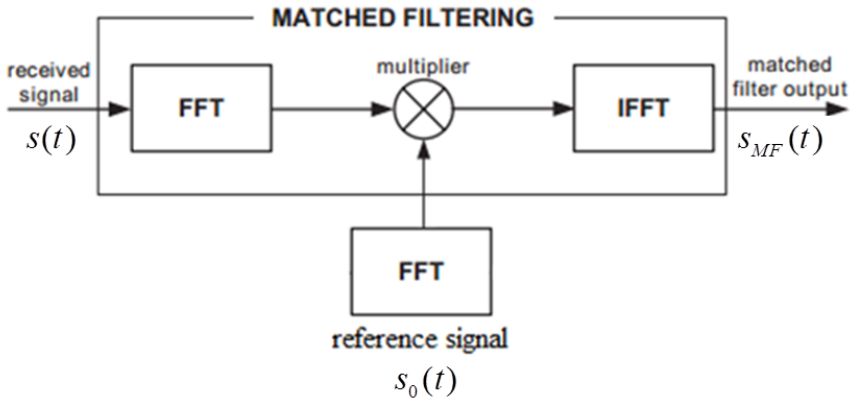

Figure 19. Illustration of matched filter via FFT processing, from [4].

B. CROSS-RANGE RECONSTRUCTION

1. Cross-range Matched Filtering

In Chapter III, we observed that the distance of the i^{th} target from the radar receiver depends on the target and the synthetic aperture positions. That is, the received echoed signal varies with fast-time t as well as position u. The matched filter or ideal signal, located at $(X_c, 0)$, is expressed as

$$\begin{aligned} s_0(t,u) &= p(t) \otimes \delta\left(t - \frac{2\sqrt{X_c^2 + u^2}}{c}\right) \\ &= p\left(t - \frac{2\sqrt{X_c^2 + u^2}}{c}\right) \end{aligned} \tag{38}$$

where $2\sqrt{X_c^2 + u^2}/c$ is the round trip propagation time from the receiver to the target scene center [14].

For cross-range reconstruction, the transmitted signal we consider is a pure sinusoid; therefore, $p(t) = \exp(j\omega t)$ is the analytic representation of the single frequency radar signal used to recover the target in the cross-range-domain [2], [14]. We

then correlate the phase history, which is related to the synthetic aperture position with the reference signal in (38) [14].

Using $p(t) = \exp(j\omega t)$, we get the reference signal

$$s_0(t,u) = \exp\left[-j\omega\left(t - \frac{\sqrt{X_c^2 + u^2}}{c}\right)\right]. \tag{39}$$

We obtain the baseband representation of the reference signal by multiplying (39) by $\exp(-j\omega t)$. The baseband representation is expressed as

$$\begin{aligned} s_0(\omega,u) &= \exp\left(-j2\frac{\omega}{c}\sqrt{X_c^2 + u^2}\right) \\ &= \exp\left(-j2k\sqrt{X_c^2 + u^2}\right), \end{aligned} \tag{40}$$

where $k = \omega/c$ is the wavenumber of the transmitted signal with units radians per meter. Equivalently, the received echoed signal in Equation (26) becomes

$$s(t,u) = \exp(j\omega t)\sum_{i=1}^{n}\sigma_i \exp\left[-j2k\sqrt{x_i^2 + (y_i - u)^2}\right], \tag{41}$$

and the baseband representation is expressed as

$$s(\omega,u) = \sum_{i=1}^{n}\sigma_i \exp\left[-j2k\sqrt{x_i^2 + (y_i - u)^2}\right], \tag{42}$$

which is obtained by multiplying Equation (41) by $\exp(-j\omega t)$ [2], [14].

2. Wavenumber Domain

Similar to range reconstruction, we wish to carry out the matched filter process in the frequency-domain. A spatial Fourier transform is performed on $s(\omega,u)$, which converts the signal into the spatial frequency or wavenumber domain. The spatial Fourier transform of $s(\omega,u)$ is defined as

$$S(\omega,k_u) = \int_{-\infty}^{\infty} s(\omega,u)\exp(-jk_u u)\,du \tag{43}$$

where k_u is the wavenumber that corresponds to synthetic aperture position u [14].

The spatial Fourier transform of $s(\omega,u)$ in Equation (42) becomes

$$\begin{aligned} s(\omega,k_u) &= \int_{-\infty}^{\infty}\sum_{i=1}^{n}\sigma_i \exp\left[-j2k\sqrt{x_i^2+(y_i-u)^2}\right]\exp(-jk_u u)\,du \\ &= \int_{-\infty}^{\infty}\sum_{i=1}^{n}\sigma_i \exp\left[-j2k\sqrt{x_i^2+(y_i-u)^2}-jk_u u\right]du. \end{aligned} \tag{44}$$

The integral in Equation (44) is evaluated using the principle of stationary phase discussed in [2] and [14], which involves expanding the term $\sqrt{x_n^2+(y_n-u)^2}$. The approximate spatial Fourier frequency transform $s(\omega,k_u)$ becomes

$$\begin{aligned} S(\omega,k_u) &= \sum_{i=1}^{n}\sigma_i \exp\left(-j\sqrt{4k^2-k_u^2}x_i - jk_u y_i\right) \\ &= \sum_{i=1}^{n}\sigma_i \exp\left(-jk_x x_i - jk_y y_i\right), \end{aligned} \tag{45}$$

where wavenumber $k_x=\sqrt{4k^2-k_u^2}$ is the spatial frequency coordinate for range x and wavenumber $k_y=k_u$ is the spatial frequency coordinate for cross-range y [2], [14].

Reconstruction of the cross-range target function can now be obtained by first carrying out the matched filter via

$$S_{MF}(\omega,k_u)=S(\omega,k_u)S_0^*(\omega,k_u), \tag{46}$$

followed by taking the inverse Fourier transform of the output $S_{MF}(\omega,k_u)$, where the reconstructed cross-range function becomes [14]

$$f(y)=F^{-1}\left[S_{MF}(\omega,k_u)\right]. \tag{47}$$

C. TWO-DIMENSIONAL RECONSTRUCTION

1. Stripmap SAR Reconstruction

Now that the one-dimensional range and cross-range matched filtering methods have been defined, we can expand the analysis to show how it applies to the two-dimensional stripmap SAR image reconstruction.

The spatial frequency interpolation algorithm (SFIA) presented in [14] is the chosen reconstruction algorithm used to convert the data from the received signal into a two-dimensional SAR image. The SFIA involves several steps, which are shown in Figure 20.

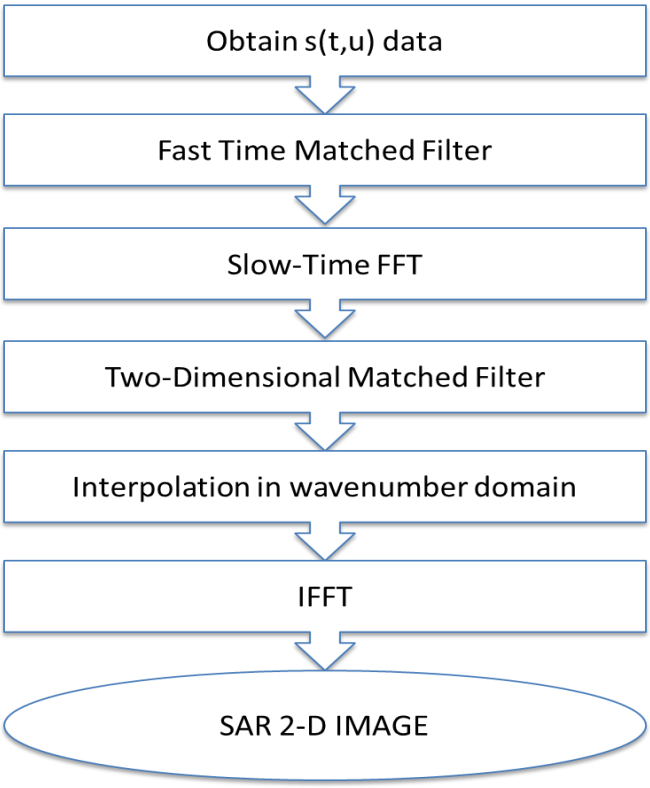

Figure 20. Reconstruction flow chart via spatial frequency interpolation for two-dimensional SAR images.

The algorithm includes a range compression that is similar to the range matched filtering algorithm described in Section IV.A, followed by a slow-time Fourier transform. We next carry out a two-dimensional matched filtering process in the wavenumber domain. The steps are explained in more detail below [14].

a. Fast-Time Matched Filter

Fast-time matched filtering is similar to the range matched filtering explained in Section IV.A. The main difference is that the two-dimensional SAR received data is a

function of both fast-time t and slow-time u. The two-dimensional SAR fast-time matched filtering consists of three steps:

1. Obtain $s(\omega,u)$ by performing a one-dimensional Fourier transform of $s(\mathrm{t},u)$ in Equation (26) with respect to fast-time t. The received fast-time Fourier transform of the received signal is

$$s(\omega,u)=P(\omega)\sum_{i}^{n}\sigma_i\left[-j2k\sqrt{x_i^2+(y_i-u)^2}\right], \tag{48}$$

where $k=\omega/c$ is the wavenumber of the transmitted radar signal [14].

2. Obtain the reference signal $s_0(\omega,u)$ by performing a one-dimensional Fourier transform on $s_0(t,u)$ with respect to fast-time t. The fast-time Fourier transform of the reference signal is [14]

$$s_0(\omega,u)=P(\omega)\exp\left[-j2k\sqrt{X_c^2-u^2}\right]. \tag{49}$$

3. Apply the matched filter in the frequency domain via

$$s_{MF}(\omega,u)=s(\omega,u)s_0^*(\omega,u) \tag{50}$$

where $s_o^*(\omega,u)$ is the fast-time conjugate of the Fourier transform of the reference signal, and $s_{MF}(\omega,u)$ is the matched filtered signal or range compressed signal [14].

b. Slow-Time Fast Fourier Transform

The purpose of this step is to transform the compressed signal to the synthetic aperture frequency k_u domain. Transforming the signal to the k_u domain allows spatial directional information data extraction, which is useful in the succeeding steps of the SFIA algorithm [14]. Performing the one-dimensional slow-time FFT involves taking the Fourier transform of the compressed signal $s(\omega,u)$ with respect to slow-time variable u. Using the fact that $k_x=\sqrt{4k^2-k_u^2}$ and $k_y=k_u$ which was introduced in Section B.2, we can express the two-dimensional spectrum of the compressed signal as [2], [14].

$$S(\omega, k_u) = P(\omega) \sum_{i=1}^{n} \sigma_i \exp\left(-j\sqrt{4k^2 - k_u^2 x_i} - jk_u y_i\right). \quad (51)$$

c. Two-Dimensional Matched Filtering

The next reconstruction algorithm step is two-dimensional matched filtering of the SAR signal, which occurs in the wavenumber domain. The input signal $S(\omega, k_u)$ to this portion of the algorithm is already in the synthetic aperture frequency k_u domain. The matched filter is applied to the input signal $S(\omega, k_u)$

$$S_{MF}(\omega, k_u) = S(\omega, k_u) S_0^*(\omega, k_u). \quad (52)$$

It is important to note that wavenumbers k_x and k_y are defined over a different set of coordinates or spacing than t and u [2], [14].

After matched filtering, we can define the two-dimensional target function in the spatial frequency-domain as [2], [14],

$$F(k_x, k_y) = \sum_{i=1}^{n} \sigma_i \exp\left(-jk_x x_i - jk_y y_i\right). \quad (53)$$

d. Interpolation

The next step is an interpolation method presented in [14]. Applying the two-dimensional Fourier Transform in the previous step resulted in frequency data that is non-uniform and, therefore, does not lie on a rectangular grid on the $k_x - k_y$ plane [4]. The unevenness of the data results from the nonlinear function $k_x = \sqrt{4k^2 - k_u^2}$. The need to approximate k_x is to enable data mapping onto a rectangular grid that allows for a two-dimensional IFFT to be performed [14].

The interpolation method involves interpolating k_x to reformat the data points into a function of evenly spaced data [14] [15]. After the data is evenly spaced, we execute a two-dimensional inverse Fourier transform on $S_{MF}(\omega, k_u)$ to recover the two-

dimensional SAR image function $f(x,y)$ [14]. An illustration of how the k_x and k_y data are mapped onto a rectangular grid before and after the interpolating k_x is shown in Figure 21.

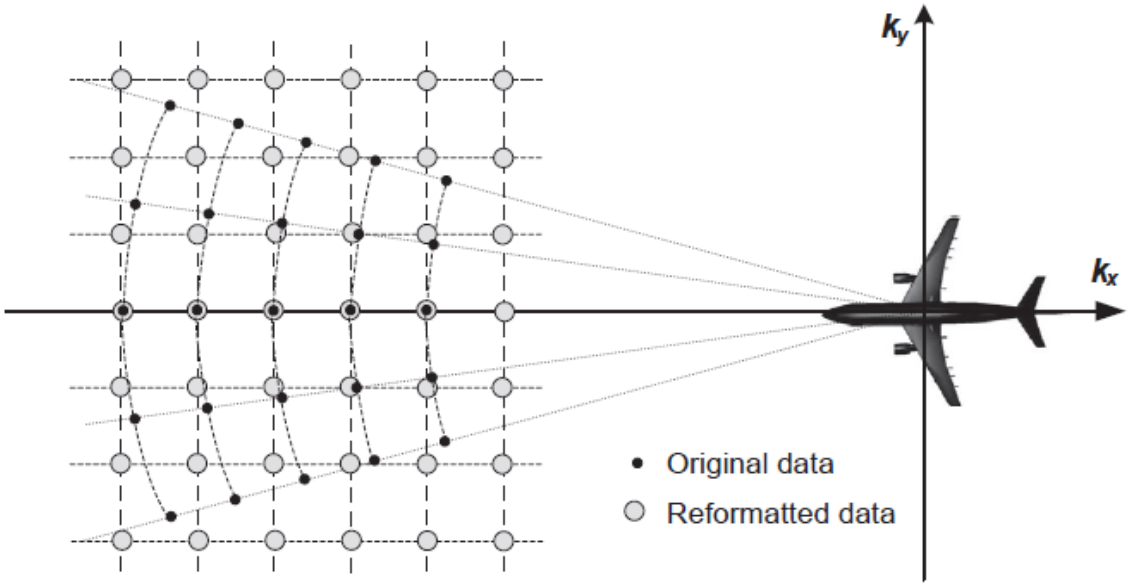

Figure 21. Depiction of interpolation of k_x data, from [4].

e. Inverse Fast Fourier Transform

The final step in recovering the target function is to perform the IFFT on Equation (53), which transforms the SAR data from the spatial frequency-domain to the time-domain. Therefore, the two-dimensional SAR image function, which represents the targets in the target scene, is [14]

$$f(x,y)=\sum_{i=1}^{n}\sigma_i\delta(x-x_i,y-y_i). \tag{54}$$

D. SAMPLING REQUIREMENTS

In the previous sections, we discussed the proposed methods utilized to reconstruct the range function, cross-range function and, finally, the two-dimensional SAR image. An important consideration in radar signal processing is the sampling rate of

both the transmitted and received signals. The sampling spacing requirements must be considered to avoid aliasing as well as to accurately reconstruct the radar signal. This section is provided to introduce the sampling spacing requirements used to process the two-dimensional SAR data. We also discuss the importance of resampling at the end of the section.

1. Nyquist Sampling Theorem

Consider that a radar signal $p(t)$ of bandwidth *B* illuminates a target scene. The received signals consist of *N* fast-time samples and *M* slow-time samples. In order to accurately recover a SAR image, the received signals must be sampled at a rate that satisfies the Nyquist sampling theorem. This theorem states that a band-limited signal can be reconstructed from its samples if the signal is sampled at a rate of at least twice the highest frequency of the signal [10], in other words,

$$F_s \geq 2B, \tag{55}$$

where *B* is the signal bandwidth and F_s is the sampling rate [10].

Violation of the Nyquist sampling criterion results in aliasing. In terms of target reconstruction, aliasing means that targets may be indistinguishable or possibly appear in inaccurate locations [16].

a. Fast-time Domain Sampling Requirements

Fast-time sampling of the received echo signals occur within the fast-time interval $t \in \left[T_s, T_f\right]$ where start time T_s is the echo signal arrival time from the target closest to the receiver and T_f is the echo signal arrival time from the target furthest from the receiver [14].

The fast-time index is sampled to correspond with the Nyquist sampling theorem (Equation (55)) applied to the transmitted radar signal bandwidth. Range resolution

depends on the radar signal bandwidth as explained in Section III.B.2. The fast-time sampling spacing requirement is shown in Equation (56), where Δt is the sampling time interval between two data points [14]

$$\Delta t = \frac{1}{F_s} \leq \frac{1}{2B}. \tag{56}$$

b. Slow-Time Domain Sampling Requirements

Next we consider the slow-time sampling requirement that depends on the divergence angle ϕ_d of a SAR antenna. Recall from Section III.D.3.a that the divergence angle of a planar radar antenna is

$$\phi_d = \arcsin\left(\frac{\lambda}{D}\right). \tag{57}$$

The Nyquist sampling criterion for the slow-time spacing Δu is given in [14] and expressed as

$$\Delta u \leq \frac{D}{4\sin\phi_d}. \tag{58}$$

We derive the Nyquist sampling criterion for a planar radar aperture by substituting Equation (57) into Equation (58). Therefore, the slow-time sampling spacing requirement becomes

$$\Delta u \leq \frac{D}{4}. \tag{59}$$

This relationship is a common rule of thumb used for slow-time SAR sampling [14].

c. Frequency-Domain Sampling Requirements

Performing the Fourier transform with respect to the fast-time variable t introduces the frequency-domain variable ω. The fast-time samples are directly related to the time-domain samples. The sampling spacing of the received echoed signal's Fourier transform is

$$\Delta\omega \leq \frac{2\pi}{N\Delta t}, \tag{60}$$

where $\Delta\omega$ is the spacing between two sample points, N is the total number of time samples and Δt is the fast-time sampling spacing requirement [14].

d. Spatial Frequency-Domain Sampling Requirements

The final domain used in SAR signal processing is spatial frequency-domain. The received signal data is transitioned to the spatial frequency or wavenumber domain after performing a two-dimensional Fourier transform. It is in this domain that we reconstruct the final SAR image [14].

As discussed in Section B.2, the spatial frequency coordinates k_x and k_y correspond to the range and cross-range directions, respectively. The interval coverage or width of the k_x axis depends on the total size of the target scene in the range direction $2X_0$, while the k_y coverage depends on the synthetic aperture size $2L$. Therefore, the sampling spacing of k_x and k_y are constrained by

$$\Delta k_x \leq \frac{2\pi}{2X_0} \tag{61}$$

and

$$\Delta k_y \leq \frac{2\pi}{M\Delta_u} \tag{62}$$

where Δk_x and Δk_y are the spacing requirement of spatial frequency k_x and k_y, M is the total number of slow-time samples and Δu is the slow-time domain spacing requirement [14].

2. Resampling via Ideal Low Pass Filter

Resampling signal data is a common procedure performed in digital and radar signal processing. Resampling is the process of changing the signal sampling rate after sampling at the Nyquist rate in (55) [17]. This procedure is carried out to obtain

interpolated values of the received echo and reference signal in positions that the transmitted radar signal sampling does not provide [2], [17].

Consider that the transmitted radar signal $p(t)$ is sampled at the Nyquist interval. We refer to the Nyquist interval as $T_{s,orig}$ as it is used before the resampling procedure. Therefore, the original discrete samples $p\left(n_{orig}\right)$ of the radar signal are expressed as

$$p\left(n_{orig}\right) = p\left(n_{orig} T_{s,orig}\right), \tag{63}$$

where n_{orig} represents the original discrete time samples. Now, consider that $p\left(n_{orig}\right)$ is transmitted onto the target scene, and the received echoed signal $s(t)$ is returned. The received signal $s(t),$ whose discrete equivalent is $s\left(n_{new}\right),$ contains data that correspond to the delay times. This data is not at the same time-sample locations as n_{orig}. Thus, recovering $s\left(n_{new}\right)$ at the original sampling time $T_{s,orig}$ is only possible if we resample the signal using a low-pass or interpolation filter [17].

The ideal interpolation formula is given by

$$x\left(t_{new}\right) = \sum_{n_{orig}=-\infty}^{\infty} x\left(n_{orig} T_{s,orig}\right) \mathrm{sinc}\left(\frac{t_{new} - n_{orig} T_{s,orig}}{T_{s,orig}}\right), \tag{64}$$

where n_{orig} represents the original samples obtained from the original signal. In this example, n_{orig} corresponds to the transmitted radar signal samples, and t_{new} represents the times corresponding the new signal. The output $x\left(t_{new}\right)$ contains the interpolated samples that can now be used to successfully recover the target locations [17] .

THIS PAGE INTENTIONALLY LEFT BLANK

V. RADAR SIGNALS

Military forces have relied on SAR systems to generate high-resolution imagery in all-weather conditions dating back to the 1950s [4]. A critical component in producing high quality imagery is the signal type transmitted by the SAR antenna [14]. As mentioned earlier, all radar systems use an electromagnetic signal reflected from a target to determine useful information about the target. There are several signal types a radar system can transmit, each having its advantages and disadvantages. In this section, we discuss the signal types used for SAR processing throughout this research.

A. PULSE COMPRESSION BASICS

The transmitted radar signal characteristics largely determine a radar's ability to produce high quality images. One of these characteristics is pulse duration. From Equation (8), it is seen that range resolution can be improved by using short pulses. However, there are limitations and system consequences when using short-pulse transmissions. For example, short pulses require a much higher peak power, which is undesirable for airborne radars. One way to reduce the peak power of the transmitted pulse is to increase the pulse duration; however, doing so results in decreased resolution. One way to attain good range resolution while not degrading the energy output is by using pulse compression techniques [13].

Pulse compression is a signal-processing technique that allows for obtaining the transmitted power of a long pulse while at the same time maintaining the range resolution of a short pulse transmission.

Pulse compression works by frequency modulating a long pulse, spreading its characteristics to that of a short pulse within its envelope [6]. The most common signal type used by SAR systems is the pulsed linear frequency modulated (LFM) waveform [6]. LFM waveforms are also referred to as chirp signals. The main advantage of using LFM signals for SAR processing is that they allow for using pulse compression techniques [6].

The analytic representation of a single LFM signal of duration T_p is defined as

$$p(t) = a(t)\exp(j2\pi f_0 t + j\pi\alpha t^2) \tag{65}$$

where f_0 is the radar carrier frequency, t is the time variable, α is the rate at which the instantaneous frequency increases or decreases as a function of time and $a(t)$ is the window function defined as

$$a(t) = \begin{cases} 1, & 0 \le t \le T_p, \\ 0, & \text{otherwise.} \end{cases} \tag{66}$$

The instantaneous frequency of $p(t)$ varies with time *t* and is given as

$$f(t) = 2\pi f_0 + 2\pi\alpha t\,. \tag{67}$$

The LFM signal bandwidth is $B = \alpha T_p$; therefore, the range resolution equation given in (11) becomes

$$\Delta R \approx \frac{c}{c}\frac{1}{\alpha T_p}. \tag{68}$$

A pulsed LFM time-domain signal representation example is illustrated in Figure 22, where it can be seen that there is an increase in frequency linearly in time.

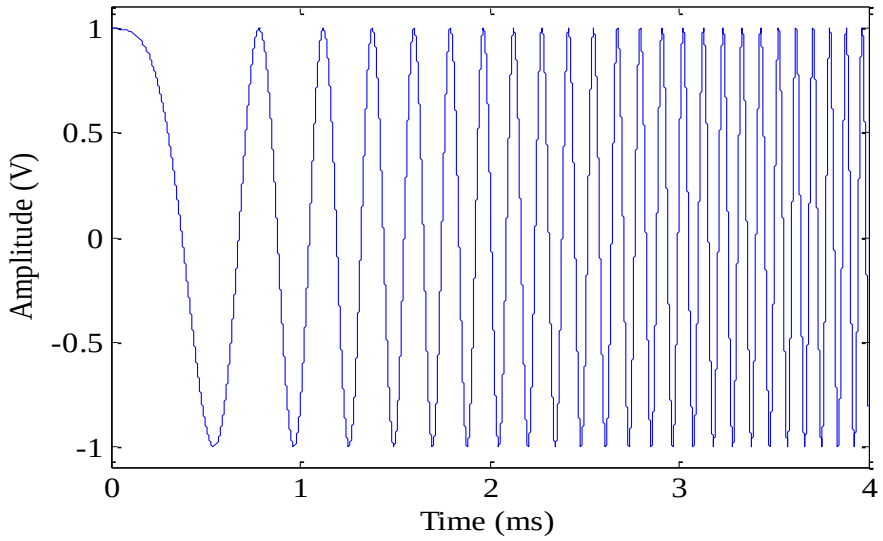

Figure 22. Linear frequency modulated signal with $T_p = 4$ ms, $\alpha = 3\times10^9$ Hz/s.

The SAR transmits many of these LFM signals to illuminate the target [2].

B. OFDM BASICS

An OFDM signal is comprised of several orthogonal subcarriers that are transmitted over a single transmission path. Each subcarrier carries a small portion of the entire signal. The OFDM signal properties make it a potential option for use as a SAR transmitted waveform. Particularly, the signal bandwidth, duration, energy, and individual subcarrier modulation can be varied to enhance the resulting SAR imagery [7].

1. Modulation Scheme

The purpose of this section is to discuss the chosen subcarrier modulation scheme used to generate an OFDM signal. In communications, the signal information is conveyed by bits. Each modulation scheme (i.e., binary phase-shift keying (BPSK), quadrature phase-shift keying (QPSK), or quadrature amplitude modulation (QAM)) contains a certain number of bits per symbol. The collection of bits within a particular scheme makes up a symbol. The OFDM signals generated for this work use the BPSK and QPSK modulation schemes on each subcarrier.

a. Binary Phase-Shift Keying

BPSK is a modulation technique that uses two phases, separated by 180 degrees, to represent two binary digits; a binary 0 or a binary 1. A BPSK symbol of bit duration T can be identified as

$$s(t)=\begin{cases} A\cos(2\pi f_c t) \\ A\cos(2\pi f_c t+\pi) \end{cases}=\begin{cases} A\cos(2\pi f_c t) & \text{for symbol 1} \\ -A\cos(2\pi f_c t) & \text{for symbol 0,} \end{cases} \tag{69}$$

where A is a constant and f_c is the carrier frequency and $0 \le t \le T$ [18].

b. Quadrature Phase-Shift Keying

QPSK is a modulation technique that uses four phases, separated by 90 degrees to represent two bits. A QPSK symbol with bit duration T can be identified as

$$s(t)=\begin{cases} A\cos\left(2\pi f_c t+\dfrac{\pi}{4}\right) & \text{for symbol 11} \\ A\cos\left(2\pi f_c t+\dfrac{3\pi}{4}\right) & \text{for symbol 01} \\ A\cos\left(2\pi f_c t-\dfrac{3\pi}{4}\right) & \text{for symbol 00} \\ A\cos\left(2\pi f_c t-\dfrac{\pi}{4}\right) & \text{for symbol 10,} \end{cases} \tag{70}$$

where $0 \le t \le 2T$ [18].

2. OFDM Transmitted Radar Signal

The first step in simulating an OFDM signal is generating a random set of bits. The randomized bits are then mapped into one of the above modulation schemes. The modulated symbols are then distributed over a chosen number of subcarriers. Finally, by taking the modulated data IFFT, we simulate a single OFDM symbol. The OFDM signal is, therefore, the sum of subcarriers with one of the modulation schemes applied. A simplified example of OFDM signal implementation is shown in Figure 23.

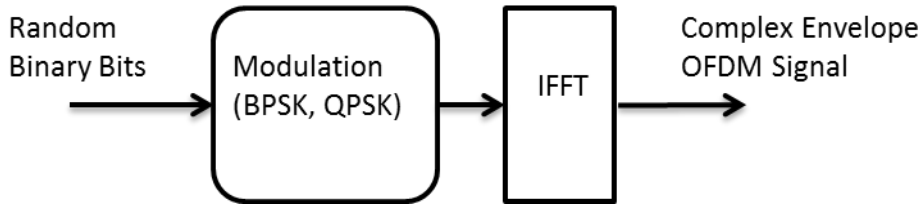

Figure 23. OFDM waveform generation.

The complex envelope representation of a single OFDM transmitted symbol $p(t)$ of bandwidth B and pulse duration T_p is represented as

$$p(t) = a(t)\sum_{k=0}^{N-1} s(k)\exp(j2\pi k\Delta f t) \tag{71}$$

where

$$a(t) = \begin{cases} 1, & 0 \le t \le T_p, \\ 0, & \text{elsewhere,} \end{cases} \tag{72}$$

N represents the total number of subcarriers, $s(k) = [s_0, s_1, ..., s_{N-1}]$ are the modulation symbols and $\Delta f = 1/T_p$ is the spacing between adjacent subcarriers. Although the subcarriers overlap, they are orthogonal and do not interfere with each other.

If we sample the OFDM signal $p(t)$ at sampling interval $T_s = T_p/N$, we obtain the discrete-time OFDM signal, which is

$$p(n) = p(t = nT_s) = \sum_{k=0}^{N-1} s(k)\exp(j2\pi k\Delta f n T_s), \tag{73}$$

where $n \in [0,1,..., N-1]$ is the discrete sequence corresponding to the sampled values.

The OFDM signal spectrum is obtained by performing the DFT via

$$P(f) = T_s\sum_{k=0}^{N-1} p(n)\exp(-j2\pi kn/N), \tag{74}$$

where the condition

$$f = \frac{k}{NT_s} \tag{75}$$

must be satisfied to yield the IFT relation. Therefore $P(f)$ becomes

$$P\left(\frac{k}{NT_s}\right) = T_s \sum_{k=0}^{N=1} p(n) \exp(-j2\pi kn / N). \tag{76}$$

The bandwidth of the signal is related to the total number of subcarriers *N* and spacing between subcarriers Δf and is expressed as

$$B = N\Delta f\ . \tag{77}$$

where $\Delta f = 1/NT_s$. Therefore,

$$B = N\frac{1}{NT_s} = \frac{1}{T_s}\ . \tag{78}$$

The symbol duration T_p of a single OFDM symbol is expressed as

$$T_p = NT_s\ . \tag{79}$$

As a result, increasing the number of subcarriers while keeping T_s constant directly increases the OFDM signal duration but keeps the bandwidth constant.

A time-domain OFDM signal example is shown in Figure 24. The signal is generated using the WiMAX standard, where $N = 128$, and $T_p = 6.4\ \mu s$ and $B = 20\,\text{MHz}$ [7].

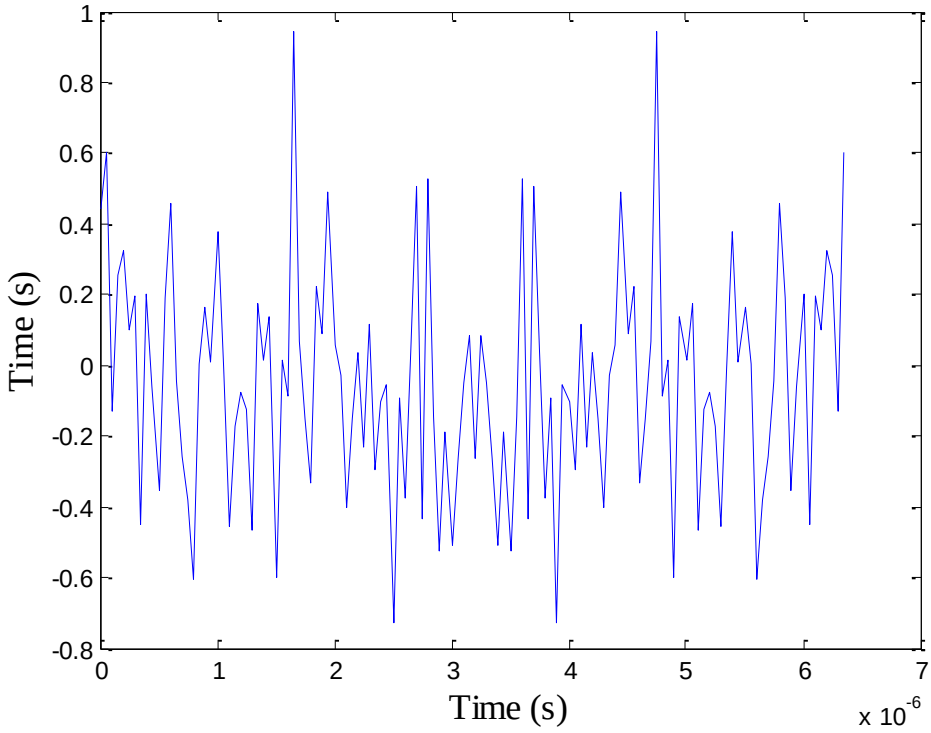

Figure 24. OFDM Signal modulated using BPSK scheme where $T_p = 6.4\ \mu s$, $N = 128$ and $B = 20\,\text{MHz}$.

THIS PAGE INTENTIONALLY LEFT BLANK

VI. SIMULATION IMPLEMENTATION AND RESULTS

In this section, we provide a detailed explanation of the SAR simulation algorithm for the range and two-dimensional SAR image cases. Following each explanation are the simulation results obtained for the range imaging case and two-dimensional case, respectively. All simulations were conducted in MATLAB, and the code was derived from the initial code outlined in [14]. The simulation software is in the Appendix.

A. ONE-DIMENSIONAL RANGE RECONSTRUCTION

1. Range MATLAB Implementation

The goal of the one-dimensional range reconstruction algorithm is to transmit a radar signal and accurately recover the target function or point target location.

The MATLAB code is broken down into sections, where each section performs a portion of the overall reconstruction algorithm. The flow chart shown in Figure 25 demonstrates how each of the codes is interconnected and how the reconstruction process takes place in MATLAB.

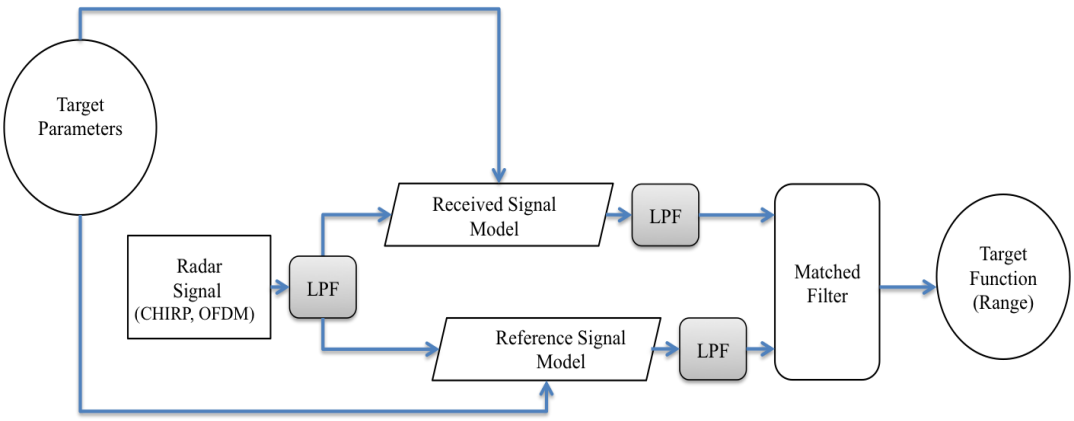

Figure 25. Range imaging simulation flow chart.

We begin by defining the target scene parameters, which for the one-dimensional range case consist of a set of points located within the one-dimensional target scene detailed in Figure 6. The user can define the target point quantity and range location in

the target scene. Placing point targets closer together allows for testing on which modulation scheme provides more accurate target resolution.

The target parameters and the desired radar signals are the inputs into the received echoed signal model and the reference signal model. As seen in the flowchart, we apply a low-pass interpolation filter model to the transmitted radar signal and the outputs from the echoed signal and reference signal models. Discussion on the purpose of this filtering operation is in Section IV.D.2.

The two resampled signals are the inputs into the matched filter function. The matched filter function's purpose is to recover each target's location. The matched filter output shows a peak from the energy received for each target location; therefore, the recovered target function $f(x)$ is formed via

$$x_i = \frac{ct_i}{2}$$

where x_i is the range to point target i and t_i is the matched filter output peak value.

2. Range-Imaging Simulation Results

The range-imaging simulation results are presented to show the ability to accurately reconstruct the range target function using each radar signal. A series of simulations are conducted where the radar signal parameters are varied to determine the effect on the SAR range profile and which parameters are more important for range reconstruction. A table containing the selected transmitted radar signal parameters is provided before showing each simulation result set. Also included in each table are the original transmitted sampling intervals that satisfy the Nyquist sampling theorem in Equation (55) and the interpolated sampling interval discussed Section IV.D.2. The interpolated sampling interval value is lower than the transmitted sampling interval, and, therefore, provides an increased number of samples. The interpolated sampling interval is the same for all range-imaging simulations. We also include the signal energy corresponding to the transmitted radar signal. Similarly, the interpolated signal energy corresponding to the interpolated sample interval is included in each table. The exact

signal energy does not vary with the sampling interval; however, the approximate signal energies, which are calculated using the sample values, do vary slightly.

We first present the simulation results for the LFM transmitted signal followed by the BPSK-OFDM and QPSK-OFDM signals results, respectively.

a. Linear Frequency Modulated Signal

The LFM transmitted signal simulation results are presented in this section.

A total of five point targets were used in the simulation. Targets one, two and three are spaced one kilometer apart, and targets four and five are spaced 125 meters apart. The two closely spaced targets allow for testing the transmitted signal's ability to differentiate or resolve the targets. All targets are located within the one-dimensional target scene (i.e., $x_i \in [5.5 \text{ km}, 10.5 \text{ km}]$). The target scene parameters used for both the LFM and OFDM signals are shown in Table 1.

Table 1. Range imaging target scene parameters.

Parameter	**Value**
Target Center, X_c	8000 m
Half Size of Target Area, X_0	2500 m
Target Scene Interval, $[X_c - X_0, X_c + X_0]$	[5500 m , 10500 m]
Target 1 Range and Reflectivity, x_1, σ_1	8000 m, 0.1
Target 2 Range and Reflectivity, x_2, σ_2	7000 m, 0.3
Target 3 Range and Reflectivity, x_3, σ_3	9000 m, 0.5
Target 4 Range and Reflectivity, x_4, σ_4	10125 m, 0.7
Target 5 Range and Reflectivity, x_5, σ_5	10250 m, 1.0

As described in Section V.A, the LFM signal bandwidth is determined by its chirp rate α and signal duration T_p. To increase the signal's bandwidth, we either increase α or T_p.

For range imaging simulation one, we held the duration of the pulse constant at $T_p = 0.1\mu s$ while increasing α. The resulting bandwidth, along with the sampling time T_s, carrier frequency f_c and transmitted signal energy E are recorded in Table 2.

Table 2. LFM signal parameters for range simulation one.

Parameter	**Values**			
Pulse Duration, $T_p(\mu s)$	1	1	1	1
Carrier Frequency, $f_c\ (\mathrm{GHz})$	0.1	0.1	0.1	0.1
Signal Bandwidth, $B\ (\mathrm{MHz})$	10	20	50	70
Transmitted Signal Energy, $E\ (\mu J)$	1.01	1.01	1.01	1.01
Nyquist Sampling Interval, $T_s\ (\mu s)$	0.001	0.001	0.001	0.001
Chirp Rate, $\alpha\ (Hz/s)$	1×10^{13}	2×10^{13}	5×10^{13}	7×10^{13}
Interpolated Sampling Interval, $T_s\ (\mu s)$	0.01	0.01	0.01	0.01
Interpolated Signal Energy, $E\ (\mu J)$	1	1	1	1

The range profile corresponding to the transmitted signal generated with $\alpha = 1\times10^{13}$ Hz/s, resulted in a 10 MHz total bandwidth and a corresponding 15 meter range resolution as per Equation (11). All five targets are recovered; however, the returns from targets four and five overlap but remain differentiable. The wide main lobes of each target return or point spread function signify poor range resolution.

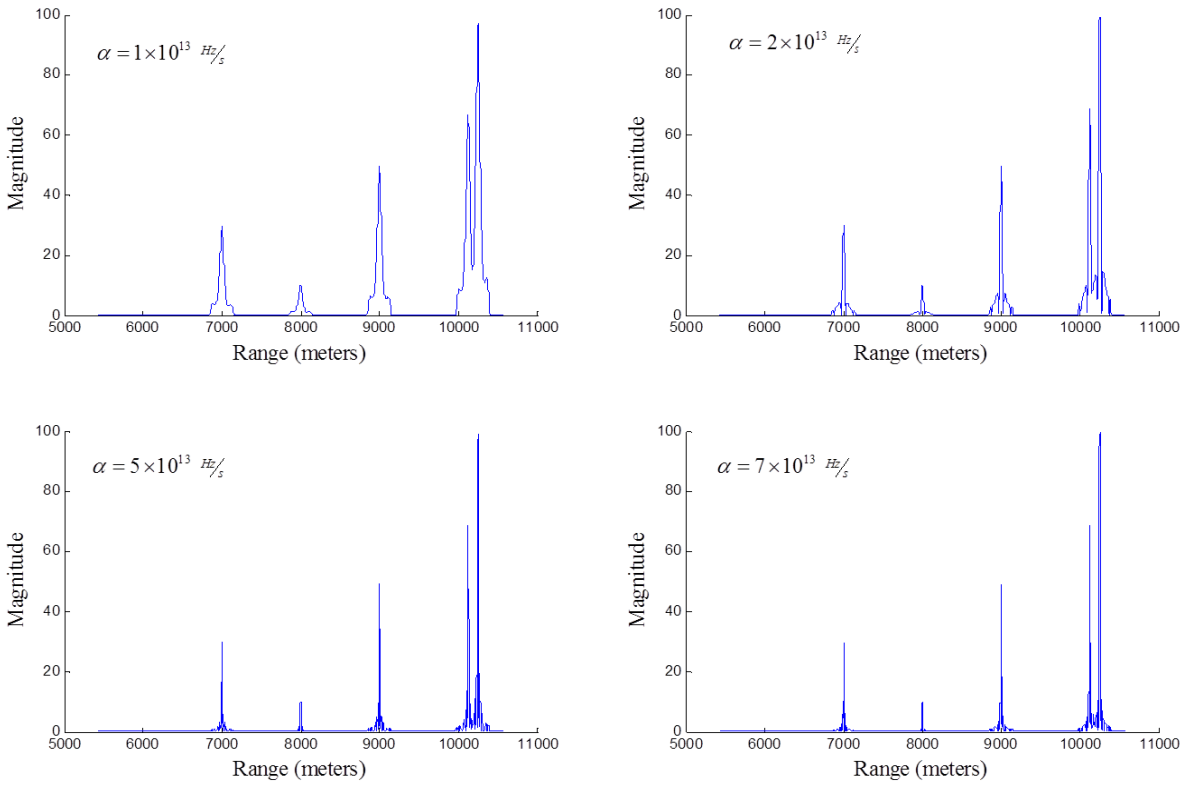

Figure 26. LFM reconstructed range target function at chirp rate, $\alpha = 1\times10^{13}$ Hz/s, 2×10^{13} Hz/s, 5×10^{13} Hz/s, 10×10^{13} Hz/s.

The range reconstruction results when the transmitted LFM signal is generated with parameters in Table 2 are illustrated in Figure 26. We can see that the point spread function improved with the increasing chirp rate for the range profiles corresponding to the signals generated with $\alpha = 2\times10^{13}$ Hz/s, 5×10^{13} Hz/s, and 10×10^{13} Hz/s, which resulted in an increased bandwidth of 20, 50 and 70 MHz, respectfully. This is an expected result because increasing α directly increases signal bandwidth.

The parameters duration, energy, carrier frequency and sample interval were all held constant; therefore, an important observation is that increasing the LFM signal chirp rate directly increased signal bandwidth, which improved the range resolution.

The second simulation was conducted to observe how LFM signal duration affects range resolution. Since LFM signal bandwidth depends on the signal duration and chirp rate, increasing duration while keeping chirp rate constant directly increases

bandwidth. For this simulation, the chirp rate was held constant at $\alpha = 5\times10^{13}$ Hz/s while varying T_p. The value of T_p was chosen so that the total signal bandwidth matched the previous simulation value. The signal energy is normalized for this simulation and matches the values from simulation one. All other signal parameters remained the same. The parameters are shown in Table 3.

Table 3. LFM signal parameters for range simulation two.

Parameter	**Values**			
Pulse Duration, T_p (μs)	0.2	0.4	1.0	1.4
Carrier Frequency, f_c (GHz)	0.1	0.1	0.1	0.1
Signal Bandwidth, B (MHz)	10	20	50	70
Transmitted Signal Energy, E (μJ)	1.01	1.01	1.01	1.01
Nyquist Sampling Interval, T_s (μs)	0.001	0.001	0.001	0.001
Chirp Rate, α (Hz/s)	5×10^{13}	5×10^{13}	5×10^{13}	5×10^{13}
Interpolated Sampling Interval, T_s (μs)	0.01	0.01	0.01	0.01
Interpolated Signal Energy, E (μJ)	0.9981	0.9979	0.9981	0.9985

The range reconstruction results when the transmitted LFM signal is generated with parameters in Table 3 are illustrated in Figure 27. All five targets are resolved at the selected pulse duration. The important observation from this simulation is that the improvement in range resolution is due to the increase in $T_{p,}$ which directly increased the transmitted signal bandwidth.

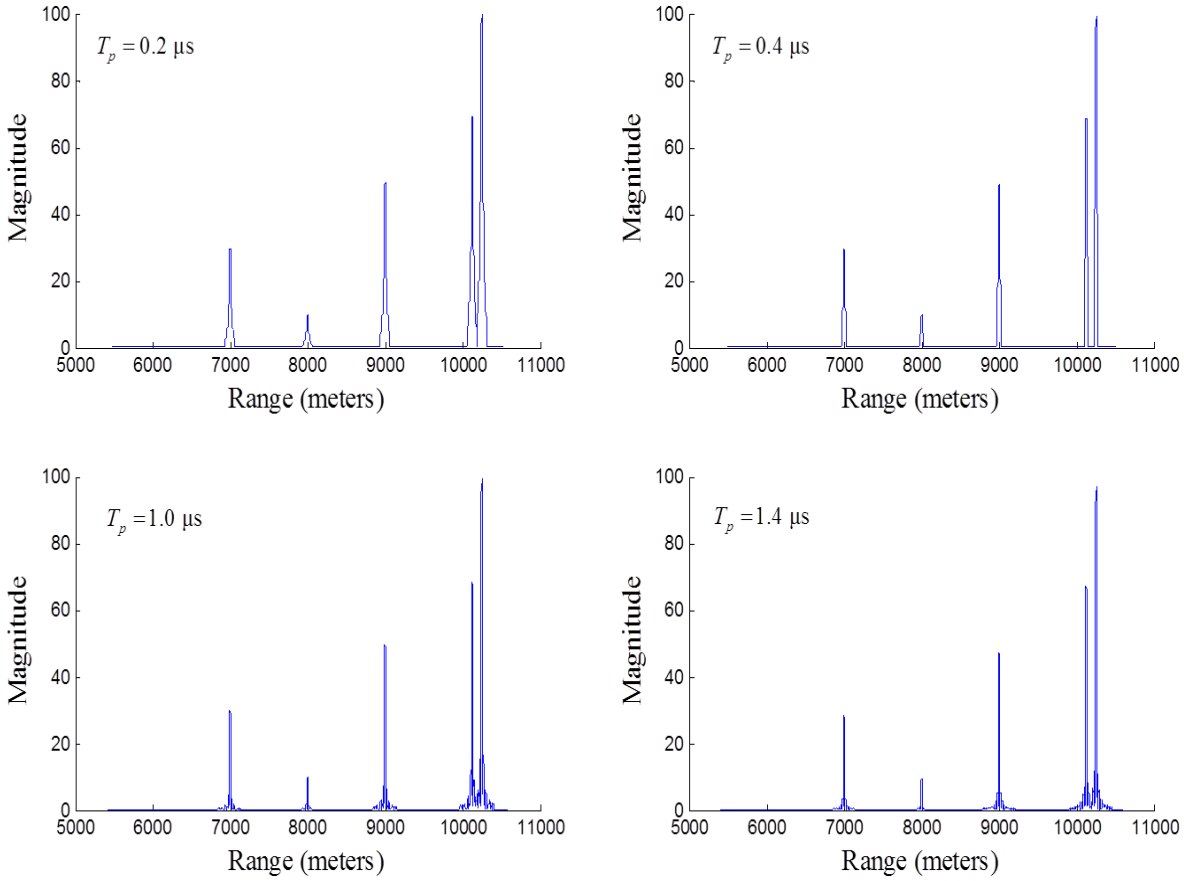

Figure 27. LFM reconstructed range target function at pulse duration, $T_p = 0.2\,\mu s,\ 0.4\,\mu s,\ 1.0\,\mu s,$ and $1.4\,\mu s$.

From the results in simulations one and two, we conclude that range resolution improves as either chirp rate or pulse duration increases. This makes intuitive sense since both parameters have a linear relationship with bandwidth as per Equation (68).

b. Orthogonal Frequency Division Multiplexing

Next, we present the results obtained from transmitting the BPSK-OFDM and the QPSK-OFDM radar signals. The OFDM signals were implemented according to the method explained in V.B.2.

Signal bandwidth is the first BPSK-OFDM signal parameter examined. As discussed in Section V.B.2, the OFDM signal bandwidth is determined by the sampling time T_s used to generate the waveform. We keep the number of subcarriers constant at

$N = 64$ while changing T_s to control the signal bandwidth. Sampling interval T_s is chosen so that the OFDM signal bandwidth matches the LFM signal's bandwidth in the previous simulations. The number of OFDM symbols is changed for each signal so that the pulse duration remains constant. The signal parameters are shown in Table 4.

Table 4. BPSK-OFDM signal parameters for range simulation three.

Parameter	**Values**			
Total OFDM Symbols	1	2	5	7
Total Subcarriers, N	64	64	64	64
Pulse Duration, T_p (μs)	6.4	6.4	6.4	6.4
Carrier Frequency, f_c (GHz)	0.1	0.1	0.1	0.1
Transmitted Signal Energy, E (μJ)	0.8	0.8	0.8	0.8
Nyquist Sampling Interval, T_s (μs)	0.1	0.05	0.02	0.01429
Signal Bandwidth, B (MHz)	10	20	50	70
Interpolated Sampling Interval, T_s (μs)	0.01	0.01	0.01	0.01
Interpolated Signal Energy, E (μJ)	0.7933	0.7860	0.7989	0.7991

The range reconstruction results for the BPSK-OFDM transmitted signal generated with 64 subcarriers are shown in Figure 28.

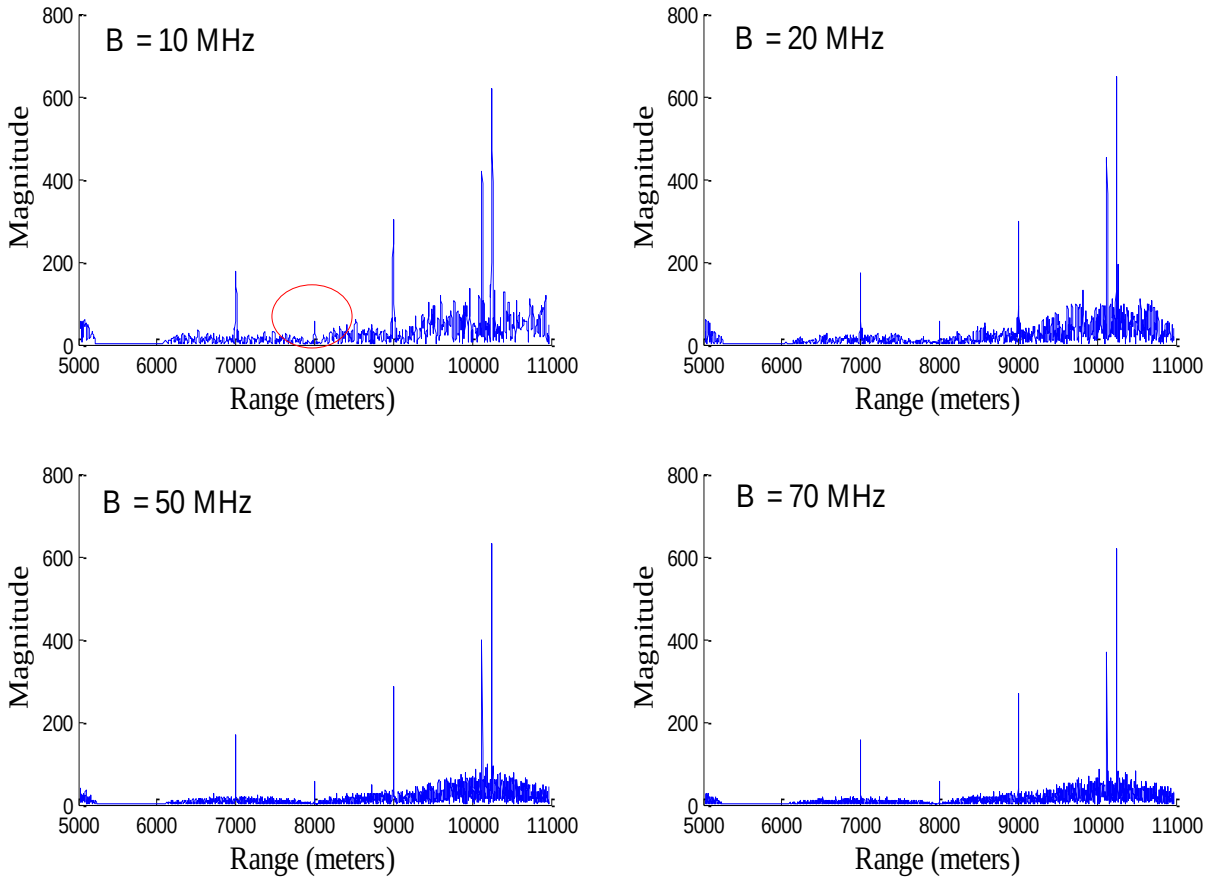

Figure 28. BPSK-OFDM reconstructed range target function with $N = 64$, $B = 10$ MHz, 20 MHz, 50 MHz, and 70 MHz.

By observing the range profile for the signal generated with $B = 10$ MHz, we see that target two, circled in red, is masked by the high side lobes from the other signal returns. The effect of side lobe leakage decreased for signals generated with wider bandwidth, as seen in the range profiles generated with 20, 50 and 70 MHz. The range resolution improvement for these profiles, however, is minor.

In simulation four, the number of subcarriers used to generate the BPSK-OFDM signals were decreased to $N = 8$, which directly decreased each signal's duration. The signals were generated with the same bandwidth as in the previous simulation where $N = 64$ subcarriers were used. All other transmitted signal parameters remained the same. The transmitted signal energy values for each signal in simulation four decreased

due to the decreased pulse duration and contain $1/8$ the transmitted signal energy of simulation three. The signal parameters for simulation four are shown in Table 5.

Table 5. BPSK-OFDM signal parameters for range simulation four.

Parameter	**Values**			
Total OFDM Symbols	1	2	5	7
Total Subcarriers, N	8	8	8	8
Pulse Duration, T_p (μs)	0.8	0.8	0.8	0.8
Carrier Frequency, f_c (GHz)	0.1	0.1	0.1	0.1
Signal Energy, E (μJ)	0.2828	0.2828	0.2828	0.2828
Sampling Interval, T_s (μs)	0.1	0.05	0.02	0.01429
Signal Bandwidth, B (MHz)	10	20	50	70
Interpolated Sampling Interval, T_s (μs)	0.01	0.01	0.01	0.01
Interpolated Signal Energy, E (μJ)	0.2725	0.2733	0.27686	0.2818

The reconstruction results for the signals in Table 5 can be seen in Figure 29.

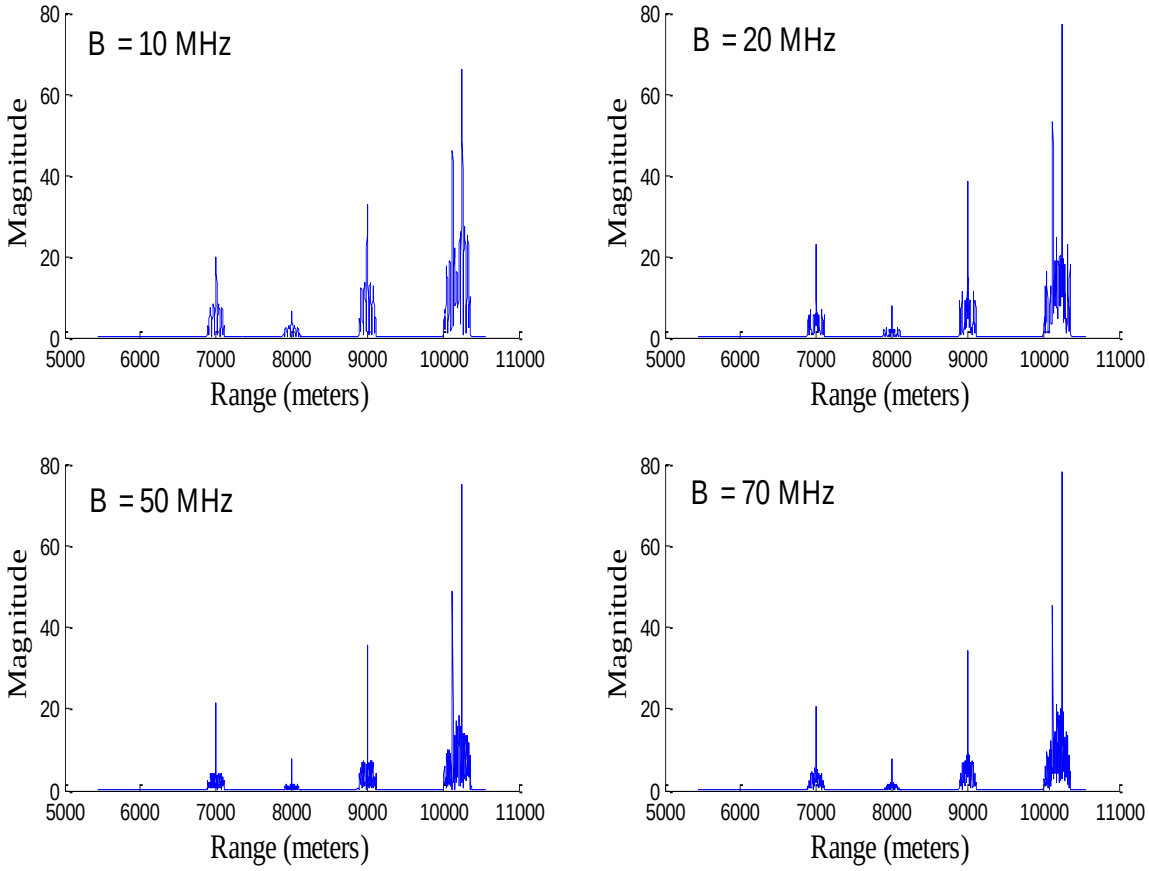

Figure 29. BPSK-OFDM reconstructed range target function: $N = 8$, $B = 10\,\text{MHz}$, $20\,\text{MHz}$, $50\,\text{MHz}$, and $70\,\text{MHz}$.

The main observation for this simulation is the diminished effect of side lobe leakage when compared to the results in simulation three. This leakage reduction is due to the decreased number of subcarriers (and, thus, pulse duration) used to implement the signals. Specifically, decreasing the number of subcarriers from 64 to eight directly decreased each signal's duration by a factor of $1/8$. Furthermore, since the point spread function duration is double the signal pulse duration, the point spread function for each target return is $1/8$ the width of the point spread function in simulation three.

In simulation five, we keep the signal bandwidth constant at 20 MHz and generate each signal with four subcarriers. Each signal's duration is increased by increasing the number of OFDM symbols. Therefore, the focus of this simulation is determination of

how BPSK-OFDM signal duration affects range reconstruction. All other signal parameters were held constant. The signal parameters for simulation five are shown in Table 6.

Table 6. BPSK-OFDM signal parameters for range simulation five.

Parameter	**Values**			
Total OFDM Symbols	1	2	3	4
Total Subcarriers, N	4	4	4	4
Pulse Duration, T_p (μs)	0.2	0.4	0.6	0.8
Carrier Frequency, f_c (GHz)	0.1	0.1	0.1	0.1
Signal Energy, E (μJ)	0.1	0.1	0.1	0.1
Sampling Interval, T_s (μs)	0.05	0.05	0.05	0.05
Signal Bandwidth, B (MHz)	20	20	20	20
Interpolated Sampling Interval, T_s (μs)	0.01	0.01	0.01	0.01
Interpolated Signal Energy, E (μJ)	0.0958	0.0951	0.0935	0.0937

The plots in Figure 30 correspond to the range reconstruction results for the parameters shown in Table 6 where pulse duration is increased from 0.2 to 0.8 in increments of 0.2 μs.

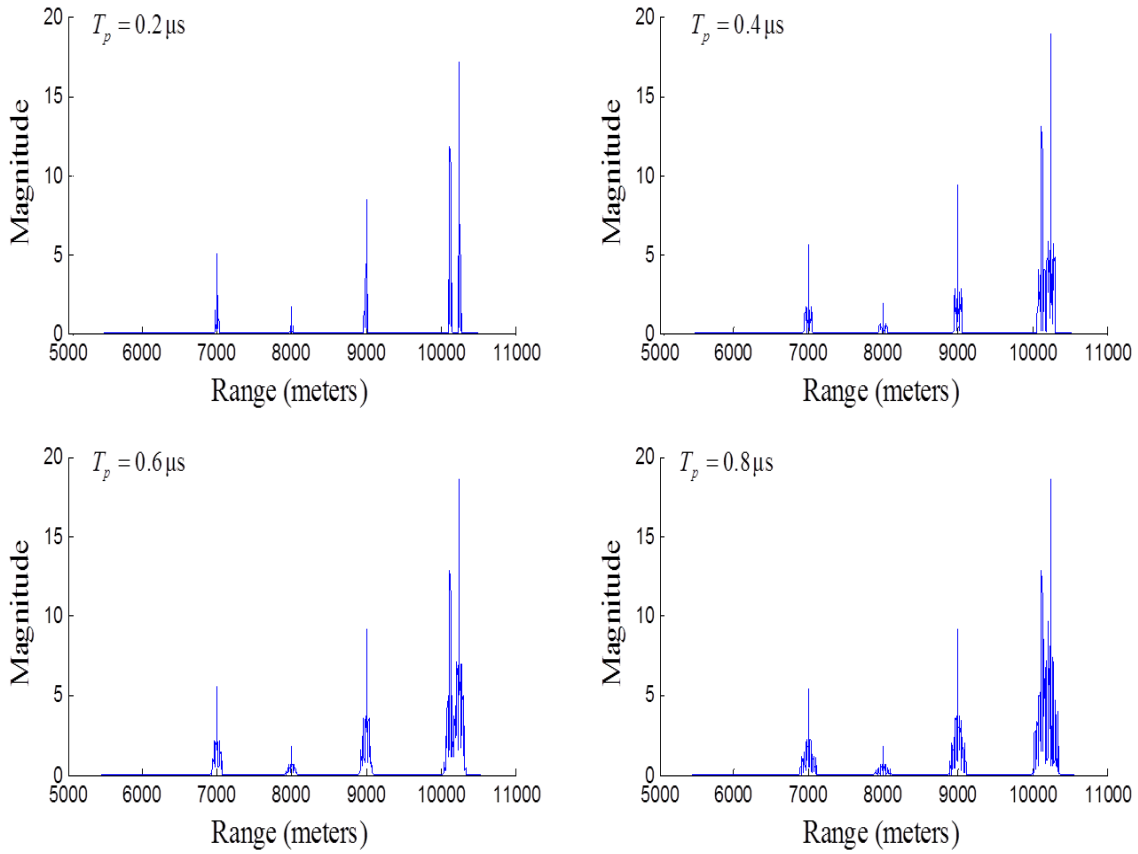

Figure 30. BPSK-OFDM reconstructed range target function with $T_p = 0.2$ μs, 0.4 μs, 0.6 μs, and 0.8 μs.

All five targets are recovered at the selected pulse duration. Range resolution appears constant for all four signals; however, increasing the each signal's duration resulted in an increased amount of side lobes in each range profile. For this simulation, implementing the BPSK-OFDM signal with only one OFDM symbol is sufficient in recovering each point target with fine range resolution.

The QPSK-OFDM signals were generated in the same manner as the OFDM-BPSK signal. Specifically, the sampling time T_s and number of subcarriers *N* assigned to the BPSK-OFDM were also used to produce the range reconstruction results for the QPSK-OFDM signals.

Simulation six was conducted to observe how increasing bandwidth affects range reconstruction while keeping the number of QPSK-OFDM signal subcarriers constant. The signal is implemented with the same number of subcarriers and pulse duration as simulation three. The transmitted signal energy values for this simulation were normalized so that the signals are transmitted with the same signal energy as in simulation three. The signal parameters are shown in Table 7.

Table 7. QPSK-OFDM signal parameters for range simulation six.

Parameter	**Values**			
Total OFDM Symbols	1	2	5	7
Total Subcarriers, N	64	64	64	64
Pulse Duration, T_p (μs)	6.4	6.4	6.4	6.4
Carrier Frequency, f_c (MHz)	0.1	0.1	0.1	0.1
Signal Energy, E (μJ)	0.8	0.8	0.8	0.8
Sampling Interval, T_s (μs)	0.1	0.05	0.02	0.01429
Signal Bandwidth, B (MHz)	10	20	50	70
Interpolated Sampling Interval, T_s (μs)	0.01	0.01	0.01	0.01
Interpolated Signal Energy, E (μJ)	0.7986	0.7951	0.7899	0.7973

The reconstruction results for simulation six can be seen in Figure 31.

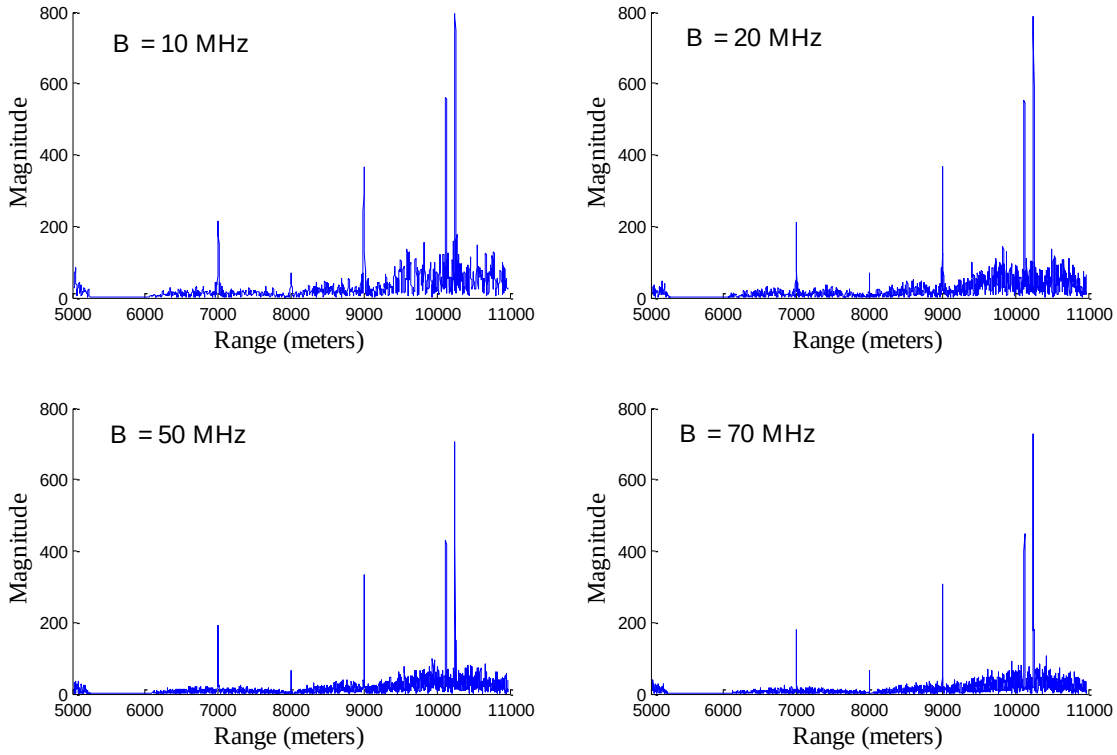

Figure 31. QPSK-OFDM reconstructed range target function with $N = 64$, $B = 10$ MHz, 20 MHz, 50 MHz, and 70 MHz.

The results are very similar to the BPSK-OFDM range profile results. The five point targets are recovered for each transmitted signal. We compared reconstruction results in Figure 31 for simulation six with that in Figure 28 for simulation three, where the BPSK-OFDM signals were implemented in the same manner. The most noticeable difference for this comparison is that the targets return main lobes are narrower, and the side lobes are lower for the QPSK-OFDM range profile than for the BPSK-OFDM signals. The decreased side lobe floor in this simulation presents an advantage for the QPSK-OFDM signals. Specifically, smaller targets are more easily detected, which is observed in the range profile corresponding to the QPSK-OFDM signal generated with 10 MHz when compared to that of the BPSK-OFDM signal in simulation three.

For simulation seven, the QPSK-OFDM signals were implemeted with eight subcarriers instead of the 64 in simulation six. Similar to simulation six, we increased signal bandwidth to match that from simulations one through four. More importantly,

simulation seven was conducted to compare the results with the BPSK-OFDM results in simulation four, where the signals were generated with the same number of subcarriers. The signal parameters are shown in Table 8.

Table 8. QPSK-OFDM signal parameters for range simulation seven.

Parameter	**Values**			
Total OFDM Symbols	1	2	5	7
Total Subcarriers, N	8	8	8	8
Pulse Duration, T_p (μs)	0.8	0.8	0.8	0.8
Carrier Frequency, f_c (GHz)	0.1	0.1	0.1	0.1
Signal Energy, E (μJ)	0.2828	0.2828	0.2828	0.2828
Sampling Interval, T_s (μs)	0.1	0.05	0.02	0.01429
Signal Bandwidth, B (MHz)	10	20	50	70
Interpolated Sampling Interval, T_s (μs)	0.01	0.01	0.01	0.01
Interpolated Signal Energy, E (μJ)	0.2816	0.2798	0.2801	0.2796

The range reconstruction results that correspond to the QPSK-OFDM signals in Table 8 are shown in Figure 32.

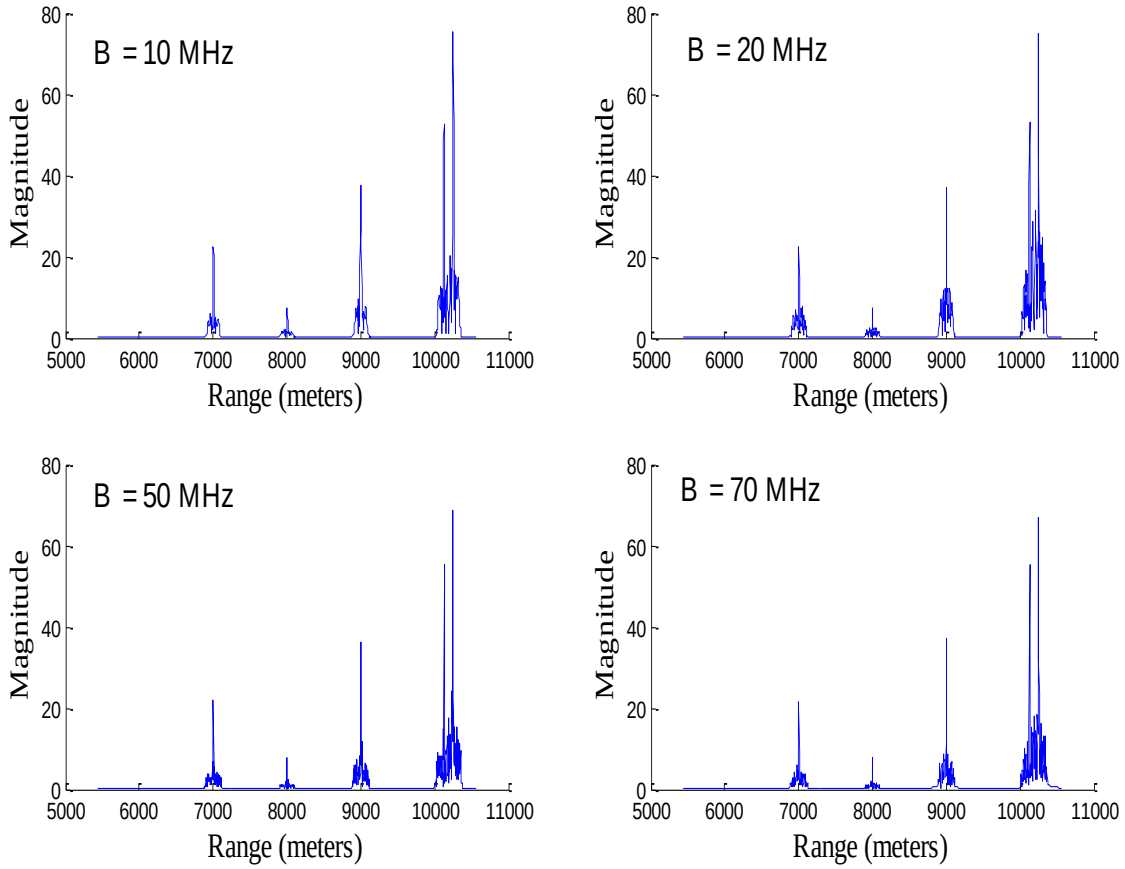

Figure 32. QPSK-OFDM reconstructed range target function with $N = 8$, $B = 10$ MHz, 20 MHz, 50 MHz, and 70 MHz.

The results are very similar to those corresponding to the BPSK-OFDM signals in simulation four. The main difference is that the side lobes for each target return are lower for QPSK-OFDM signals. Similar to the results from simultion four, the pulse spread function also narrowed by a factor of $1/8$ when compared to results from simulation six where the QPSK-OFDM signals were implemeted with 64 subcarriers.

The final simulation was conducted to observe how QPSK-OFDM signal pulse duration affects the SAR range profile. Similar to the BPSK-OFDM simulation, the signal bandwidth and the number of subcarriers were kept constant at $B = 20$ MHz and

$N = 4,$ respectively. We increased the total number of OFDM symbols for each signal, which directly increased signal duration. The signal parameters for simulation 8 are shown in Table 9.

Table 9. QPSK-OFDM signal parameters for simulation eight.

Parameter	**Values**			
Total OFDM Symbols	1	2	3	4
Total Subcarriers, N	4	4	4	4
Pulse Duration, T_p (μs)	0.1	0.2	0.3	0.4
Carrier Frequency, f_c (GHz)	0.1	0.1	0.1	0.1
Signal Energy, E (μJ)	0.1	0.1	0.1	0.1
Sampling Interval, T_s (μs)	0.05	0.05	0.05	0.05
Signal Bandwidth, B (MHz)	20	20	20	20
Interpolated Sampling Interval, T_s (μs)	0.01	0.01	0.01	0.01
Interpolated Signal Energy, E (μJ)	0.0984	0.988	0.0992	0.0979

The range profiles shown in Figure 33 correspond to the signal generated with $T_p = 0.2\ \mu s,\ 0.4\ \mu s,\ 0.6\ \mu s,$ and $0.8\ \mu s,$ respectively.

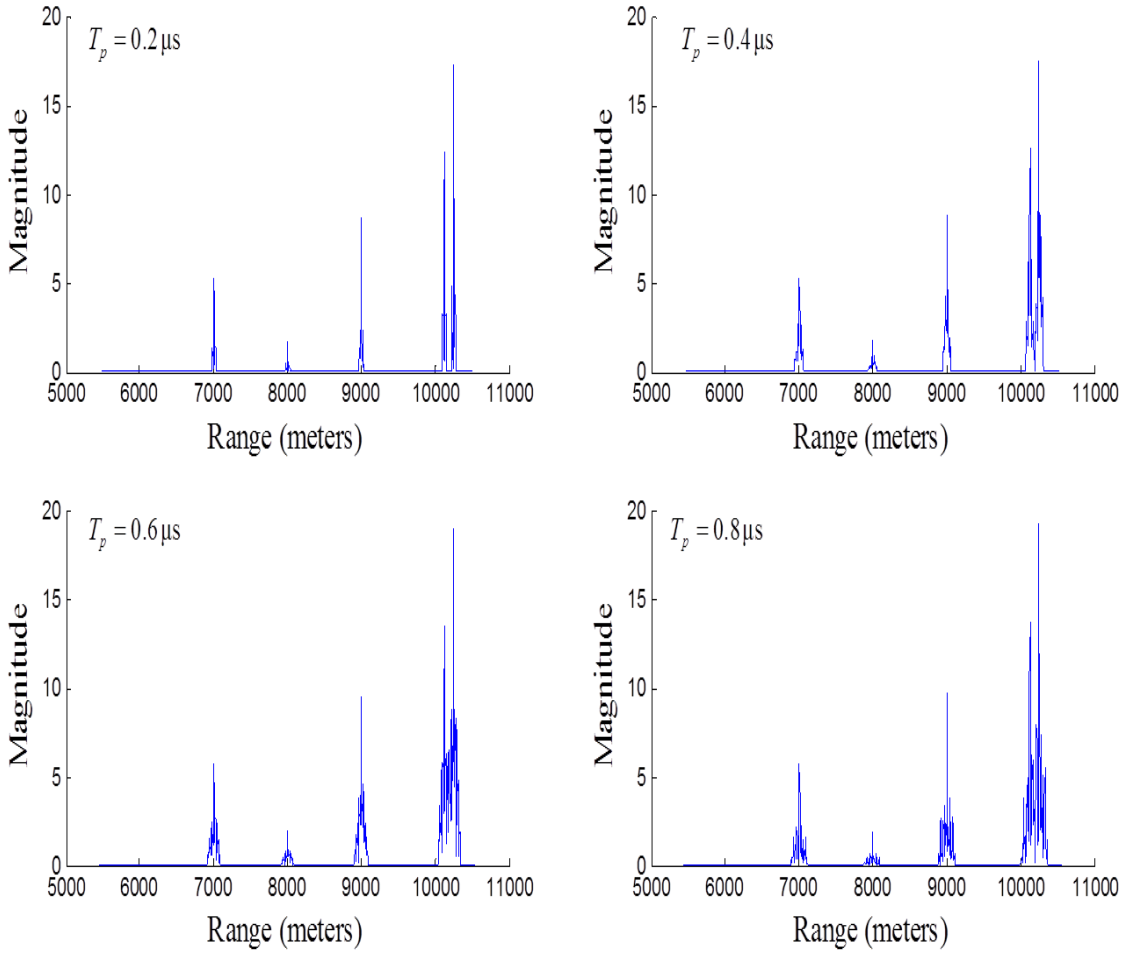

Figure 33. QPSK-OFDM reconstructed range target function with $T_p = 0.2$ μs, 0.4 μs, 0.6 μs, and 0.8 μs.

The results are comparable to the BPSK-OFDM reconstruction results obtained in simulation five. Range resolution remained relatively constant with the increase in pulse duration. Furthermore, increasing pulse duration resulted in higher side lobes around each target return.

B. TWO-DIMENSIONAL IMAGE RECONSTRUCTION

1. Two-dimensional SAR with MATLAB Implementation

The simulation algorithm for the two-dimensional SAR case is more complex than the range case. However, like the range-reconstruction algorithm, each operation discussed in Section IV.C.1 is broken into functions allowing for a more user-friendly and understandable program.

The two-dimensional image reconstruction algorithm requires generated samples from the transmitted radar signal, radar position and the planar array antenna pattern. We first define and derive the fast-time, slow-time, wavelength and wavenumber parameters shown in Figure 34.

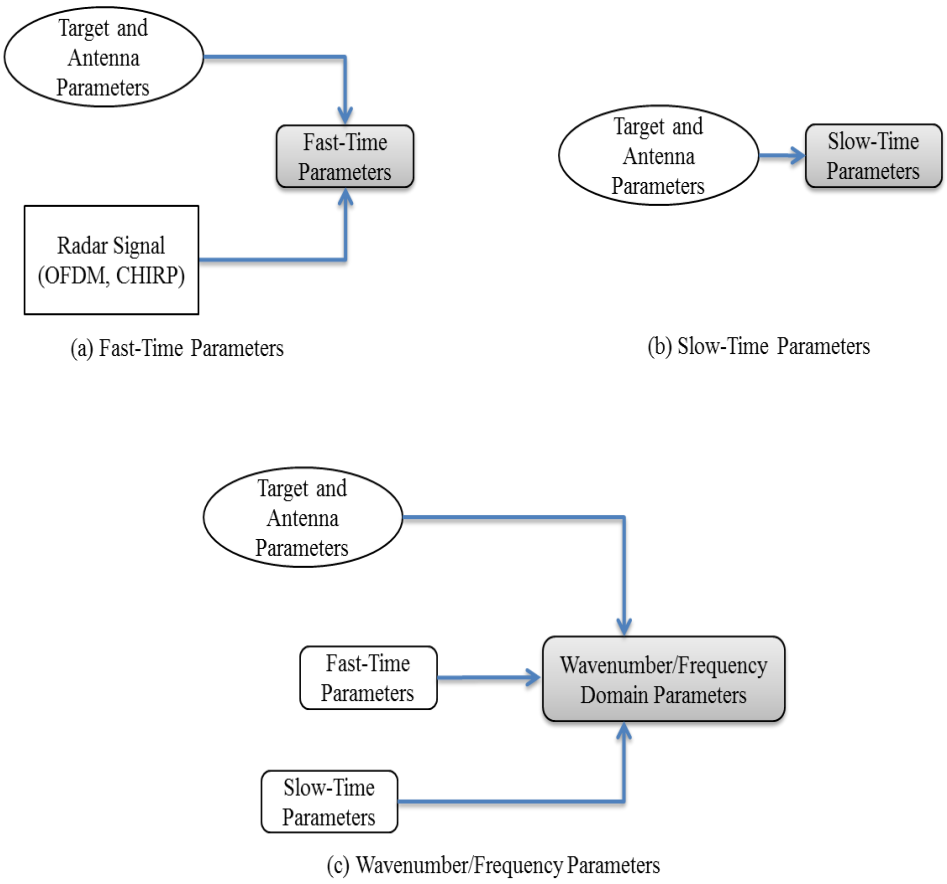

Figure 34. Two-dimensional initial parameters flow charts.

As seen in Figure 34, the target location information from the target and antenna parameters as well as the reconstructed transmitted radar signal comprise the two inputs into the fast-time parameter model. These two inputs are required to derive the fast-time sampling measurements, specifically the sampling start time T_s, stop time T_f and the fast-time interval $t \in \left[T_s, T_f \right]$ discussed in Section IV.D.1.a. The fast-time vector is size $N \times 1$ where N is the total number of fast-time samples. The fast-time parameters are used to generate the received echo signal, reference signal and fast-time matched filtered signal.

Next, we assign the slow-time parameters derived from the antenna parameters. Specifically, the parameters are derived from the synthetic aperture length, which is a function of the antenna size and type as discussed in Section III.D.3.a. The slow-time vector is size $1 \times M$, where M is the total number of slow-time samples. The slow-time parameters are also used to generate the received echo, reference and matched filtered signal.

The next set of parameters are derived in the wavenumber or frequency parameter model with inputs from the both the fast-time and slow-time parameter models as well as the target and antenna information from target and antenna parameter model. The k_u, k_x and k_y arrays are the main outputs from the wavelength/frequency parameters model. The criterion for each of these arrays is discussed in Section IV.B.2.

The next step in the MATLAB reconstruction implementation is based on the SFIA algorithm introduced in Section IV.C.1. We present a simple flow chart in Figure 35 to illustrate how each section is interconnected and depends on the parameters discussed above.

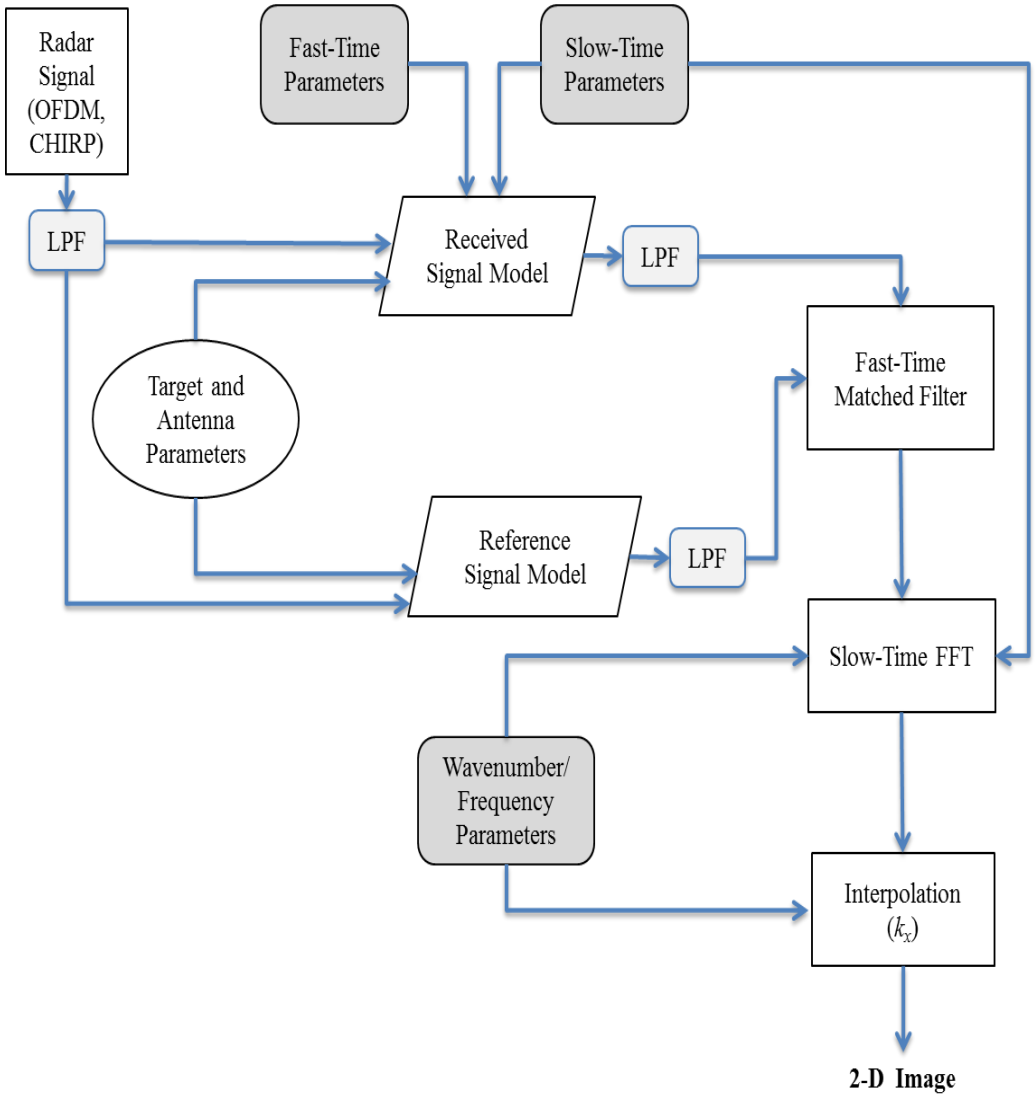

Figure 35. Two-dimensional image reconstruction flow chart.

We begin by generating the received signal model whose inputs are obtained from the three models explained above. The other inputs to the received signal model include the reconstructed transmitted radar signal and the target scene information from target and antenna parameters. The received signal model takes into account the physical characteristics of the planar array antenna radiation pattern discussed in Section III.D.3.a. In this model, we first generate the received signal discussed in Section III.D.3.b, which is an $N \times M$ matrix. We then incorporate the planar array antenna divergence angle to derive its radiation pattern. A Hanning window is applied to the radiation pattern to

reduce the side lobes [14]. Finally, we multiply the ideal received echo signal by the radiation pattern, which results in a received echo signal dictated by the planar array antenna pattern.

The next step in the MATLAB algorithm is to generate the reference signal model. The inputs to this model are the reconstructed transmitted radar signal, the fast-time vector and the target scene information. The target scene center is used as the reference position for the reference signal. The reference signal is comprised of returns from the reference position at times specified in the fast-time vector; therefore, the reference signal size is also $N \times 1$.

The output from both the received signal and reference signal models are the input into the fast-time matched filtering model. As mentioned in Section IV.C.1.a, the matched filtering operation is carried out in the frequency-domain; therefore, we perform the FFT with respect to fast-time on both the $N \times M$ received signal matrix and $N \times 1$ reference signal vector. We then perform the IFFT operation on the product of the two signals. This model's output is the fast-time matched filtered stripmap SAR signal, which is an $N \times M$ sized matrix.

The fast-time matched filtered stripmap SAR signal is the input into the slow-time FFT model. To perform the FFT with respect to slow-time, we first transpose the fast-time filtered $N \times M$ sized signal so that it becomes an $M \times N$ matrix. Next, we perform the FFT operation and then transpose the matrix back to its original dimensional construct. The slow-time FFT model output is an $N \times M$ sized matrix that corresponds to the signal in Equation (42).

The next algorithm step occurs in the two-dimensional matched filtering model. The inputs into this model include the stripmap SAR data in the frequency-domain, the k_x and k_y arrays and the target information. Performing the two-dimensional matched filtering operation involves multiplying the $N \times M$ sized SAR data matrix obtained in the previous step by the reference signal complex conjugate. The reference signal conjugate is derived in terms of wavenumbers k_x and k_y; therefore, the output of the two-

dimensional matched filtering model is a matrix of the same size as $N \times M$. The data is now mapped to wavenumber or spatial frequency-domain.

The next step in the algorithm is to perform an interpolation of the k_x data as discussed in Section IV.C.1.d. The k_x array derived in the wavelength or frequency parameters model is the input into this interpolation model.

The final step in the MATLAB algorithm is the two-dimensional IFFT. The input into this IFFT is the interpolated k_x samples from the interpolation model and the $N \times M$ spatial frequency-domain data from the two-dimensional matched filtering model. The two dimensional IFFT is accomplished by taking the IFFT with respect to the dimension that corresponds to k_x, followed by transposing the matrix, then taking the IFFT with respect to the k_y dimension. The output of the two-dimensional IFFT model displays the reconstructed two-dimensional SAR image.

2. Two-Dimensional Results

The simulation results for the two-dimensional stripmap SAR are presented in this section. Similar to the range-imaging simulation, we provide a table that contains the selected radar signal parameters shown before each simulation's results. We also include the Nyquist and interpolated sampling intervals. Similar to the range imaging reconstruction, the interpolated sampling interval is the same for all two-dimensional SAR simulations.

The target scene parameters are chosen by the user and remain the same throughout the analysis. The distance to each target and the target scene dimensions directly impact the speed of each simulation. Since the focus of this thesis is radar signal parameters and not target scene parameters, we choose a shorter distance for the two-dimensional SAR reconstruction. The target scene parameters used for the stripmap SAR are shown in Table 10.

Table 10. Stripmap SAR target scene parameters.

Parameter	Description	Value(s)
$2X_0$	Target Scene Range Width	200 m
$2Y_0$	Target Scene Cross-range Length	300 m
X_c	Target Range Center	250 m
$[X_c - X_0 : X_c + X_0]$	Target Scene (Range)	[150 m : 350 m]
$[-Y_0 : Y_0]$	Target Scene (Cross-range)	[-300 m : 300 m]
(x_1, y_1)	Target 1	(0 m, 0 m)
(x_2, y_2)	Target 2	(300 m , -100 m)
(x_3, y_3)	Target 3	(250 m , -150 m)
(x_4, y_4)	Target 4	(200 m , 100 m)
(x_5, y_5)	Target 5	(250 m , 100 m)

As discussed in Section III.D.3.a, the planar antenna parameters (i.e., aperture diameter and divergence angle) vary with the radar beamwidth. The antenna parameters that correspond to the transmitted radar signals used in the two-dimensional SAR simulations are provided Table 11.

Table 11. Stripmap SAR planar array antenna parameters.

Parameter	**Description** / **Signal Bandwidth (MHz)**	20	3	40	50
D	Diameter (m)	7.5	8.57	10	12
B_n	Radiation Pattern (Beamwidth) (m)	[53.03, 202.07]	[41.93, 202.07]	[32.91, 202.07]	[25.35, 202.07]
φ_d	Divergence Angle (degrees)	0.3398	0.2726	0.216	0.1674
L	Synthetic Aperture (m)	352.0726	325.0726	352.0726	352.0726
Parameter	Description / Signal Bandwidth (MHz)	60	70	80	90
D	Diameter (m)	15	20	30	60
B_n	Radiation Beamwidth (m)	[18.90, 202.07]	[13.29, 202.07]	[8.35, 202.07]	[3.95, 202.07]
φ_d	Divergence Angle (degrees)	0.1253	0.0884	0.0556	0.0263
L	Synthetic Aperture (m)	352.0726	352.0726	352.0726	352.0726

For simplicity, we first show the reconstruction results of a single point target, designated as target one. We then add four point targets to the imaging scene, where targets four and five are spaced only $45\,\mathrm{m}$ apart. The two closely spaced targets provide an approach to assess resolvability.

The results for the first simulation are presented to validate the MATLAB algorithm and show the geometry of the measured echoed signal $s(t,u)$, the fast-time matched filtered signal $s_{MF}(t,u)$ and, finally, the reconstructed target function $f(x,y)$. For this trial, we simulate a single point target located at $(x_i, y_i) = (0,0)$, which is at the target scene center. We show the results obtained from transmitting the three signals.

The three signals are each implemented using a signal bandwidth B = 50 MHz, which, for the OFDM signals requires a sampling time of $0.02\,\mu\mathrm{s}$. The LFM signal is implemented with the same sampling time. The OFDM signals are generated with four subcarriers. The signal parameters for simulation one is shown in Table 12.

Table 12. Stripmap SAR simulation one signal parameters.

	LFM	**BPSK-OFDM**	**QPSK-OFDM**
Total OFDM Symbols	-	2	1
Pulse Duration, T_p (μs)	0.08	0.08	0.08
Carrier Frequency, f_c (MHz)	0.1	0.1	0.1
Signal Bandwidth, B (MHz)	50	50	50
Transmitted Energy, E_t (μJ)	0.08	0.08	0.08
Transmitted Sampling Time, T_s (μs)	0.02	0.02	0.02
Subcarrier, N	-	4	4
Interpolated Sampling Time, T_s (μs)	0.005	0.005	0.005
Interpolated Signal Energy, E_i (μJ)	0.07893	0.07671	0.07739

Illustrated in Figures 36, 37, and 38 are the measured echoed signal, the fast-time matched-filtered signal and the reconstructed target function, respectively.

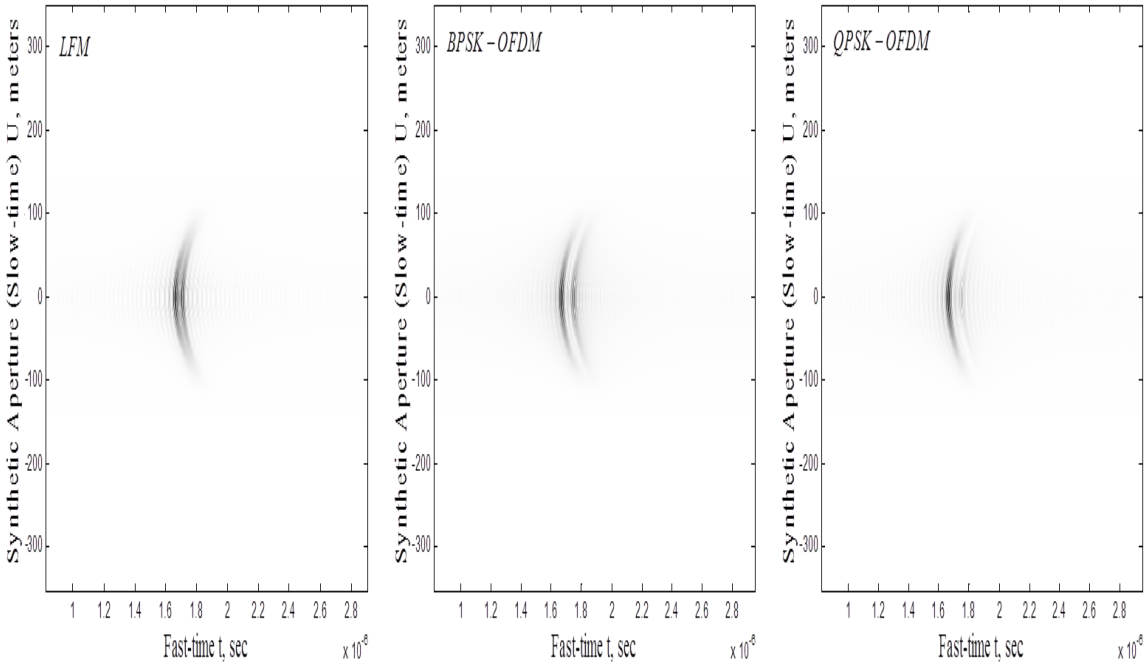

Figure 36. Measured echoed signal $s(t,u)$ for single point target located at center of target scene

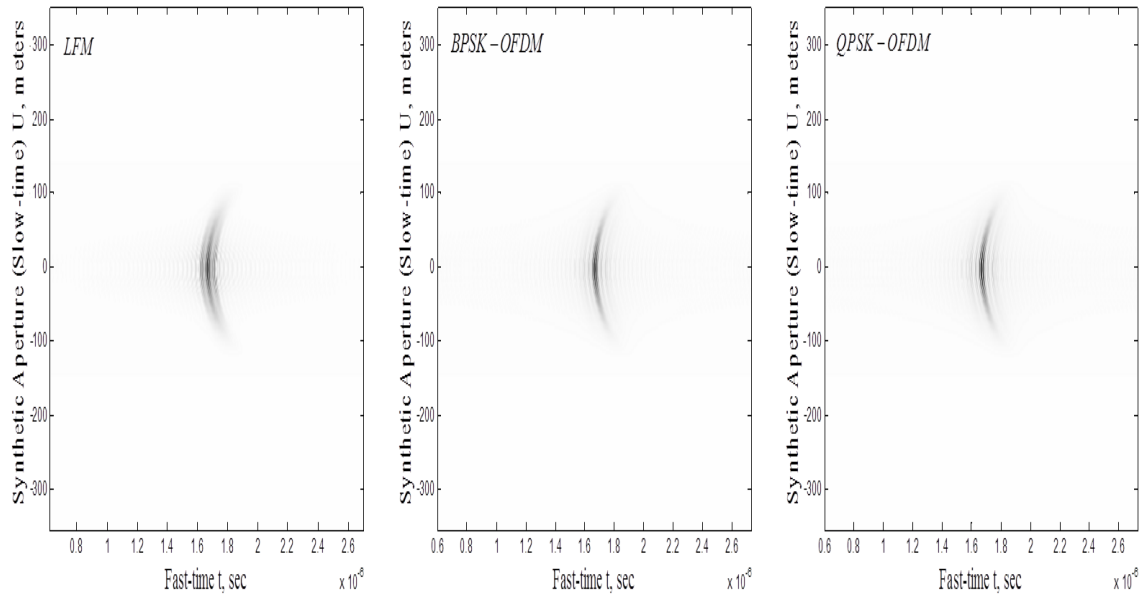

Figure 37. Fast-time matched filtered signal $s_{MF}(t,u)$ for single point target located at center of target scene.

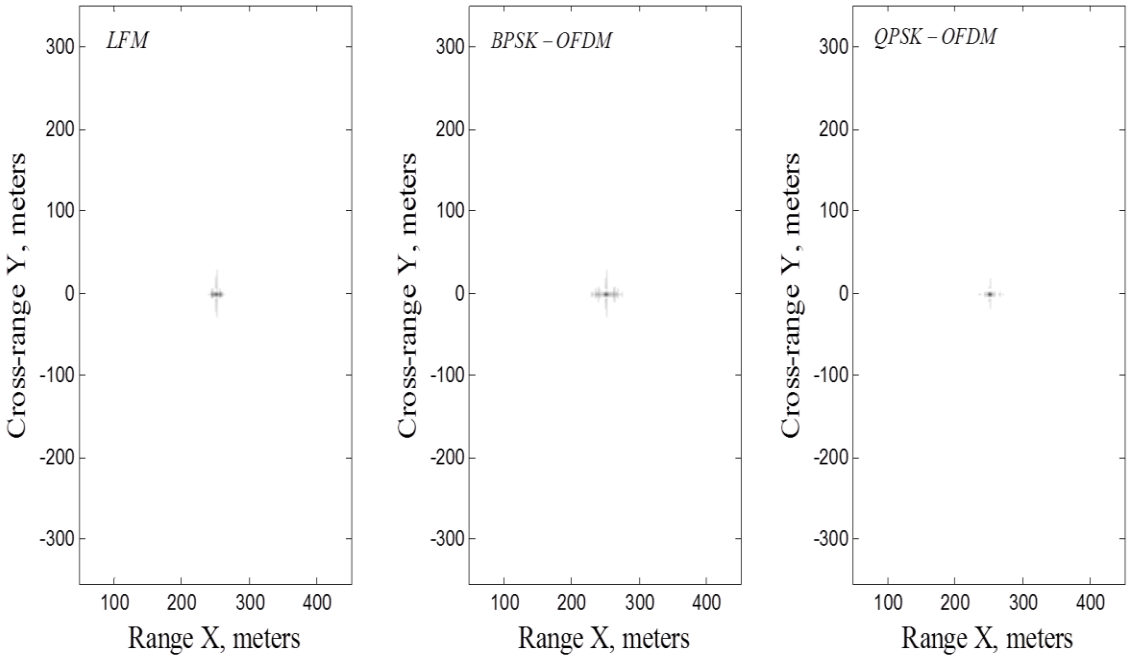

Figure 38. Reconstructed target function $f(x,y)$ for single point target located at center of target scene.

a. LFM

The additional four targets were added to the two-dimensional target scene for the remainder of the analysis. A series of simulations were conducted to determine which signal parameters have the most impact on the two-dimensional reconstructed target function. We tested this effect by varying the signal parameters and comparing the reconstructed results against the original signal and then against all three signals.

The first LFM parameter examined is bandwidth. Since LFM signal bandwidth is determined by its chirp rate and pulse duration, we expect image resolution to improve as chirp rate or pulse duration increases. In simulation two, we vary chirp rate while keeping the signal duration constant. In simulation three, chirp rate was held constant while pulse duration was increased. The amplitudes for each signal are normalized in both simulations; therefore, the transmitted signal energy values remained constant. The interpolated signal energy values are within one percent of the transmitted signal energy values. The signal parameters for simulations two and three are shown in Table 13.

Table 13. LFM signal parameters for simulations two and three.

	Simulation 2				**Simulation 3**			
Pulse Duration, T_p (μs)	0.02	0.02	0.02	0.02	0.01	0.02	0.03	0.04
Carrier Frequency, f_c (MHz)	100	100	100	100	100	100	100	100
Signal Bandwidth, B (MHz)	20	40	60	80	20	40	60	80
Transmitted Signal Energy, E_t (μJ)	0.03	0.03	0.03	0.03	0.03	0.03	0.03	0.03
Nyquist Sampling Interval, T_s (μs)	0.01	0.01	0.01	0.01	0.01	0.01	0.01	0.01
Chirp rate, α (Hz/s)	$6.28\text{x}10^{15}$	$1.26\text{x}10^{16}$	$1.89\text{x}10^{16}$	$2.51\text{x}10^{16}$	$2\text{x}10^{15}$	$2\text{x}10^{15}$	$2\text{x}10^{15}$	$2\text{x}10^{15}$
Interpolated Sampling Interval, T_s (μs)	0.005	0.005	0.005	0.005	0.005	0.005	0.005	0.005
Interpolated Signal Energy, E_i (μJ)	0.02796	0.02882	0.02896	0.02913	0.02774	0.02786	0.02806	0.02899

The reconstruction results corresponding to the signal in Table 13 are shown in Figures 39 and 40.

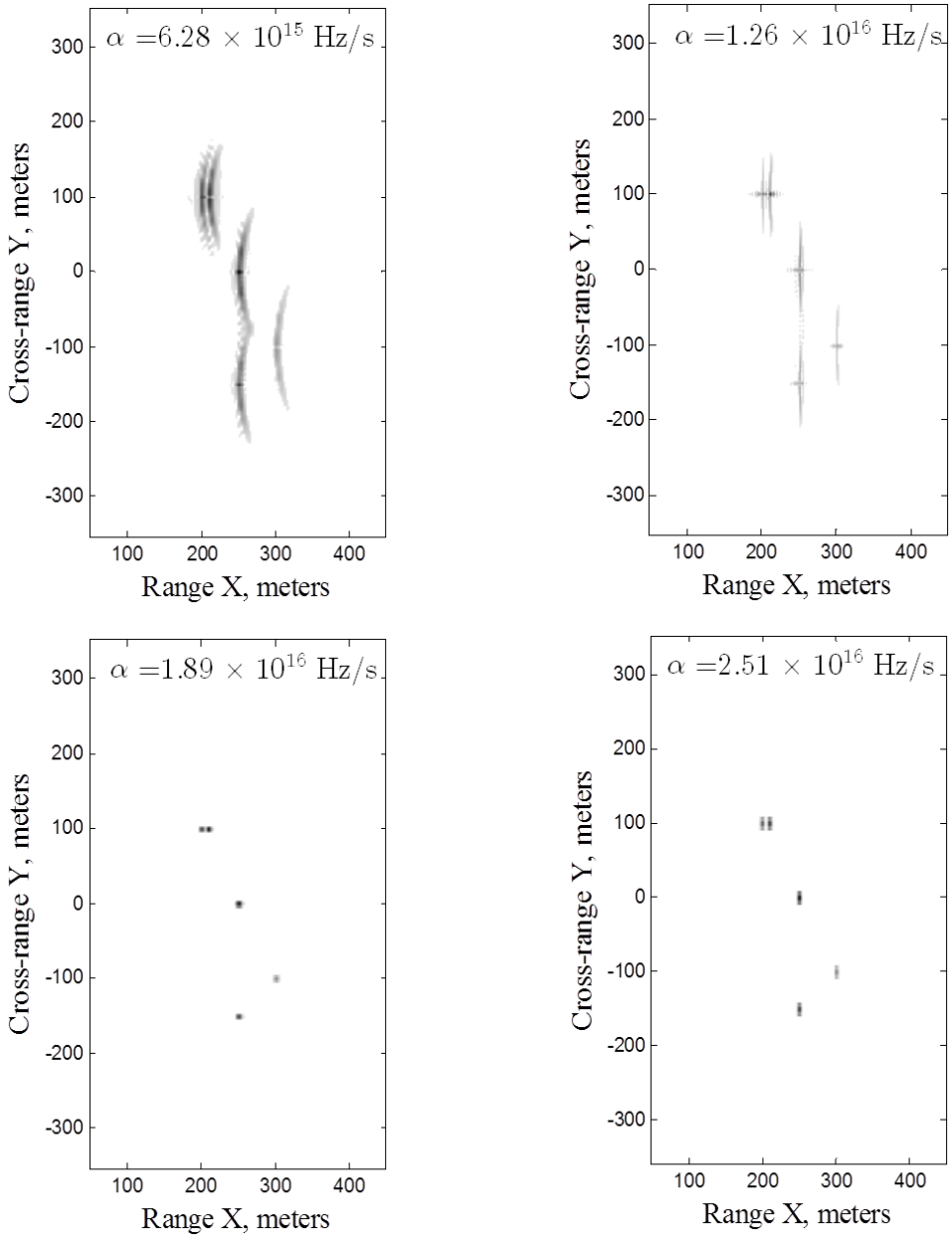

Figure 39. Simulation 2: Reconstructed target function for LFM signal with varying chirp rate.

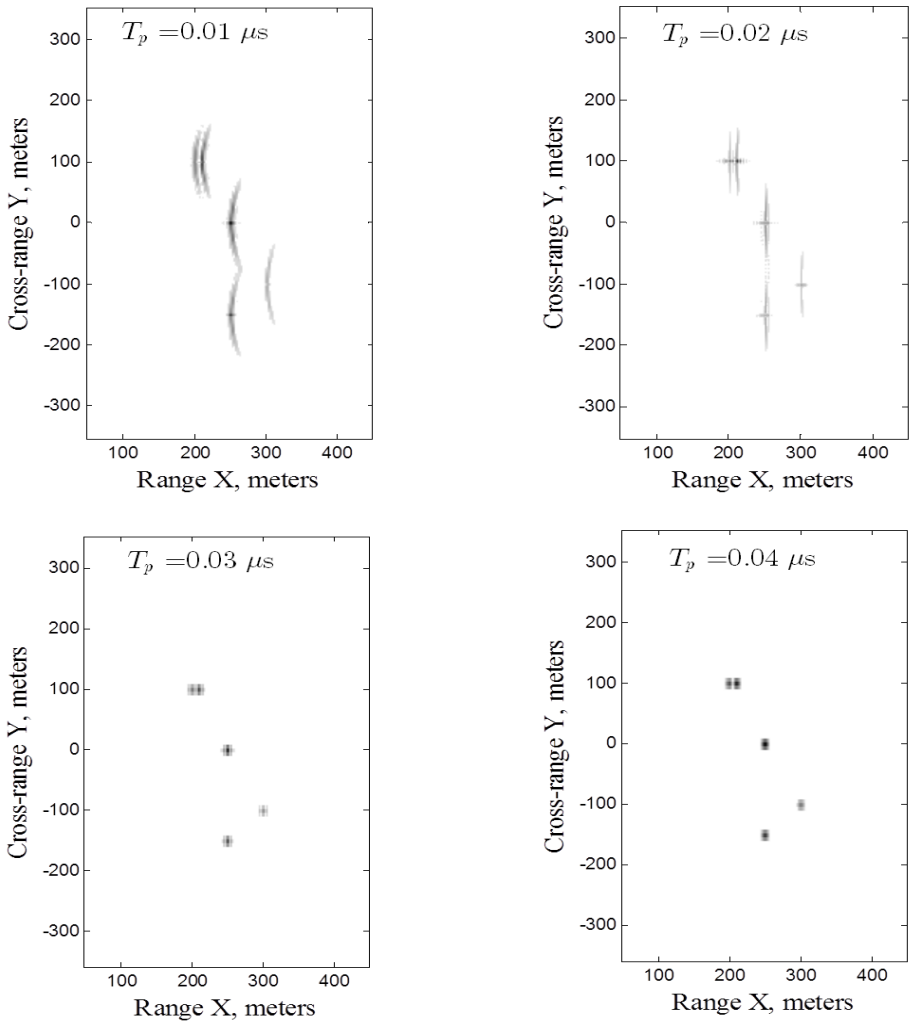

Figure 40. Simulation 3. Reconstructed target function for LFM signal with varying pulse duration.

The chirp rate values in simulation two are selected so that the signal bandwidth is equal to 20 MHz, 40 MHz, 60 MHz, and 80 MHz, respectively. Similarly, for simulation three, the pulse duration values are selected to match the signal bandwidth listed for simulation two. By observing the results for simulation two and three in Figures 39 and 40, we see that the resolution improves as either the chirp rate or pulse duration increases. For the lower bandwidth signals at 20 and 40 MHz, the targets are recovered; however, the exact target location is smeared or distorted. For both simulations, the best SAR images are obtained when the signal bandwidth is 60 MHz.

Surprisingly, the image resolution did not improve when signal bandwidth was increased to 80 MHz, indicating there may be a point of diminishing returns in terms of cross-range resolution vs. signal bandwidth.

b. BPSK-OFDM

In this section, we present the results of transmitting a BPSK-OFDM signal. In simulation four, we examine how BPSK-OFDM signal bandwidth affects the two-dimensional reconstruction results. We ran two sets, where four and 16 subcarriers were used to generate the signals in set one and two, respectively. Signal bandwidth was increased from 20 to 80 MHz in increments of 20 MHz within each set. We increased the number of symbols for each signal and each iteration, which kept signal duration constant for each set. The transmitted signal energy values within each set were normalized so that only bandwidth varies for this simulation with parameters contained in Table 14.

Table 14. BPSK-OFDM signal parameters for simulation four.

	Set 1			
Total OFDM Symbol	2	4	6	8
Pulse Duration, T_p (μs)	0.4	0.4	0.4	0.4
Signal Bandwidth, B (MHz)	20	40	60	80
Transmitted Energy, E_t (μJ)	0.2	0.2	0.2	0.2
Sampling Time, T_s (μs)	0.05	0.025	0.01667	0.0125
Subcarrier, N	4	4	4	4
Interpolated Sampling Time, T_s (μs)	0.005	0.005	0.005	0.005
Interpolated Signal Energy, E_t (μJ)	0.1891	0.1898	0.1976	0.1996
	Set 2			
Total OFDM Symbol	2	4	6	8
Pulse Duration, T_p (μs)	1.6	1.6	1.6	1.6
Signal Bandwidth, B (MHz)	20	40	60	80
Transmitted Energy, E_t (μJ)	0.4	0.4	0.4	0.4
Sampling Time, T_s (μs)	0.05	0.025	0.01667	0.0125
Subcarrier, N	16	16	16	16
Interpolated Sampling Time, T_s (μs)	0.005	0.005	0.005	0.005
Interpolated Signal Energy, E_t (μJ)	0.3766	0.3935	0.3977	0.3974

The reconstruction results corresponding to the signal in Table 14 are shown in Figures 41 and 42.

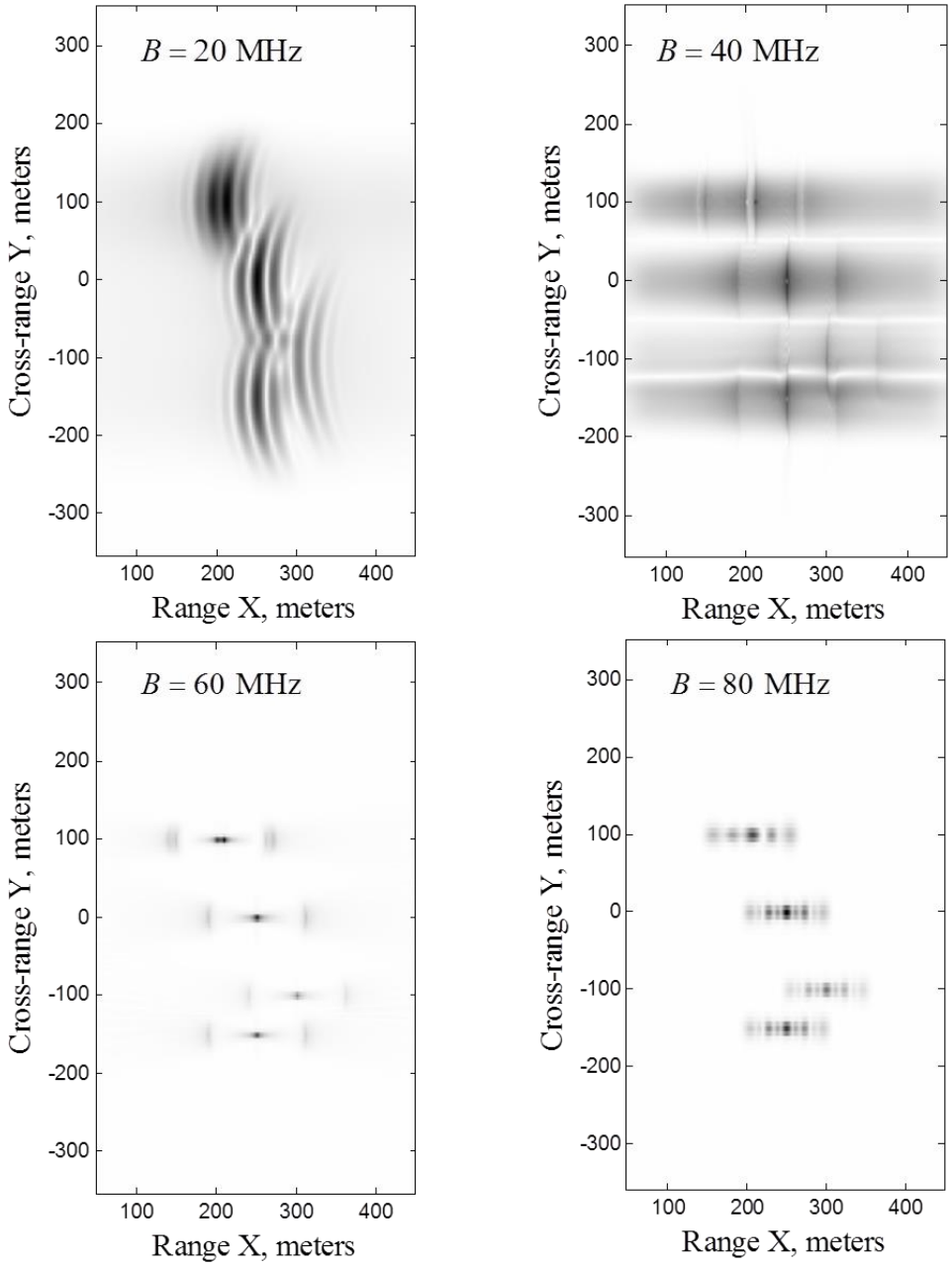

Figure 41. Reconstructed target function for simulation four, set one for BPSK-OFDM signal with $N = 4$

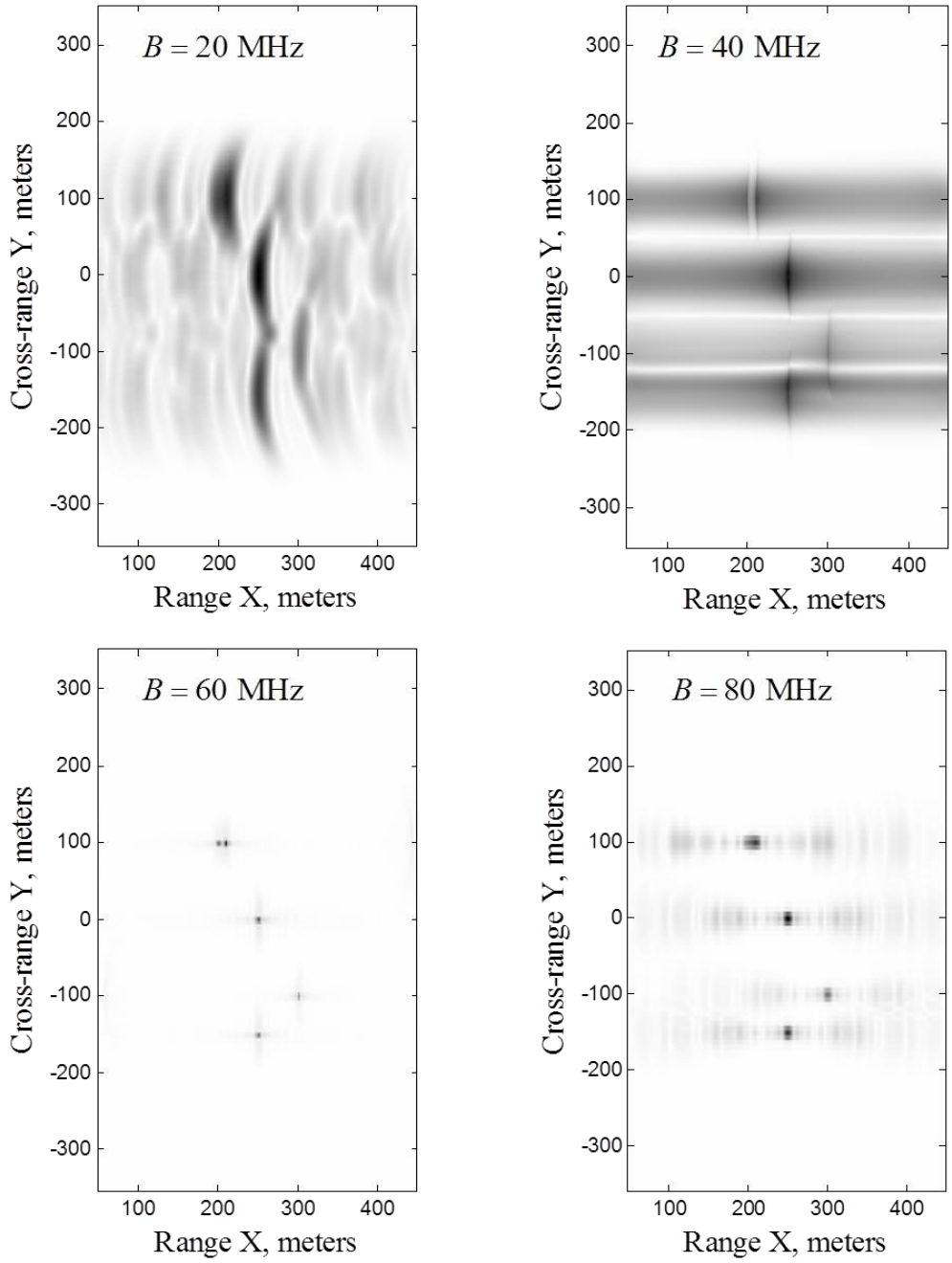

Figure 42. Reconstructed target function for simulation four, set two for BPSK-OFDM signal with $N = 16$.

Observing the results in Figure 41, where the BPSK-OFDM signal was implemented with four subcarriers and 20 MHz, we can see that the model was successful at recovering the five point targets; however, the target locations appear to be smeared and ambiguous. Furthermore, the two closely spaced targets could easily be

mistaken as one larger target. Image resolution improves when the bandwidth is increased to 40 MHz and the two closely spaced targets are more distinguishable; however, the targets returns are still smeared, making their exact locations unclear. Further, the result is a higher resolution image if signal bandwidth was increased to 60 MHz. The targets appear very clearly, and the two closely spaced targets are very distinct from each other. Interestingly, the targets do not appear to be any clearer when the bandwidth is increased to 80 MHz. In fact, there is grey area surrounding each point, and the two closely spaced targets are not as distinguishable as they were for the 60 MHz bandwidth signal. This is likely due to diminishing returns in terms of bandwidth versus cross-range resolutions.

The reconstruction results corresponding to the BPSK-OFDM signal implemented with 16 subcarriers in Figure 42 display similar results to that of the signal transmitted with four subcarriers. The main difference is that the added subcarriers resulted in additional smearing around the location of each point target. It can be seen that resolution improved from 20 to 40 MHz, but the target locations are still unclear. Image resolution is best at 60 MHz and at 80 MHz and the size of each point target increased, which implies lower image resolution.

For simulation five, we examined how the duration of a BPSK-OFDM signal affects the SAR image quality. The number of subcarriers was kept constant at $N = 4$. We ran four sets, where signal bandwidth remained constant within each iteration but increased for each set. Each signal's duration within a set is increased by increasing the number of OFDM symbols per signal. The signal parameters for simulation five are shown in Table 15.

Table 15. BPSK-OFDM signal parameters for simulation five.

	Set 1				Set 2			
Total OFDM Symbols	1	2	3	4	1	2	3	4
Pulse Duration, T_p (μs)	0.08	0.16	0.24	0.32	0.06667	0.1333	0.2	0.26667
Signal Bandwidth, B (MHz)	50	50	50	50	60	60	60	60
Transmitted Energy, E (μJ)	0.04	0.04	0.04	0.04	0.0333	0.0333	0.0333	0.0333
Transmitted Sampling Time, T_s (μs)	0.02	0.02	0.02	0.02	0.0167	0.0167	0.0167	0.0167
Subcarrier, N	4	4	4	4	4	4	4	4
Interpolated Sampling Time, T_s (μs)	0.005	0.005	0.005	0.005	0.005	0.005	0.005	0.005
Interpolated Signal Energy, E (μJ)	0.0379	0.0388	0.0390	0.0390	0.03166	0.03162	0.03214	0.03283
	Set 3				Set 4			
Total OFDM Symbols	1	2	3	4	1	2	3	4
Pulse Duration, T_p (μs)	0.0571	0.1143	0.1714	0.2286	0.05	0.1	0.15	0.2
Signal Bandwidth, B (MHz)	70	70	70	70	80	80	80	80
Transmitted Energy, E (μJ)	0.02857	0.02857	0.02857	0.02857	0.025	0.025	0.025	0.025
Transmitted Sampling Time, T_s (μs)	0.0143	0.0143	0.0143	0.0143	0.0125	0.0125	0.0125	0.0125
Subcarrier, N	4	4	4	4	4	4	4	4
Interpolated Sampling Time, T_s (μs)	0.005	0.005	0.005	0.005	0.005	0.005	0.005	0.005
Interpolated Signal Energy, E (μJ)	0.02553	0.02739	0.02581	0.02687	0.02487	0.02296	0.02381	0.02437

The simulation results for the BPSK-OFDM transmitted signal in Table 15 are shown in Figures 43 through 46.

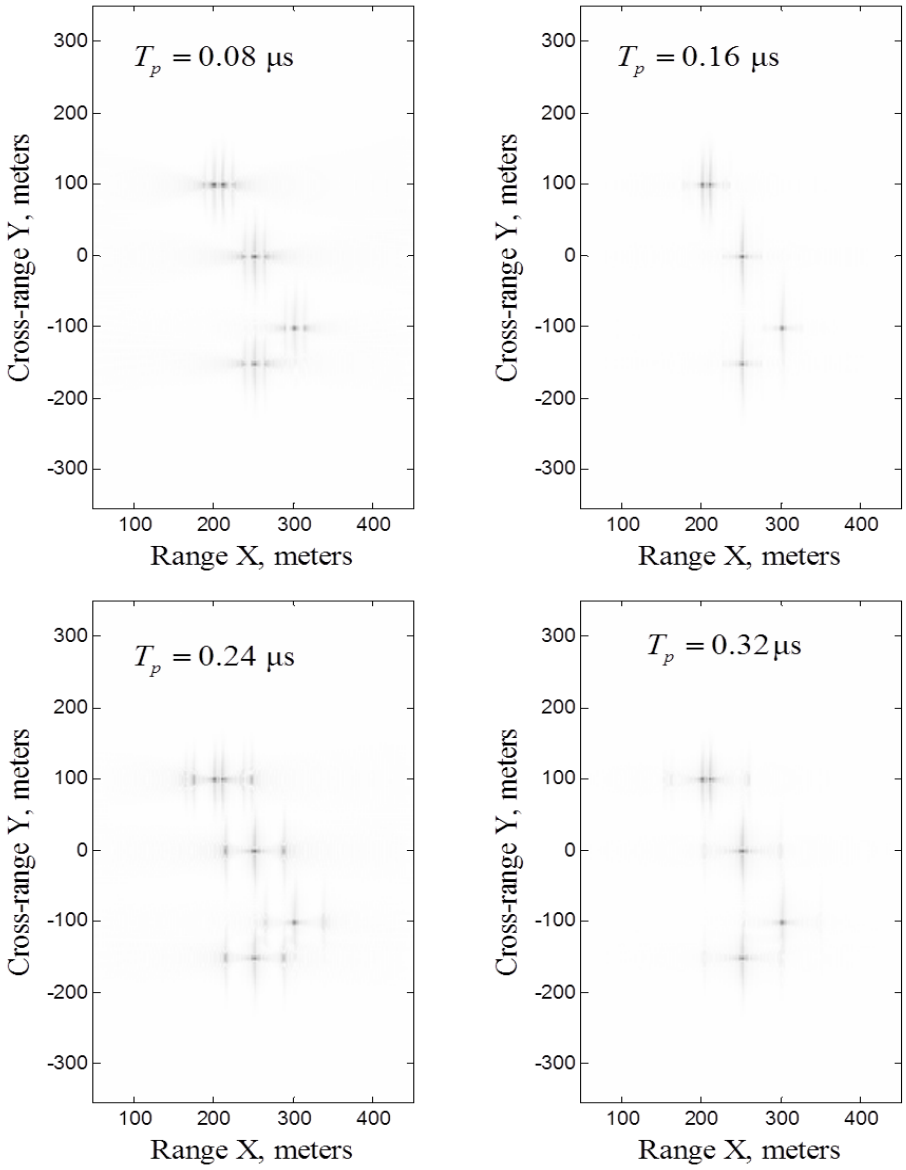

Figure 43. Reconstructed target function for simulation five, set one for BPSK-OFDM signal with $B = 50\,\text{MHz}$.

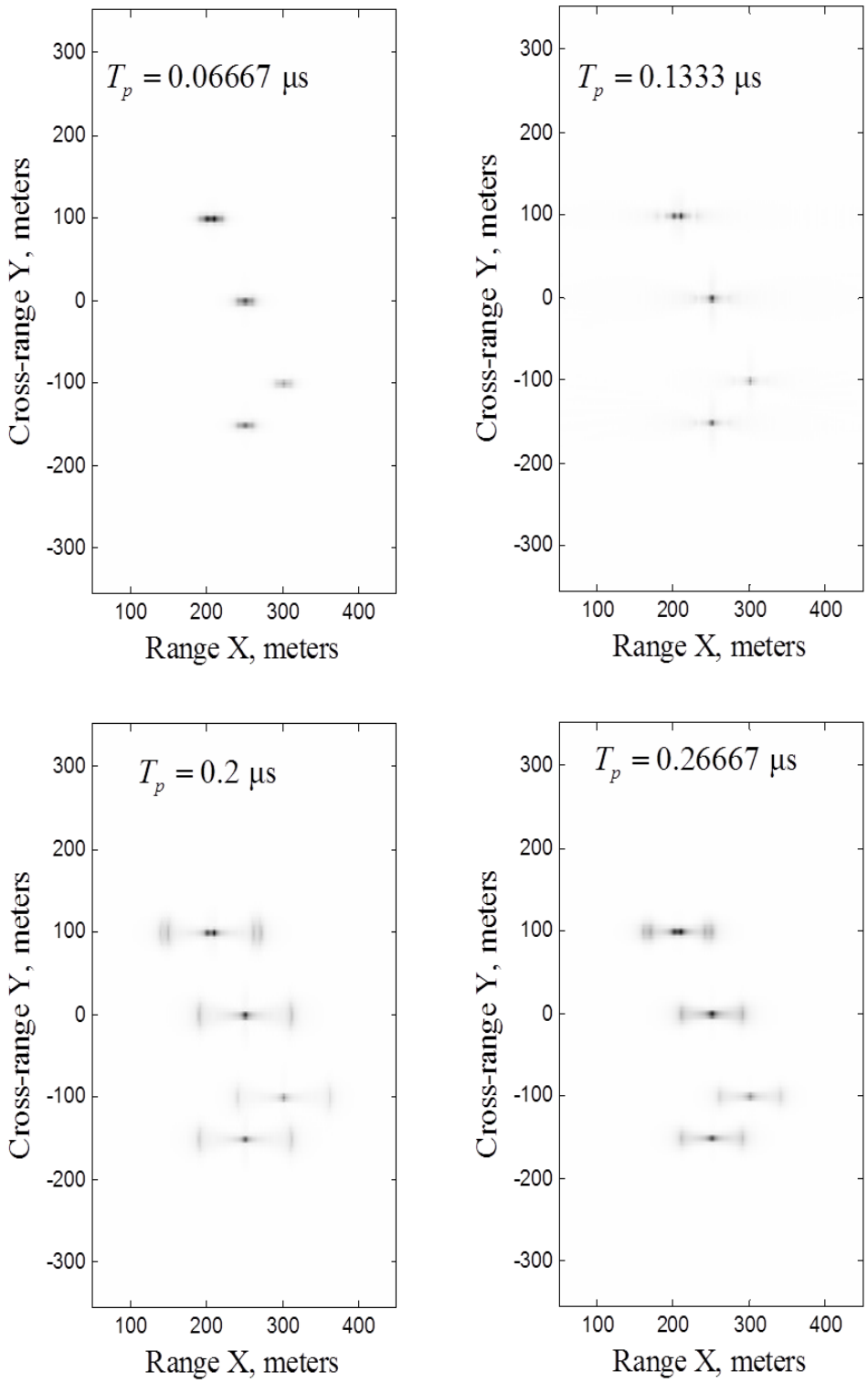

Figure 44. Reconstructed target function for simulation five, set two for BPSK-OFDM signal with $B = 60$ MHz.

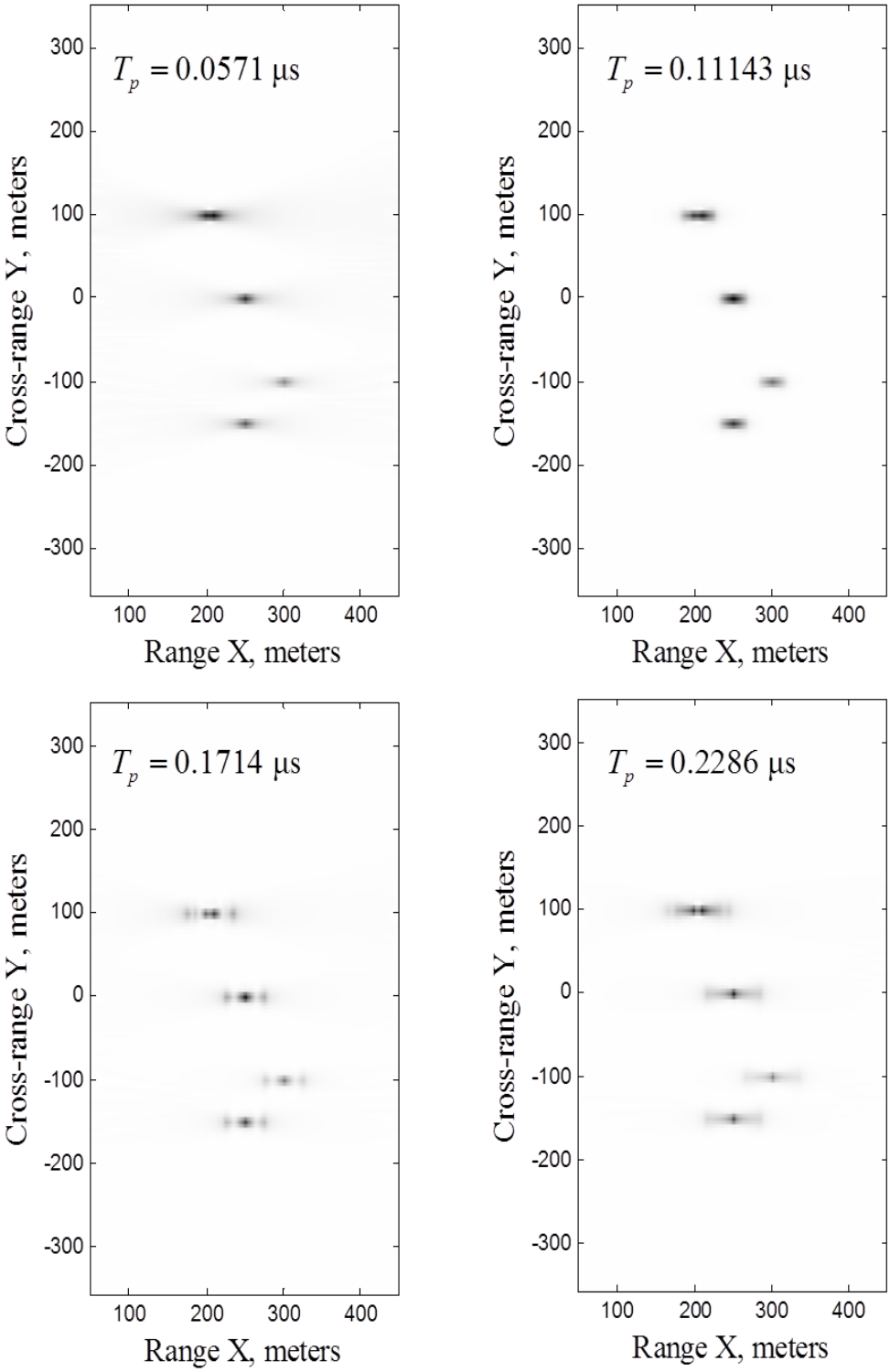

Figure 45. Reconstructed target function for simulation five, set three for BPSK-OFDM signal with $B = 70$ MHz.

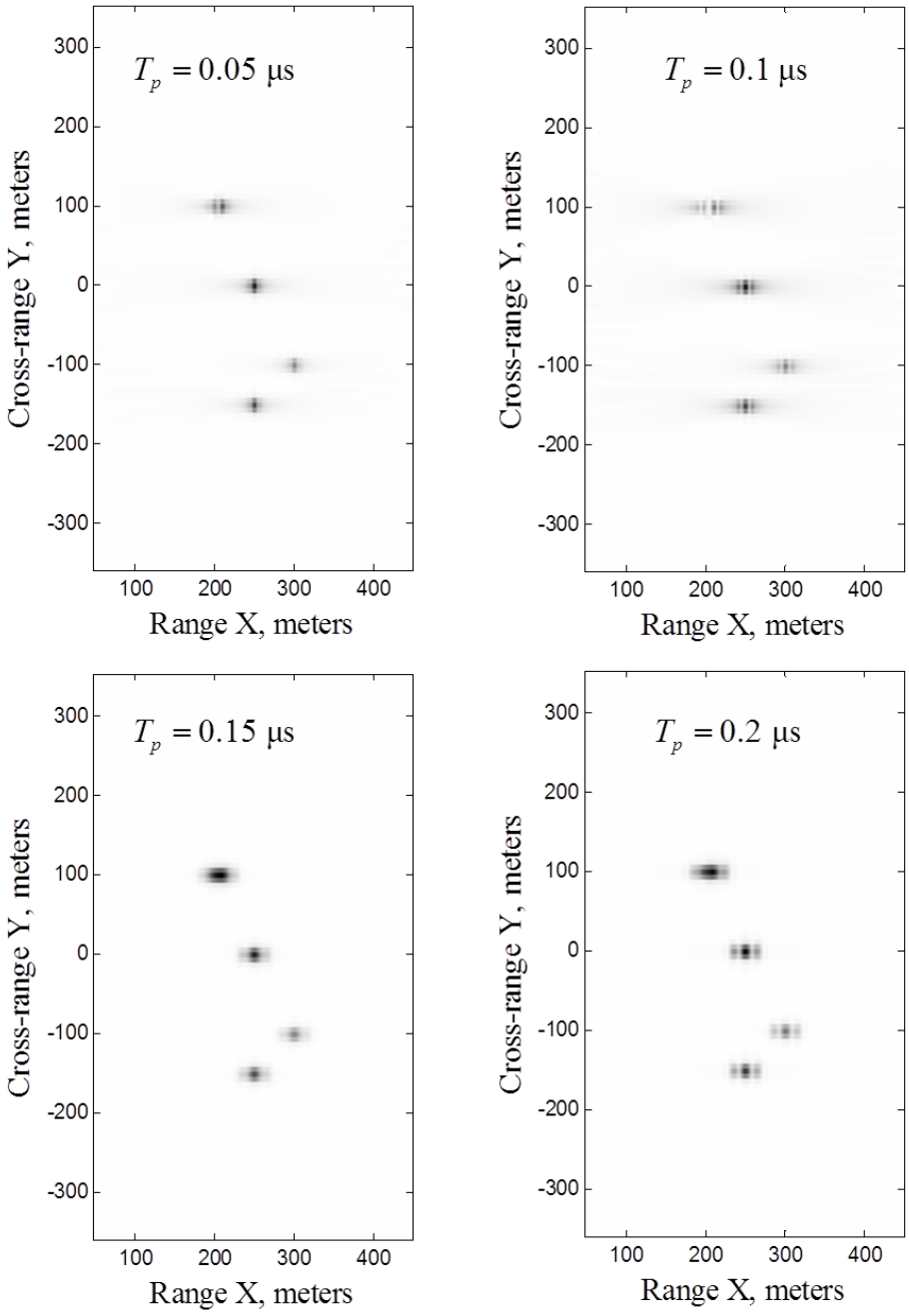

Figure 46. Reconstructed target function for simulation five, set four for BPSK-OFDM signal with $B = 80$ MHz.

In set one, four BPSK-OFDM signals are generated with 50 MHz and 1, 2, 3 and 4 symbols, respectively. The reconstruction results obtained from generating the four signals in set one are shown in Figure 43. All five point targets are recovered for each of the signals; however, there appear to be grey smearing around the vicinity of each

target's location for all results. Nonetheless, the five point targets are recognizable due to the solid black contrast in the correct location of each target. The least amount smearing occurred in the signal with the longest pulse duration at $T_p = 0.32\ \mu s$. Overall in set one, increasing pulse duration directly improved the SAR image quality, but the improvement was not very significant.

The reconstructed images for set two, where the signals were generated with 60 MHz, are shown in Figure 44. First, it can be seen that resolution improved with the increased signal bandwidth. Further, image resolution improved with the increased duration of each signal, but the improvement is not significant. Increasing the signal's duration resulted in an increased amount of grey smearing around the vicinity of each target. This occurs because of the increased number of symbols used to implement the signals.

The results corresponding to the signals generated with 70 MHz in set three are shown in Figure 45. Similar to previous simulations, lower resolution was obtained when bandwidth was increased beyond 60 MHz. It can be seen that the point targets are smeared for the results corresponding to $T_p = 0.0571\ \mu s$ and $T_p = 0.11143\ \mu s,$ and the two closely spaced targets appear as one. Increasing the signal duration, as in the results corresponding to $T_p = 0.1714\ \mu s$ and $T_p = 0.2286\ \mu s,$ respectively, we see that resolution improved and closely spaced targets are more distinguishable.

The results for the signals implemented with 80 MHz in set four can be seen in Figure 46. The most desirable results were obtained for the shorter duration signal at $T_p = 0.05\ \mu s.$ Although the targets are recovered for the longer duration signals, lower resolution was obtained and the closely spaced targets are indistinguishable.

Overall, increasing the duration of the BPSK-OFDM signals directly improved the image quality for signals generated with 50, 60, and 70 MHz. However, the images became increasingly distorted when the duration was increased for signals generated with 80 MHz. We can conclude that shorter duration signals are sufficient for obtaining fine resolution for wider bandwidth BPSK-OFDM signals.

c. QPSK-OFDM

In this section, we present the QPSK-OFDM two-dimensional SAR reconstruction results. Similar to the BPSK-OFDM case, we perform a series of simulations while changing various parameters of the signal to determine how they affect the SAR image.

Simulation six is similar to simulation four where the QPSK-OFDM signal bandwidth is increased within each set while signal duration and the number of subcarriers are kept constant. Simulation six signal parameters are shown in Table 16.

Table 16. QPSK-OFDM signal paramters for simulation six.

	Set 1			
Total OFDM Symbol	2	4	6	8
Pulse Duration, T_p (μs)	0.4	0.4	0.4	0.4
Signal Bandwidth, B (MHz)	20	40	60	80
Transmitted Energy, E_t (μJ)	0.4	0.4	0.4	0.4
Sampling Time, T_s (μs)	0.05	0.025	0.01667	0.0125
Subcarrier, N	4	4	4	4
Interpolated Sampling Time, T_s (μs)	0.005	0.005	0.005	0.005
Interpolated Signal Energy, E_t (μJ)	0.3847	0.3853	0.3926	0.3964
	Set 2			
Total OFDM Symbol	2	4	6	8
Pulse Duration, T_p (μs)	1.6	1.6	1.6	1.6
Signal Bandwidth, B (MHz)	20	40	60	80
Transmitted Energy, E_t (μJ)	0.8	0.8	0.8	0.8
Sampling Time, T_s (μs)	0.05	0.025	0.01667	0.0125
Subcarrier, N	16	16	16	16
Interpolated Sampling Time, T_s (μs)	0.005	0.005	0.005	0.005
Interpolated Signal Energy, E_t (μJ)	0.7808	0.7907	0.7923	0.7950

The results for simulation six are shown in Figures 47 and 48.

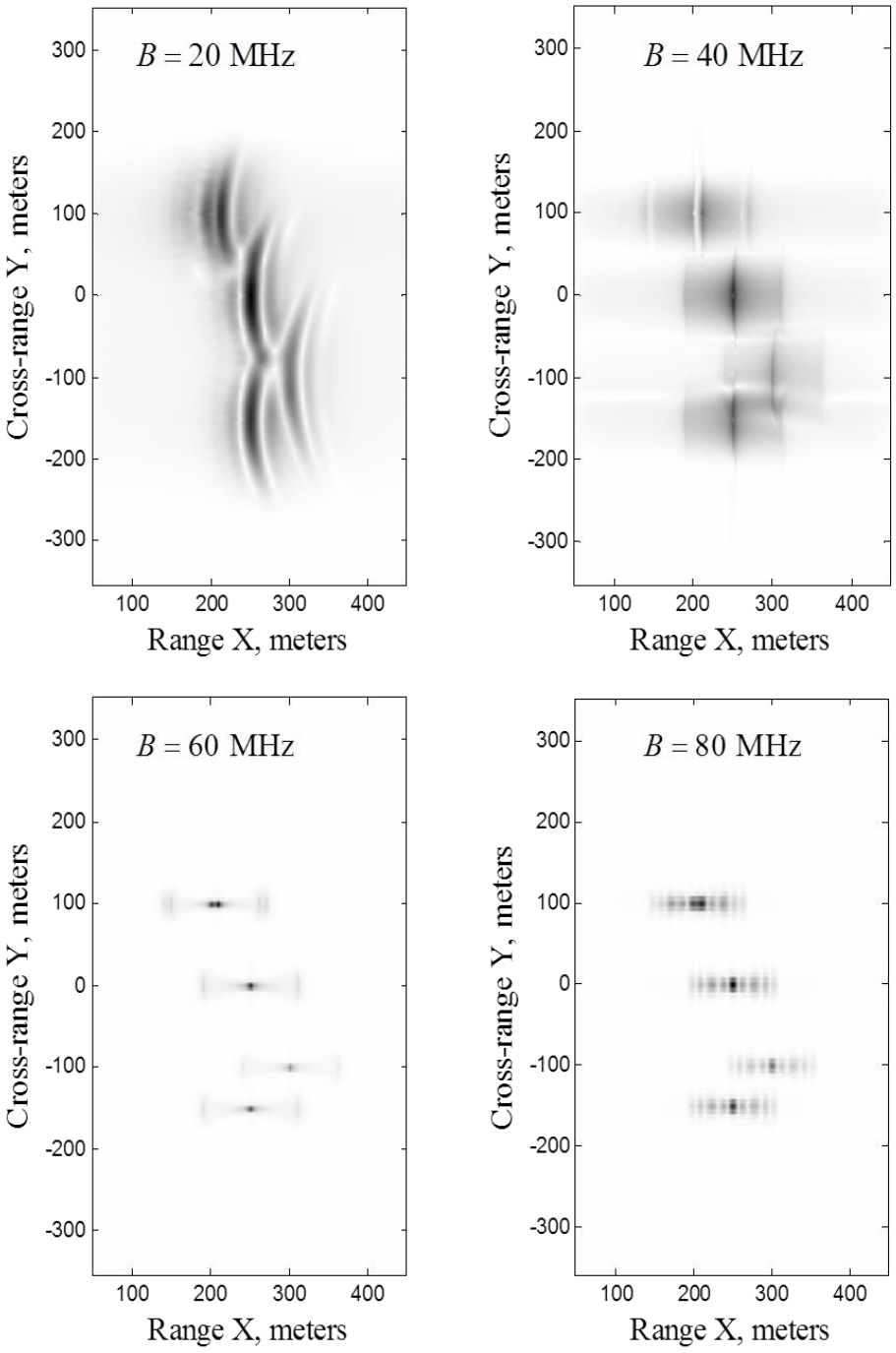

Figure 47. Reconstructed target function for simulation six, set one for QPSK-OFDM with $N = 4$.

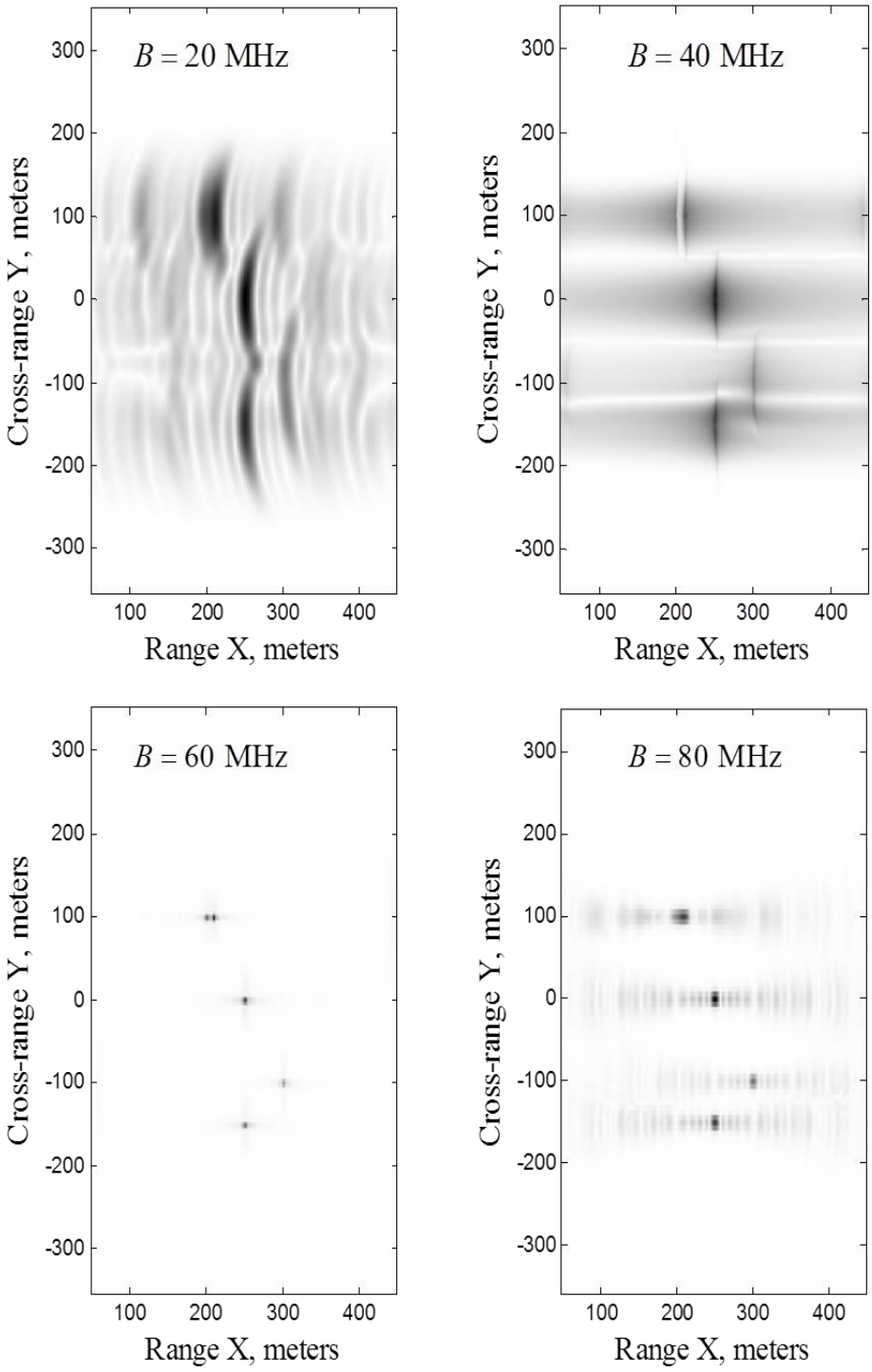

Figure 48. Reconstructed target function for simulation six, set two for QPSK-OFDM with $N = 16$.

Similar to the results obtained from transmitted the BPSK-OFDM signal in simulation four, resolution improved as the signal bandwidth increased. At both 20 and 40 MHz, the results showed grey smearing around each point target that increased with the number of subcarriers. For each iteration, the best resolution was obtained when the signal was implemented with 60 MHz. Overall, the results were similar to that of the BPSK-OFDM results in simulation four. The main difference is the change in the transmitted and interpolated signal energy, which both increased by a factor of two for the QPSK-OFDM signals.

Simulation seven was conducted to assess how the QPSK-OFDM signal duration affects the SAR image. There are four sets in this simulation, where bandwidth in increased for each set, and the number of subcarriers was kept constant at $N = 4$. We increased the signal duration within a set by increasing the number of symbols. The signal parameters for simulation seven are shown in Table 17.

Table 17. QPSK-OFDM signal parameters simulation seven.

	Iteration 1				Iteration 2			
Total OFDM Symbols	1	2	3	4	1	2	3	4
Pulse Duration, T_p (μs)	0.08	0.16	0.24	0.32	0.06667	0.1333	0.2	0.26667
Signal Bandwidth, B (MHz)	50	50	50	50	60	60	60	60
Transmitted Energy, E (μJ)	0.08	0.08	0.08	0.08	0.06667	0.06667	0.06667	0.06667
Transmitted Sampling Time, T_s (μs)	0.02	0.02	0.02	0.02	0.0167	0.0167	0.0167	0.0167
Subcarrier, N	4	4	4	4	4	4	4	4
Interpolated Sampling Time, T_s (μs)	0.005	0.005	0.005	0.005	0.005	0.005	0.005	0.005
Interpolated Signal Energy, E (μJ)	0.07650	0.07688	0.07764	0.07852	0.06481	0.06463	0.06516	0.06598
	Iteration 3				Iteration 4			
Total OFDM Symbols	1	2	3	4	1	2	3	4
Pulse Duration, T_p (μs)	0.0571	0.1143	0.1714	0.2286	0.05	0.1	0.15	0.2
Signal Bandwidth, B (MHz)	70	70	70	70	80	80	80	80
Transmitted Energy, E (μJ)	0.05714	0.05714	0.05714	0.05714	0.05	0.05	0.05	0.05
Transmitted Sampling Time, T_s (μs)	0.0143	0.0143	0.0143	0.0143	0.0125	0.0125	0.0125	0.0125
Subcarrier, N	4	4	4	4	4	4	4	4
Interpolated Sampling Time, T_s (μs)	0.005	0.005	0.005	0.005	0.005	0.005	0.005	0.005
Interpolated Signal Energy, E (μJ)	0.05569	0.05684	0.05692	0.05632	0.04781	0.04836	0.04828	0.04798

The results for simulation seven can be seen in Figures 49 through 52.

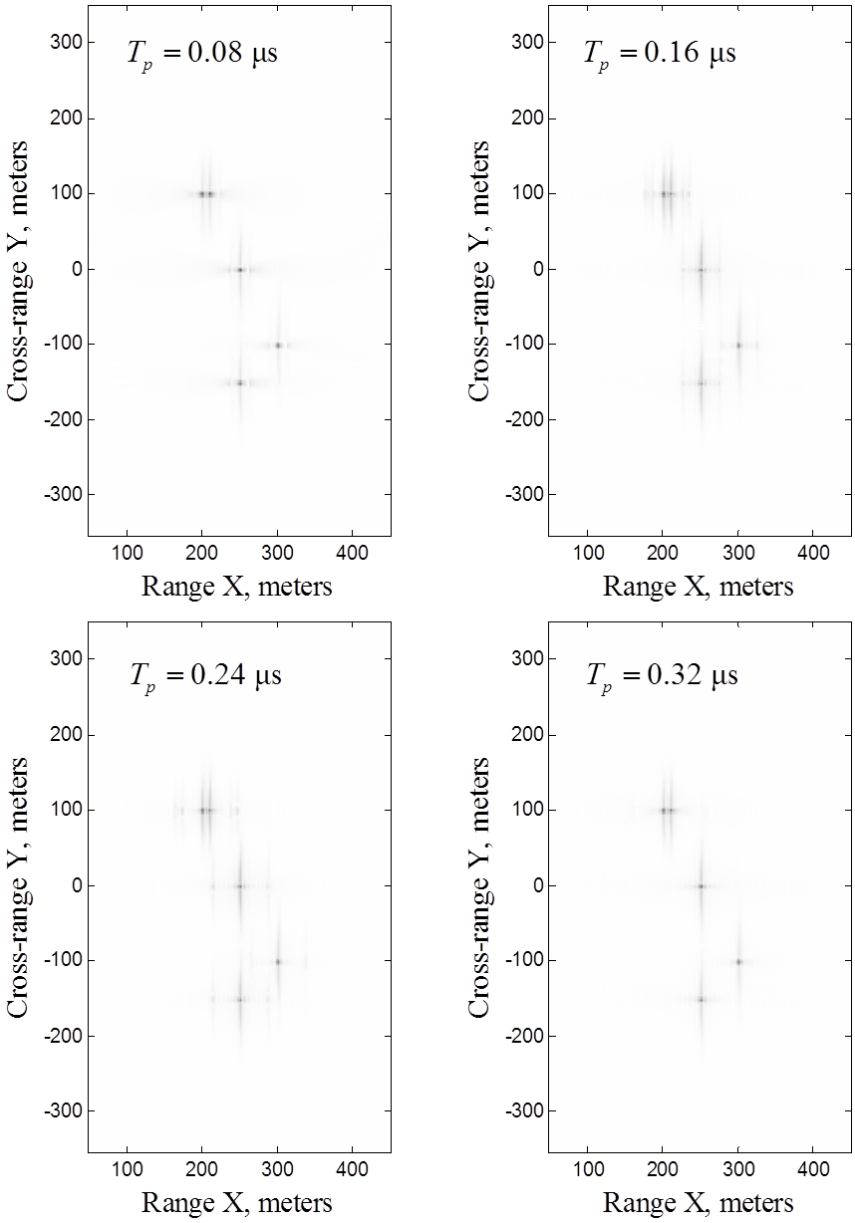

Figure 49. Reconstructed target function for simulation seven, set one with QPSK-OFDM signal with $B = 50$ MHz.

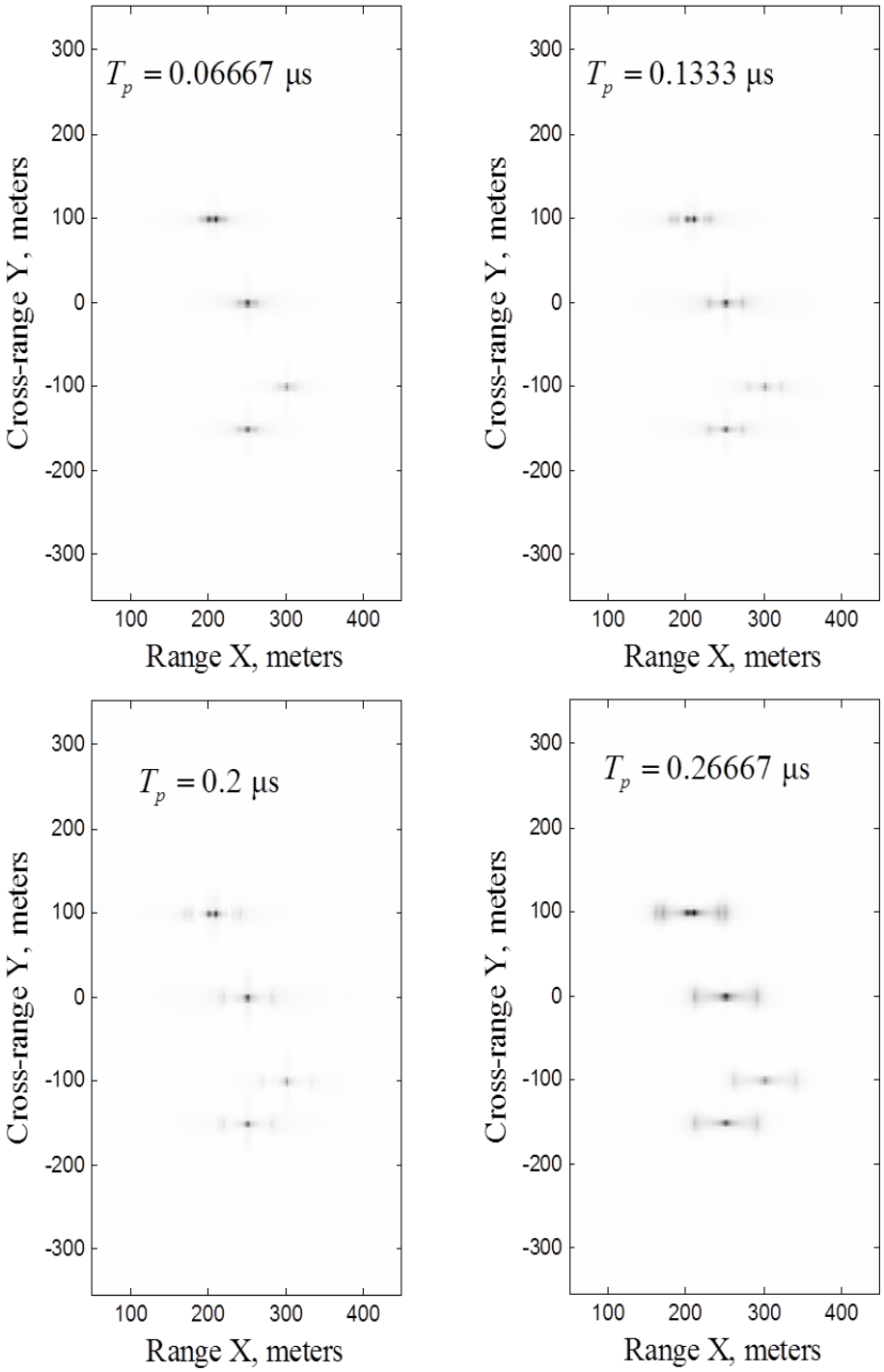

Figure 50. Reconstructed target function for simulation seven, set two for QPSK-OFDM with $B = 60$ MHz.

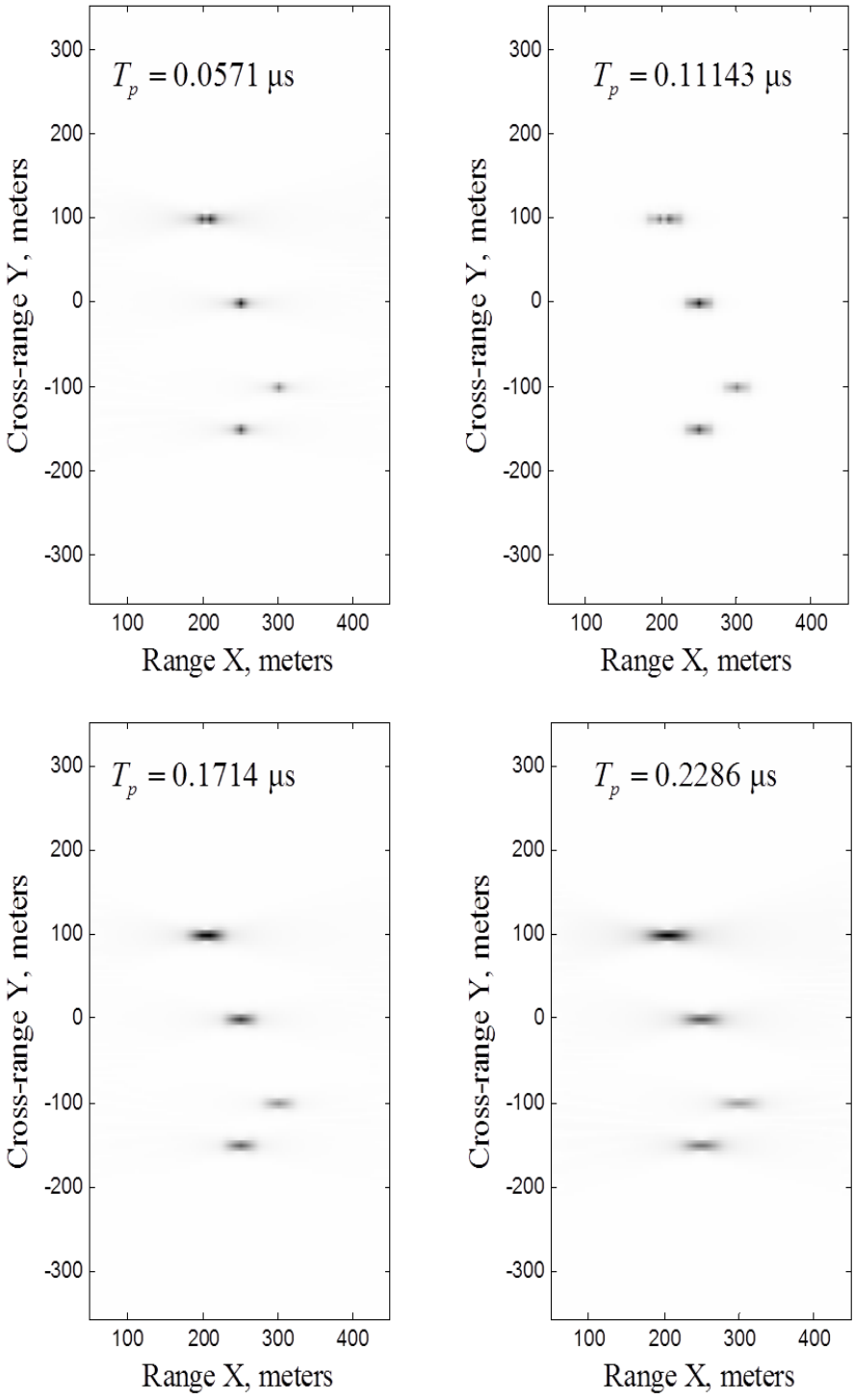

Figure 51. Reconstructed target function for simulation seven, set three for QPSK-OFDM with $B = 70$ MHz.

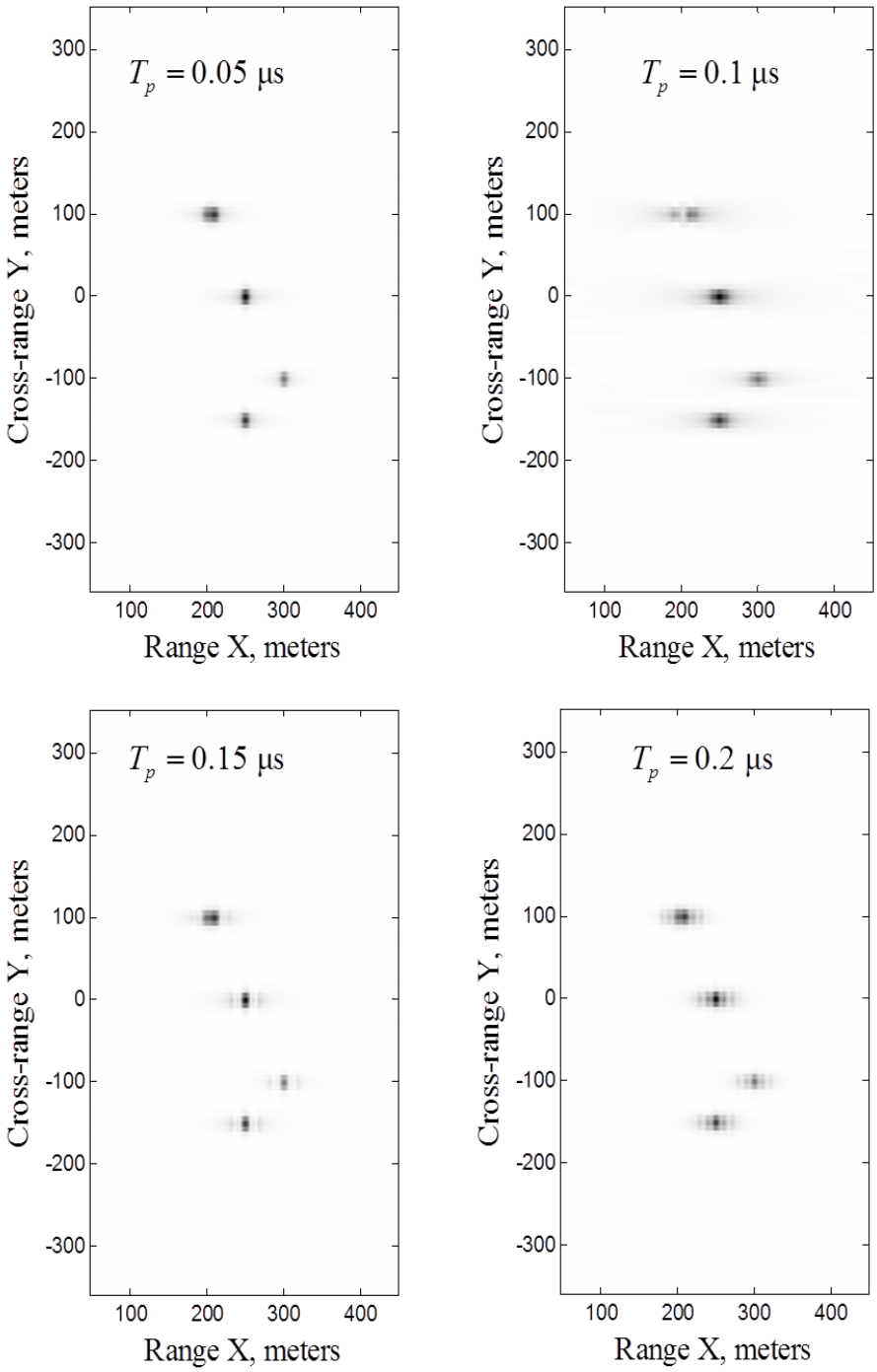

Figure 52. Reconstructed target function for simulation seven, set four for QPSK-OFDM with $B = 80$ MHz.

By observing the results for set one, where the QPSK-OFDM signal was implemented with 50 MHz, we can see that all five point targets were recovered for each

iteration. Similar to the BPSK-OFDM results in simulation five, the least amount of smearing occurred for the longest signal duration at $T_p = 0.32\ \mu s$.

At 60 MHz, in set two, the images have improved resolution with increasing signal duration; however, there is a gray smearing area around each point target. This result is similar to that observed for the BPSK-OFDM signals generated with the same bandwidth in simulation five.

At 70 MHz, in set three, the resolution improved as signal duration was doubled from $T_p = 0.0571\ \mu s$ to $T_p = 0.1143\ \mu s$; however, further increases in the duration resulted in lower image resolution. In fact, the point targets are stretched in the range direction making it difficult to pinpoint their exact location.

For the images corresponding to the signal generated with 80 MHz, we see that the best results were obtained when $T_p = 0.05\ \mu s$. Increasing the duration at this bandwidth resulted in lower image resolution.

Overall, the results in this simulation are similar to the results obtained for the BPSK-OFDM signals generated for simulation five. The main difference is the increase in the both transmitted and interpolated signal energies for the QPSK-OFDM signals.

Simulation eight and nine were conducted to compare the signals and their parameters against each other. It is worth noting that the image resolution improved for all three signals up to 60 MHz and either did not improve or degraded, which is the same phenomenon observed in the original algorithm written by Soumekh in [19].

In simulation eight, the each signal's bandwidth was held constant at 60 MHz, while the signal duration was increased from $0.06667\ \mu s$ to $0.2667\ \mu s$. We increased each OFDM signal's duration by increasing the number of OFDM symbols per signal. The OFDM signals were generated with four subcarriers. The transmitted signal energy values were normalized for all three signals. The signal parameters for simulation eight are shown in Table 18.

Table 18. Signal parameters for simulation eight.

	LFM	BPSK-OFDM	QPSK-OFDM	LFM	BPSK-OFDM	QPSK-OFDM
Total OFDM Symbols	-	1	1	-	2	2
Pulse Duration, T_p (μs)	0.06667	0.06667	0.06667	0.13333	0.13333	0.13330
Signal Bandwidth, B (MHz)	60	60	60	60	60	60
Transmitted Energy, E (μJ)	0.03333	0.03333	0.03333	0.03333	0.03333	0.03333
Transmitted Sampling Time, T_s (μs)	0.001	0.01667	0.01667	0.001	0.01667	0.01667
Subcarrier, N	-	4	4	-	4	4
Interpolated Sampling Time, T_s (μs)	0.005	0.005	0.005	0.005	0.005	0.005
Interpolated Signal Energy, E (μJ)	0.03136	0.03129	0.03213	0.03125	0.03145	0.03261
	LFM	**BPSK-OFDM**	**QPSK-OFDM**	**LFM**	**BPSK-OFDM**	**QPSK-OFDM**
Total OFDM Symbols	-	3	3	-	4	4
Pulse Duration, T_p (μs)	0.2	0.2	0.2	0.26667	0.26667	0.26667
Signal Bandwidth, B (MHz)	60	60	60	60	60	60
Transmitted Energy, E (μJ)	0.03333	0.03333	0.03333	0.03333	0.03333	0.03333
Transmitted Sampling Time, T_s (μs)	0.001	0.01667	0.01667	0.001	0.01667	0.01667
Subcarrier, N	-	4	4	-	4	4
Interpolated Sampling Time, T_s (μs)	0.005	0.005	0.005	0.005	0.005	0.005
Interpolated Signal Energy, E (μJ)	0.03171	0.03135	0.03135	0.03149	0.03208	0.03377

The results corresponding to the signal parameters in Table 18 are shown in Figures 53 through 56.

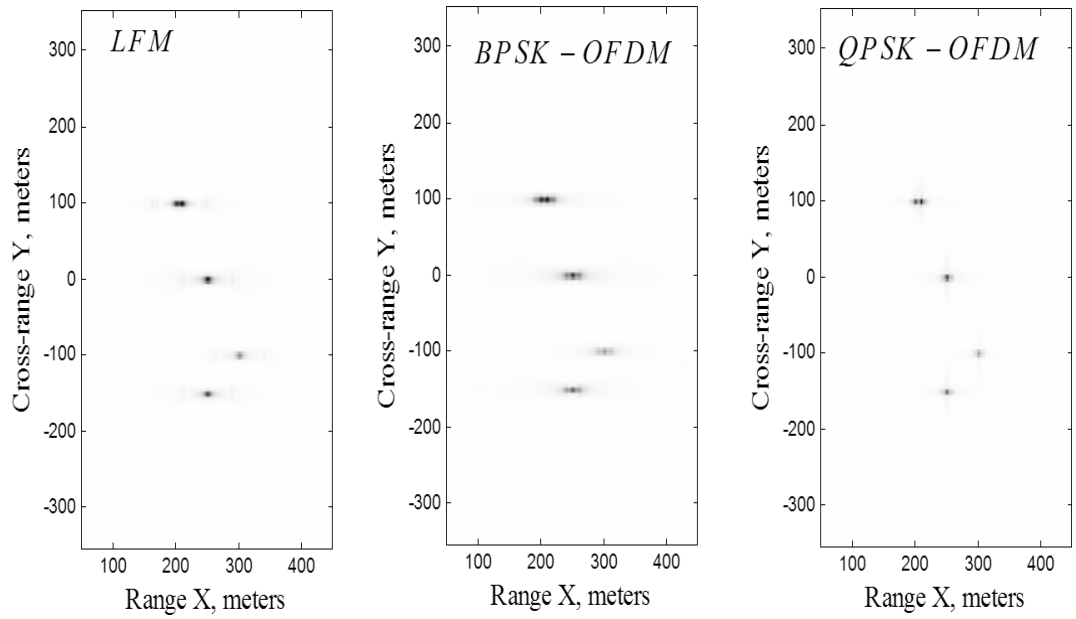

Figure 53. Reconstructed target function for simulation eight with $T_p = 0.06667\ \mu s$.

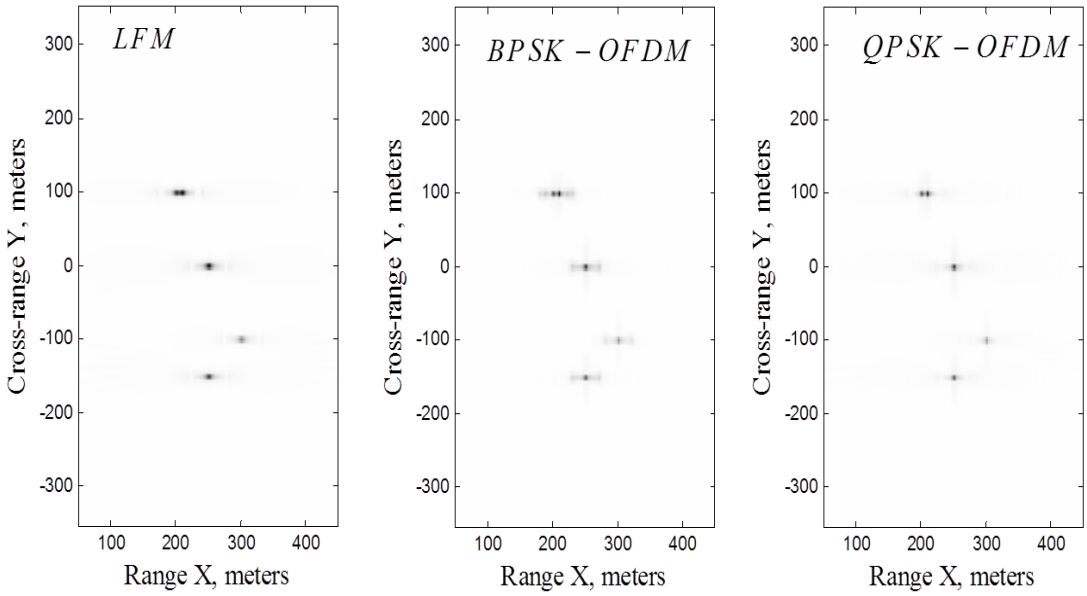

Figure 54. Reconstructed target function for simulation eight with $T_p = 0.13334\ \mu s$.

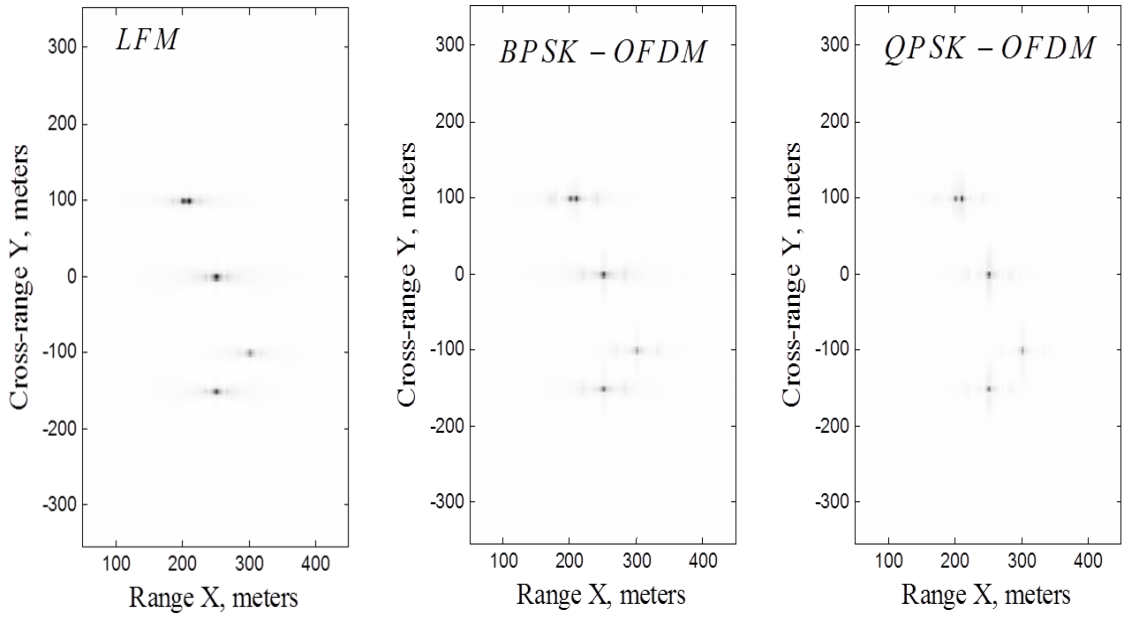

Figure 55. Reconstructed target function for simulation eight with $T_p = 0.2\ \mu s$.

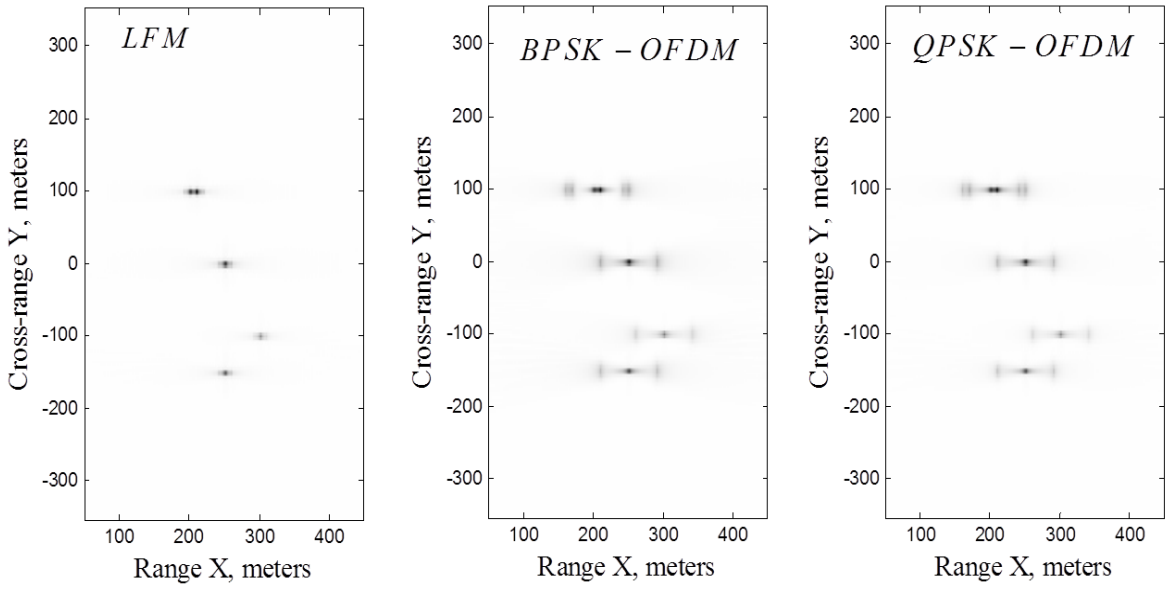

Figure 56. Reconstructed target function for simulation eight with $T_p = 0.26667\ \mu s$.

Observing the LFM results in each figure, we can see that resolution improves with every increase in T_p; however, the improvement is not significant. Similarly, image

resolution for the BPSK-OFDM and QPSK-OFDM signals improved up to $T_p = 0.2\ \mu s$; however, further increasing T_p beyond $0.2\ \mu s$ resulted in grey smearing around the point targets as seen in results corresponding to the OFDM signals with $T_p = 0.26667\ \mu s$. Comparing the three signals against each other, we see that the QPSK-OFDM signal achieved finer resolution that the LFM and BPSK-OFDM signals up to $T_p = 0.2\ \mu s$; however, when duration was further increased to $T_p = 0.26667\ \mu s$, the LFM signal exhibited finer resolution than either OFDM signals.

The main observation from simulation eight is that when all other signal parameters are held constant, resolution continued to improve with duration for the LFM signals. Conversely, elongating duration of the OFDM signals resulted in lower resolution in the images.

In simulation nine, we kept signal bandwidth and duration constant for each of the signals and recorded the resulted transmitted signal energies. We ran four sets in this simulation, where bandwidth and pulse duration was held constant for each iteration within a single set. In set one through four, signal bandwidth was kept constant at B = 50, 60, 70, and 80 MHz, respectively. Each OFDM signal was transmitted with one symbol; however, the number of subcarriers was increased for each set. The signal parameters for simulation nine are shown in Table 19.

Table 19. Signal parameters for simulation nine.

	Set 1			**Set 2**		
	LFM	BPSK-OFDM	QPSK-OFDM	LFM	BPSK-OFDM	QPSK-OFDM
Total OFDM Symbols	-	1	1	-	1	1
Pulse Duration, T_p (μs)	0.3200	0.3200	0.3200	0.3333	0.3333	0.3333
Signal Bandwidth, B (MHz)	50	50	50	60	60	60
Transmitted Energy, E (μJ)	0.3400	0.3400	0.6400	0.3300	0.3300	0.6400
Transmitted Sampling Time, T_s (μs)	0.001	0.0200	0.0200	0.001	0.0167	0.0167
Subcarrier, N	-	16	16	-	20	20
Interpolated Sampling Time, T_s (μs)	0.005	0.005	0.005	0.005	0.005	0.005
Interpolated Signal Energy, E (μJ)	0.3146	0.3122	0.6103	0.3223	0.3181	0.6400
	Set 3			**Set 4**		
	LFM	BPSK-OFDM	QPSK-OFDM	LFM	BPSK-OFDM	QPSK-OFDM
Total OFDM Symbols	-	1	1	-	1	1
Pulse Duration, T_p (μs)	0.3143	0.3143	0.3143	0.3250	0.3250	0.3250
Signal Bandwidth, B (MHz)	70	70	70	80	80	80
Transmitted Energy, E (μJ)	0.3143	0.3143	0.6286	0.3250	0.3750	0.6500
Transmitted Sampling Time, T_s (μs)	0.001	0.0143	0.0143	0.001	0.0125	0.0125
Subcarrier, N	-	22	22	-	26	26
Interpolated Sampling Time, T_s (μs)	0.005	0.005	0.005	0.005	0.005	0.005
Interpolated Signal Energy, E (μJ)	0.3005	0.3143	0.6181	0.3217	0.3217	0.6392

The reconstruction results corresponding to the parameters in Table 18 can be seen in Figures 57 through 60.

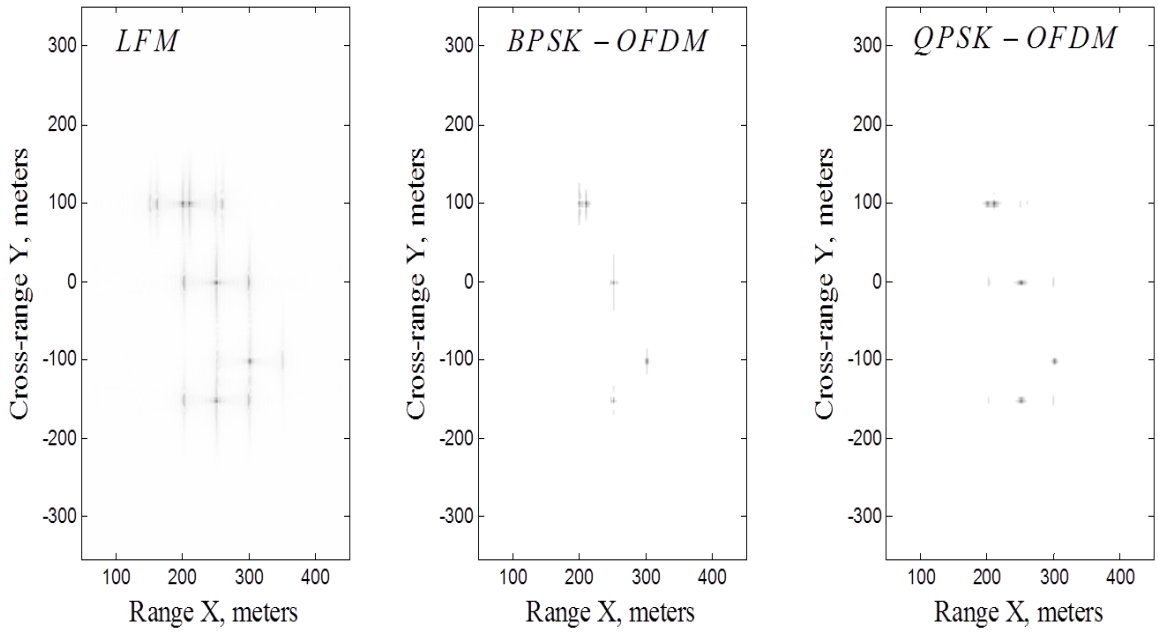

Figure 57. Reconstructed target function for simulation nine with $B = 50$ MHz.

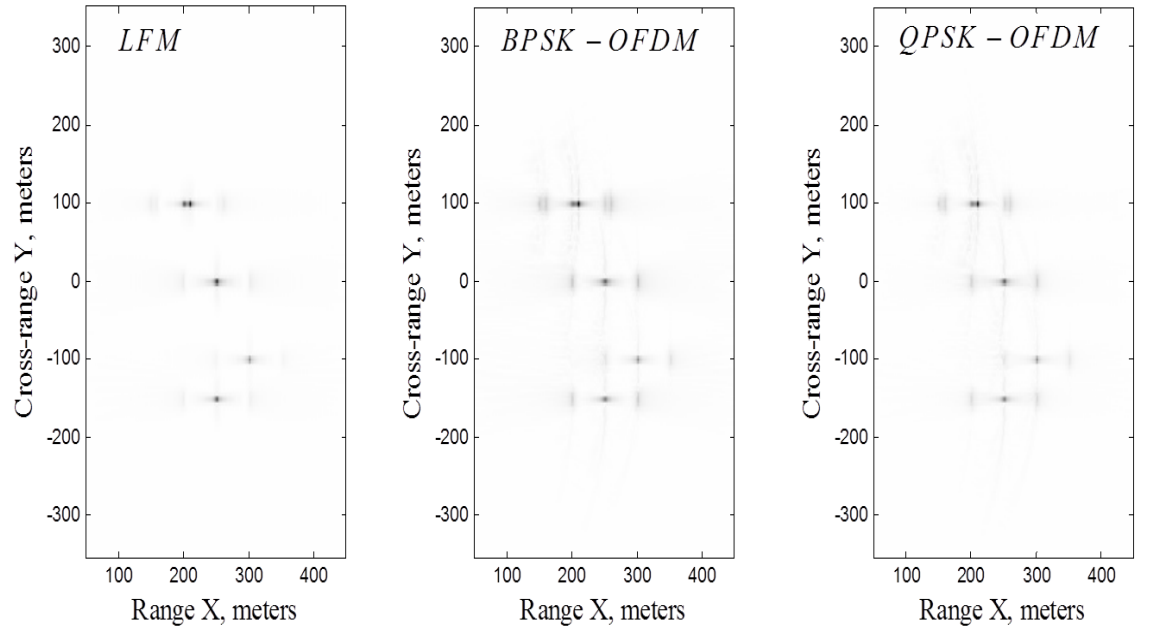

Figure 58. Reconstructed target function for simulation nine with $B = 60$ MHz.

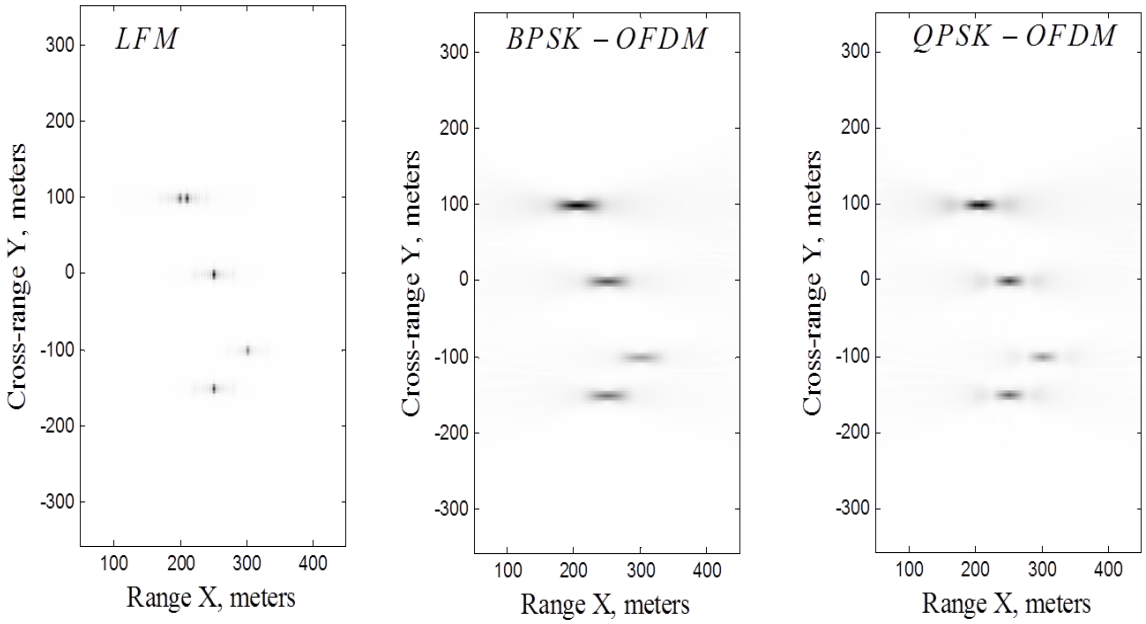

Figure 59. Reconstructed target function for simulation nine with $B = 70$ MHz.

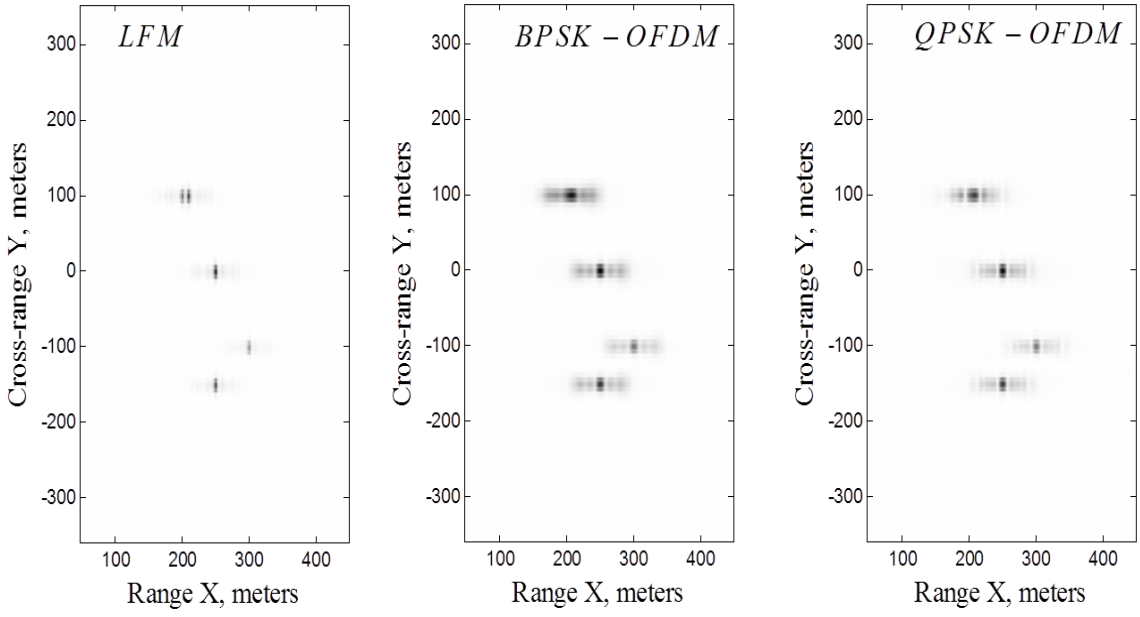

Figure 60. Reconstructed target function for simulation nine with $B = 80$ MHz.

At 50 MHz, the QPSK-OFDM signal produced the best images, and the least amount of smearing is present when compared to the BPSK-OFDM and LFM signal. Image resolution improved for all three signals when bandwidth was increased to 60 MHz; however, there is also grey smearing around each target. At this bandwidth, the least amount of grey smearing is present for the LFM signal. The images corresponding to the OFDM signals implemented with 70 and 80 MHz appear to be stretched in the range direction and the targets are blurred. Conversely, for the LFM signal results at this same bandwidth, we can see that the targets are much clearer than those of the OFDM results.

The interpolated signal energy values for all three signals are within one percent of the original transmitted signal energies. The signal energy values for the LFM and BPSK signals were the same; however, the QPSK signal energy was double that of both the LFM and BPSK signals.

Another important observation for this simulation is that lower resolution was obtained for the wider bandwidth OFDM signals, which is likely due to the elongated signal duration.

Illustrated in Figure 61 are reconstruction results for a BPSK-OFDM and a QPSK-OFDM signal generated with 70 MHz, two subcarriers and one symbol, which results in pulse duration $T_p = 0.02857\ \mu s$ for BPSK-OFDM signal and $T_p = 0.05714\ \mu s$ signals for the QPSK-OFDM signal, respectively.

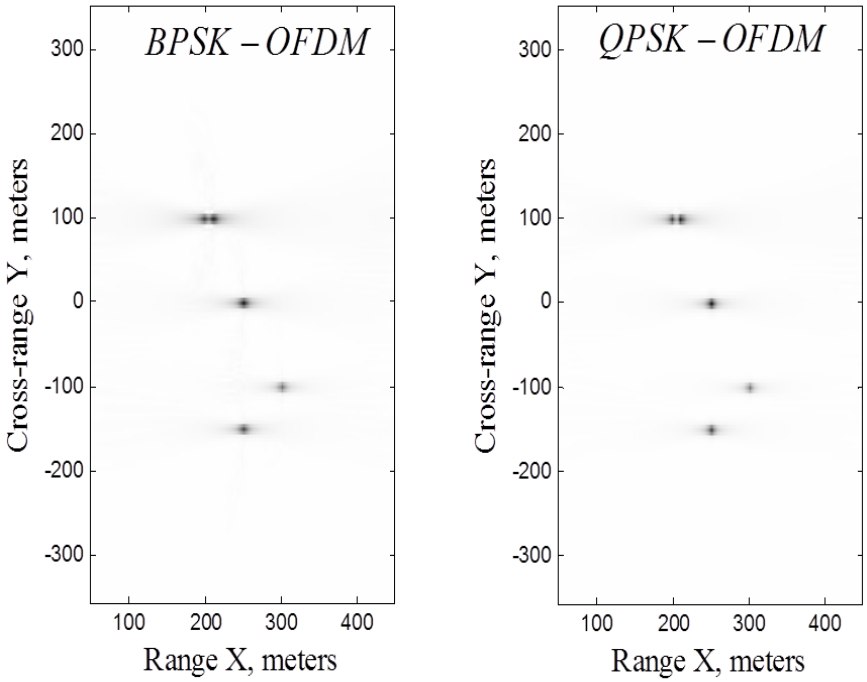

Figure 61. Reconstructed target function for BPSK OFDM and QPSK-OFDM signals generated with $B = 70$ MHz, $N = 2,$ and $T_p = 0.02857$ μs, and T_p=0.05714 μs, respectively.

When compared to the results in simulation nine, where the BPSK-OFDM and QPSK OFDM signals were generated with the same bandwidth but 22 subcarriers or $T_p = 0.3143$ μs and $T_p = 0.6286$ μs, respectively, we can see the decreased number of subcarriers and, thus, pulse duration exhibited higher image resolution.

Similarly, by increasing the bandwidth to 80 MHz for both signals and using two subcarriers and one symbol, which results in $T_p = 0.025$ μs for the BPSK-OFDM signal and $T_p = 0.5$ μs for the QPSK-OFDM signal, we can also see that higher resolution was obtained in the results when compared to those corresponding to the BPSK-OFDM and QPSK-OFDM signals generated with 26 subcarriers in simulation nine. This can be seen in Figure 62.

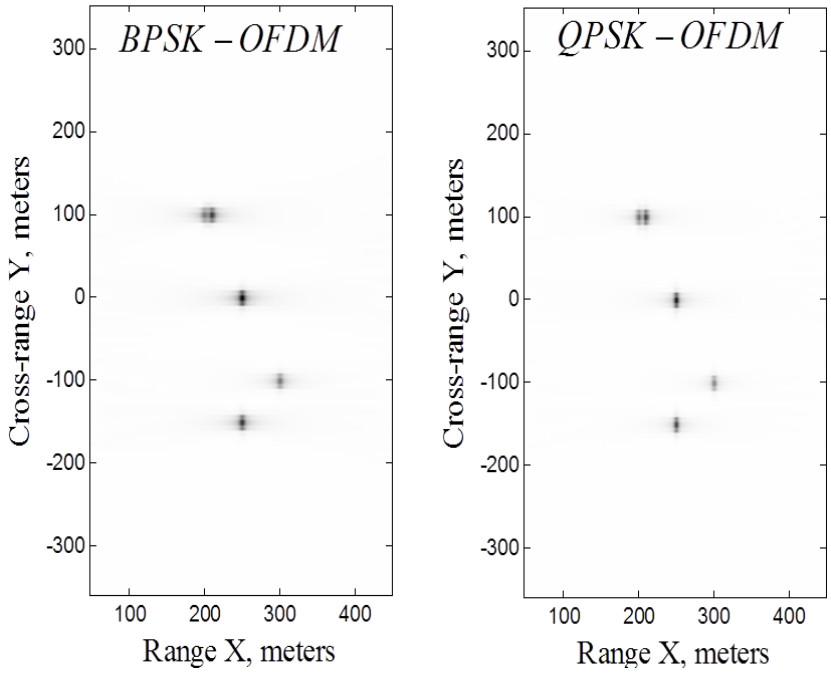

Figure 62. Reconstructed target function for BPSK OFDM and QPSK-OFDM signals generated with $B = 80$ MHz, $N = 2$, and $T_p = 0.025$ μs, and $T_p = 0.05$ μs, respectively.

We conclude from this final simulation that a shorter duration or fewer subcarriers is sufficient for achieving fine image resolution when the OFDM signal is implemented with a wider bandwidth.

VII. CONCLUSION AND FUTURE WORK

A. CONCLUSION

In this thesis, we developed a SAR MATLAB simulation tool where the user can generate any signal as an input to use as the transmitted SAR radar signal. The output of the simulation tool displays the measured echoed SAR signal, fast-time matched filtered SAR signal and two-dimensional SAR image. The two signals investigated in this thesis were the traditional LFM radar signal and the OFDM communication signal. Various parameters of each of these signals were varied and compared against each other.

The simulation results reveal that bandwidth and pulse duration are the two most important parameters for achieving the best SAR image for both signals. For the LFM signal, we observed that maintaining constant pulse duration while increasing the signal chirp rate to increase signal bandwidth directly improves image resolution. Since the pulse duration is held constant, the transmitted signal energy does not increase with the signal bandwidth. Results also revealed that increasing the LFM pulse duration also improves resolution. In all cases, the Nyquist sampling theorem must be obeyed to avoid aliasing.

Overall, we observed varying effects for the OFDM signal. Specifically, increasing the pulse duration for lower bandwidth OFDM signals directly resulted in improved image resolution. This was seen in the two-dimensional simulations four and six where the additional number of subcarriers directly improved the resulting images for the signals implemented with 40 MHz and 60 MHz. Similarly, in simulations five and seven, increasing the number of symbols for the OFDM signals directly increased the duration of the signal, which also resulted in improved images for the signals generated with 50, 60 and 70 MHz. Conversely, when a wider bandwidth OFDM signal was used, a shorter duration signal was sufficient for achieving fine resolution. Implementing the wider bandwidth OFDM signals with a longer duration resulted in distorted images. This was observed in simulation nine where elongated signal duration from implementing the OFDM signals with too many subcarriers resulted in images that were smeared and

indistinguishable. Similar results were obtained when the OFDM signals were generated with too many symbols in simulation five and seven. This is one disadvantage of using an OFDM signal for SAR systems.

SAR systems are used for obtaining high resolution imagery in various military applications. One advantage of using OFDM signals over LFM signals is that OFDM signals offers more flexibility in terms of pulse width, sampling times and, thus, usable bandwidth. In this thesis, we saw that the parameters of an OFDM signal can be adjusted to obtain fine resolution. The military can benefit from this advantage by incorporating OFDM signals as a transmitted SAR radar signal for use in various military applications. In particular, each military application can govern the way in which an OFDM signal is implemented to achieve the quality of imagery a particular mission may require.

B. FUTURE WORK

There are various means in which this subject matter and simulation can be expanded upon. First, the simulations herein were all noiseless. Further study is required to determine the efficacy of the various signal types and relative importance of the signal parameters for producing high resolution SAR imagery when the receptions are corrupted by various levels of noise. Second, many of the images displayed smearing or a light gray color around the target location. One method for alleviating this smearing is to implement a program or a threshold that can filter out the gray smearing and only display the point targets. This also allows for revealing the actual nominal target resolution. A third area requiring investigation is LTE and WIMAX signals as well as other communication signals application in SAR systems. The final area for future work is to enhance the algorithm to use SAR raw data or more complex images rather than of point targets.

APPENDIX MATLAB CODES

```
% Author: Sade A. Holder
% Last Update: 6JUN2014
% This function plots the range profile for to the selected transmitted
% radar signal.


clear all
clc

s1 = menu('Choose your input signal', 'OFDM', 'Chirp');

if s1 == 1
  s2 = input('enter number of subcarriers: ');
  s3 = menu('Choose your modulation scheme', 'BPSK', 'QPSK');
  s3 = s3 * 2;
  s4 = input('Bandwidth: ');
  s5 = input('Enter numbr of OFDM symbols: ');
  reference_sigNy = OFDMrefpulse(s2, s3, s4, s5);
  OFDMrefpulse(s2, s3, s4, s5)
else
  reference_sigNy = cosinepulse();
end

fc = 100e6; % Carrier Frequency
if s1 == 1
  reference_a_sigNY= analytic_s(reference_sigNy, fc);
else
  reference_a_sigNY = reference_sigNy;
end

% Change this number to either 1, 2, 3, or 4 to display on final plot.
% run multiplot function to display four range profiles.
subplt =4;

Tsamp = .01e-6;% Tsamp is the reciprocal of the sampling rate for the
               % reference signal and most other signals (but not the
               % Ny signals).
reference_a_sigNY= analytic_s(reference_sigNy, fc)

% t = sampling interval.
t = 0:Tsamp:reference_sigNy.duration;

reference_sig = interpolate(reference_a_sigNY, t, Tsamp, 0);

% Interpolated Signal Energy:
sigEnergy = (1/sqrt(1))*sum(abs(reference_sig.sig.^2))*Tsamp
 c = 3e8; % speed of light

% define the targets (i.e. the points that reflect the signal)
```

```
range_width = 5000;
targets= struct('x_center',    8000, ...
        'halfwidth',  0.5*range_width, ...
        'num',     5, ...
        'x_rel',    [0 -.4 0.4 .85 .9]*0.5*range_width, ...
        'sigma',    [0.1 0.3 .5 0.7 1]);


% get the echo signal. echo_sig is a structure.
echo_sig = getechosig(reference_sig, targets);

% ref_delay is the round trip propagation delay for a target in the  %
center of the target range.
ref_delay = 2*targets.x_center/c;

% echo_ref is the signal that would be reflected from a target in the
% center of the target range. echo_ref is a structure.
echo_ref = interpolate(reference_sig, echo_sig.t, reference_sig.Tsamp,
...
  ref_delay);

% mfout is the output of the matched filter. It is a structure. The %
time vector mfout.t is adjusted so that a target at location X should
cause a % peak in mfout.sig at time 2X/c.
mfout = getmfout(echo_sig, echo_ref, ref_delay);
% range(i) is the target location that would cause a peak in the mfout
%at time mfout.t(i).

range = (mfout.t*c)/2;
plot(range, (abs(mfout.sig))/1)
xlabel('Range (meters)', 'FontName', 'Times New Roman', 'Fontsize', 16)
ylabel('Magnitude', 'FontName', 'Times New Roman', 'Fontsize', 16)

fc1 = num2str(subplt); % Used for multiplot program
nm2 = 'Sade_Plot_';
filename = strcat(nm2,fc1);
savefig(filename)

% findpeaks(abs(mfout.sig))
% [pks, loc] = findpeaks(abs(mfout.sig))
% plot([900:1100], (abs(mfout.sig(900:1100))))


function  y = getechosig(reference_sig, targets)
% This function generates the received echoed signal.

c = 3e8;
y = def_sig_struct();

wc = 2*pi*100e6; % 2*pi*carrier frequency

% Ts = 2(Xc-X0)/2 + Tp
```

```
tstart = reference_sig.t(1) + 2*(targets.x_center + -
targets.halfwidth)/c;
% tstart_min = min(tstart);
y.duration = 4*targets.halfwidth/c + reference_sig.duration;
y.Tsamp = reference_sig.Tsamp;
%numsamp = ceil(y.duration/y.Tsamp);
y.t = tstart + linspace(0, y.duration, y.duration/y.Tsamp + 1);

delay = 2*(targets.x_center + targets.x_rel)/c;
y.sig = zeros(1,length(y.t));
for i = 1:targets.num
  term = interpolate(reference_sig, y.t, ...
    reference_sig.Tsamp, delay(i));
  y.sig = y.sig + targets.sigma(i)*term.sig;
  y.sig = y.sig.*exp(1i*wc*y.t); %***Baseband signal
  size(y.sig)

end
y.fourier = fft(y.sig);

function  y = interpolate(samples, tnew, Tsamp_new, delay)
% this function reconstructs signal y from its samples using an ideal
LPF.
% 1/Tsamp is the sampling rate
% t are the values of time where the reconstruction is to be
calculated.
% samples and t need to be row vectors.

y = def_sig_struct();
y.Tsamp = Tsamp_new;

%num_samp_new = round(length(samples.sig)*samples.Tsamp/y.Tsamp);
%n = 0:num_samp_new-1;  % discrete time index
y.t = tnew;

n_old = 1:(length(samples.sig));
%construct the argument for the sinc function.
  npart = n_old'*ones(1,length(y.t));
  %size(ones(length(samples.sig),1)*y.t);
  tpart = ones(length(samples.sig),1)*y.t-delay;
  targ = (tpart-npart*samples.Tsamp)/samples.Tsamp;

sincmat = sinc(targ);

y.sig = samples.sig*sincmat;
y.duration = tnew(length(tnew)) - tnew(1);
y.fourier = fft(y.sig);


function  mfout = getmfout(echo_sig, echo_ref, ref_delay)
% This function is used to generate the matched-filter output signal.

mfout = def_sig_struct();
```

```
mfout.fourier = echo_sig.fourier.*conj(echo_ref.fourier);
mftemp = ifft(echo_sig.fourier.*conj(echo_ref.fourier));

N = length(mftemp);
% n0 is the time index that we want should corresponds to location Xc;
n0 = floor(0.5*(N)); %location of Xc
% put earliest time first and latest last.
mfout.sig = [mftemp((n0+1):N) mftemp(1:n0)];
mfout.Tsamp = echo_sig.Tsamp;
%Continuous time ref_delay corresponds with discrete time n0. Use that
and
%the sample duration to determine the continuous time vector.
tstart = ref_delay-n0*mfout.Tsamp;
mfout.t = tstart + (0:(N-1))*mfout.Tsamp;
mfout.duration = mfout.t(N)-mfout.t(1);


function  y = interpolate(samples, tnew, Tsamp_new, delay)
% this function reconstructs signal y from its samples using an ideal
LPF.
%1/Tsamp is the sampling rate
%t are the values of time where the reconstruction is to be calculated.
%samples and t need to be row vectors.

y = def_sig_struct();
y.Tsamp = Tsamp_new;

%num_samp_new = round(length(samples.sig)*samples.Tsamp/y.Tsamp);
%n = 0:num_samp_new-1;  % discrete time index
y.t = tnew;

n_old = 1:(length(samples.sig));
%construct the argument for the sinc function.
  npart = n_old'*ones(1,length(y.t));
  tpart = ones(length(samples.sig),1)*y.t-delay;
  targ = (tpart-npart*samples.Tsamp)/samples.Tsamp;

sincmat = sinc(targ);

y.sig = samples.sig*sincmat;
y.duration = tnew(length(tnew)) - tnew(1);
y.fourier = fft(y.sig);

function y = cosinepulse()
% This function generates the LFM signal for the SAR range imaging
model.
y = def_sig_struct();

y.bandwidth =10e6; %Signal bandwidth
y.bandwidth= 2*pi*y.bandwidth;
alpha = 5e13; %chirp rate
fc= 100e6; % carrier frequency
```

```
wc= 2*pi*fc; %Angular carrier frequency
y.duration = .2e-6; % Signal duration Tp
y.bandwidth = alpha*y.duration;

wcm = fc-alpha*y.duration;
y.Tsamp = .001e-6; %Nyquist sampling time
y.t = 0:y.Tsamp:y.duration; % time interval
y.sig =2.2305*exp(1i*wcm*y.t+1i*alpha*(y.t.^2));
y.sigenergy = sum(abs(y.sig.^2))*y.Tsamp


function y= analytic_s(reference_sigNy, fc)
% This function generates the analytic signal representation of the
% transmitted radar signal.

t = reference_sigNy.t; %time interval
sig = reference_sigNy.sig; %original signal

y.sig= sig.*exp(1i*2*pi*fc*t); %analytic signal
y.t = t;
y.duration = reference_sigNy.duration;
y.bandwidth = reference_sigNy.bandwidth;
y.Tsamp = reference_sigNy.Tsamp;


% Author: Sade A. Holder
% Last Update: 6JUN2014
% The program returns four Range Imaging Profiles in the same plot.
% User must change the subplot value in the MAIN_Range function
%(Line38)% to 1, 2, 3, or 4.


clear all
close all

h1 = openfig('Plot_1.fig','reuse'); % open figure
ax1 = gca; % get handle to axes of figure
h2 = openfig('Plot_2.fig','reuse');
ax2 = gca;
h3 = openfig('Plot_3.fig','reuse');
ax3 = gca;
h4 = openfig('Plot_4.fig','reuse');
ax4 = gca;

h5 = figure; %create new figure
s1 = subplot(2,2,1); %create and get handle to the subplot axes
xlabel('Range (meters)', 'FontName', 'Times New Roman', 'Fontsize', 14)
ylabel('Magnitude', 'FontName', 'Times New Roman', 'Fontsize', 14)
%  ylim([0 1.05])
s2 = subplot(2,2,2);
xlabel('Range (meters)', 'FontName', 'Times New Roman', 'Fontsize', 14)
ylabel('Magnitude', 'FontName', 'Times New Roman', 'Fontsize', 14)
%  ylim([0 1.05])
s3 = subplot(2,2,3); %create and get handle to the subplot axes
```

```
xlabel('Range (meters)', 'FontName', 'Times New Roman', 'Fontsize', 14)
ylabel('Magnitude', 'FontName', 'Times New Roman', 'Fontsize', 14)
%  ylim([0 1.05])
s4 = subplot(2,2,4);
xlabel('Range (meters)', 'FontName', 'Times New Roman', 'Fontsize', 14)
ylabel('Magnitude', 'FontName', 'Times New Roman', 'Fontsize', 14)
%  ylim([0 1.05])
fig1 = get(ax1,'children'); %get handle to all the children in the
figure
fig2 = get(ax2,'children');
fig3 = get(ax3,'children');
fig4 = get(ax4,'children');
copyobj(fig1,s1); %copy children to new parent axes i.e. the subplot
axes
copyobj(fig2,s2);
copyobj(fig3,s3);
copyobj(fig4,s4);

%Author: Sade A. Holder
%Last Update: 6JUN2014
% The program is used to generate the plots for the received echoed
signal, fast-time matched filtered signal and target function. The user
will be prompted to select the desired transmitted radar signals.

clc
clear all
close all
clc

s1 = menu('Choose your input signal', 'OFDM', 'Chirp');

if s1 == 1
  s2 = input('enter number of subcarriers: ');
  s3 = menu('Choose your modulation scheme', 'BPSK', 'QPSK');
  s3 = s3 * 2;
  s4 = input('Enter desired bandwidth: ');
  s5 = input('Choose number of OFDM symbols: ');
  reference_sigNy = OFDMrefpulse_2D(s2, s3, s4, s5);
else
  reference_sigNy = chirp_pulse();
end

tic

fc = 100e6;
if s1 == 1
  reference_a_sigNY= analytic_s(reference_sigNy, fc);
else
  reference_a_sigNY = reference_sigNy;
end

reference_a_sigNY= analytic_s(reference_sigNy, fc);

subplt = 3;
```

```
% Resample sampling time
Tsamp = .005e-6;
t = 0:Tsamp:reference_sigNy.duration;
reference_sig = interpolate_2D(reference_a_sigNY, t, Tsamp, 0); %for
OFDM

%Resample transmitted signal energy
 sigPower = (1/sqrt(s2))*sum(abs(reference_sig.sig.^2))*Tsamp
%/length(reference_sig.sig))


c = 3e8; % speed of light
% Baseband Bandwidth
f0 = reference_sig.bandwidth;
w0 =2*pi*f0;
wc = 2*pi*fc;

lambda_min=  c/(fc+f0); % Wavelength of highest frequency
lambda_max= c/(fc-f0); % Wavelength of lowest frequency

% define the targets (i.e. the points that reflect the signal)
range_width = 200;
crange_length = 150;
x_center = 250;
Diameter = 2*lambda_max; %Diameter of planar radar
Bmin = (x_center - .5*range_width) *tan(asin(lambda_min/Diameter));
%Min 1/2BW
Bmax = (x_center + .5*range_width) *tan(asin(lambda_max/Diameter));
%Max 1/2BW
Beamwidth = [Bmin, Bmax];

% Target and Antenna Parameters
targets = struct(  'x_center',    250, ...
          'halfwidth',  0.5*range_width, ...
          'num',     5, ...
          'x_rel',      [0 50 0 -50 -40], ...
          'y_rel',     [0 -100 -150 100 100], ...
          'sigma',     [1 .5 .8 .8 1], ...
          'lam_max',    lambda_max,...
          'Diameter',    2*lambda_max,...
          'Beamwidth' ,   [Bmin, Bmax], ...
          'theta_d',     asin(lambda_min/Diameter), ...
          'SA_length',   (Beamwidth(2) + crange_length)) ;

clear Bmin Bmax lambda crange_length theta_d Beamwidth x_center
range_width

u = u_array(targets);
time = time_samples(targets, reference_sig);
w = wavelength_parameters(wc, lambda_max, lambda_min, targets,
reference_sig);
received_sig = get_echo_sig_2D(reference_sig, targets, wc, lambda_max,
lambda_min);
```

```
colormap(gray(256));
G= abs(received_sig.sig)';
% This plots the Measured Stripmap SAR Signal
 xg=max(max(G)); ng=min(min(G)); cg=255/(xg-ng);
 temp2 = 256-cg*(G-ng);
 figure(1)
 axis('square');axis('xy')
image(time.array,-u.u_array,temp2);
xlabel('Fast-time t, sec', 'Fontsize', 14, 'Fontname', 'Times New
Roman')
ylabel('Synthetic Aperture (Slow-time) U, meters', 'Fontsize', 14,
'Fontname', 'Times New Roman')


echo_ref = get_echo_ref(reference_sig, targets, wc);
% FMF= received_sig.fourier.*
(conj(echo_ref.fourier)*ones(1,u.u_samples));
%
FMF=fast_matched_filter(reference_sig, echo_ref, received_sig,
targets);

mm = wavelength_parameters(wc, lambda_max, lambda_min, targets,
reference_sig);

f= interpolation(FMF, targets, reference_sig, wc, lambda_max,
lambda_min );

dx = (2*pi)/(f.nx * mm.delta_kx);   % range sample spacing in
reconstructed image
x=dx*(-f.nx/2:f.nx/2-1); % range array

% %Image%
G2=abs(f.sig)';

xg=max(max(G2)); ng=min(min(G2)); cg=255/(xg-ng);
t2 = 256-cg*(G2-ng);
% threshold
t1 = t2 < 230; %0=black 255=white %everything that is not the target
black
t3 = ~t1;
t4 = 255 * t3;
t5 = t2 + t4;
% colormap('default')

 colormap(gray(256))
% subplot(121)
figure(4)
image((targets.x_center + x), u.u_array, t2);
axis([targets.x_center-2*targets.halfwidth
targets.x_center+2*targets.halfwidth -150 150]);
axis image; axis xy
```

```
xlabel('Range X, meters', 'Fontsize', 14, 'Fontname', 'Times New
Roman')
ylabel('Cross-range Y, meters', 'Fontsize', 14, 'Fontname', 'Times New
Roman')


% Uncomment to plot target function with threshold
% figure(5)
% colormap(gray(256))
% image((targets.x_center + x), u.u_array, t5);
% axis([targets.x_center-2*targets.halfwidth
targets.x_center+2*targets.halfwidth -300 300]);
% axis image; axis xy
% xlabel('Range X, meters', 'Fontsize', 14, 'Fontname', 'Times New
Roman')
% ylabel('Cross-range Y, meters', 'Fontsize', 14, 'Fontname', 'Times
New Roman')
% % title('Stripmap SAR Reconstructed Signal', 'Fontsize', 14,
'Fontname',
% % 'Times New Roman') title('Stripmap SAR Reconstruction thresholded')

toc
range_res =c/(4*reference_sig.bandwidth)
c_range_res=Diameter/2


function y = u_array(targets)
% This function gerates the parameters for the u_array. u is slow time
% and corresponds the movement of the radar

y = def_sig_struct();
% SA --the synthetic aperture length that is defined in the main
function

SA = targets.SA_length;
c= 3e8;
%fc = 200e6;
% delta_u --- the sample spacing of signal in the u (slow-time) domain.
The
% worst case scenario for delta_ u is lambda/4 or D/4 for STRIPMAP SAR
% u_samples ---is the the total number of u (slow time) samples.
% u_array --- is the the u (slow time) array.. i.e samples. The support
band
% is [-SAR length, SAR length] (SAR length is the total distance the
radar
% moves.

delta_u = targets.Diameter/4; %fspacing of u for a planar radar;
y.delta_u = (delta_u)/1.2;
u_samples = 2*ceil(SA/y.delta_u);
u_array = y.delta_u*(-u_samples/2 : u_samples/2-1);
%u_array = fliplr(u_array);
```

```
% ku is the frequency of the radar. It represents the spatial frequency
% domain for the synthryic aperture (u) domain
%delta_ku is the sample spacing for cvariable ku.
%ku_array is the support band of ku.
y.delta_ku = 2*pi/(u_samples*y.delta_u);
ku_array = y.delta_ku*(-u_samples/2:u_samples/2-1);

y.u_samples = u_samples;
y.u_array = u_array;
y.ku_array = ku_array;

end

function t = time_samples(targets, reference_sig)
%This function generates the fast-time parameters
c = 3e8;
t= def_sig_struct();
f0 = reference_sig.bandwidth;


max_beam = targets.Beamwidth(2);
tstart = reference_sig.t(1)+ 2*(targets.x_center -
targets.halfwidth)/c;
tstop = 2*sqrt((targets.x_center + targets.halfwidth)^2 + max_beam^2)/c
...
  + reference_sig.duration;

tduration = tstop-tstart; % total fast time interval

% 10 percent guard band.
tstart = tstart - .1*tduration;
tstop = tstop + .1*tduration;
t.duration = tstop - tstart; % total fast time interval (guard band)

tmin = max(t.duration, (4*targets.halfwidth)/ ...
     (c*cos( targets.theta_d)));


t.delta_t = 1/(4*f0);

t.samples = 2*ceil((.5*tmin)/t.delta_t);


t.Tsamp= reference_sig.Tsamp;
t.array = tstart + (0:t.samples-1)*t.delta_t;
t.tstop=tstop;
end


function  y = interpolate_2D(samples, tnew, Tsamp_new, delay)
% this function reconstructs signal y from its samples using an ideal
LPF.
% 1/Tsamp is the sampling rate
```

```
% t are the values of time where the reconstruction is to be
calculated.
% samples and t need to be row vectors.

y = def_sig_struct();
y.Tsamp = Tsamp_new;

%num_samp_new = round(length(samples.sig)*samples.Tsamp/y.Tsamp);
%n = 0:num_samp_new-1;  % discrete time index
y.t = tnew;

n_old = 0:(length(samples.sig)-1); %column
%construct the argument for the sinc function.


  npart = n_old'*ones(1,length(y.t));
size_n = size(npart);
  tpart = ones(length(samples.sig),1)*y.t-delay; %first part column
  size_t = size(tpart);
  targ = (tpart-npart*samples.Tsamp)/samples.Tsamp;

sincmat = sinc(targ);

y.sig = samples.sig*sincmat;
y.duration = tnew(length(tnew)) - tnew(1);
y.fourier = fft(y.sig);
y.bandwidth = samples.bandwidth


function y = wavelength_parameters(wc, lambda_max, lambda_min, targets,
reference_sig)
% The function generates the wavelength parameters
 y = def_sig_struct();
 t = time_samples(targets, reference_sig);
 u = u_array(targets);


 c = 3e8;
 % Frequency domain Parameters:
 % Frequency domain support band is w = [wc - wo, wc + w0]
 % where wc = 2*pi*fc and w0 is the bandwidth of the radar signal



 y.delta_w =(2*pi)/(t.samples*t.delta_t);% Frequency domain sampling
                    % spacing. 2pi/(t*dt). This is
                   % a scalar. PG 20

 y.freq_array = wc + y.delta_w *(-t.samples/2 : t.samples/2-1);
                     % Frequency array. This
                     % vector is the same size
                     % as the fast time array.
```

```
 y.wavenumber_array = y.freq_array/c;  % Wavenumber array. "k= w/c"
                     % This vector is also the same
                     % size as the fast time array.

 y.wavenumber_max =2*pi*lambda_min^-1;   % largest wavenumber
 y.wavenumber_min = 2*pi*lambda_max^-1;  % smallest wavenumber



 % ----------------y = u ---> ky = ku -------------------------------%%
delta_y = u.delta_u; %The sampling spacing for the cross-range domain
           % is the same as the sampling spacing for the
           % synthetic aperture "u" domain.

%y.CR_array = u.ku_array; % cross range "y" array is same as synthetic
             % aperture "u" array.

%Creating ky array
y.CR_array = ones(t.samples,1)*u.ku_array;
kx_array = (4*y.wavenumber_array(:).^2)*ones(1,u.u_samples)-
y.CR_array.^2;
y.kx_array = sqrt(kx_array.*(kx_array > 0));

y.kxmin = min(min(y.kx_array));
y.kxmax = max(max(y.kx_array));
y.delta_kx = pi/(2*targets.halfwidth); % Nyquist sample spacing in kx
domain
y.kx_samples = 2*ceil((.5*(y.kxmax-y.kxmin))/y.delta_kx); %


function  y = OFDMrefpulse_2D(N, M, B, L)

%This function generates the complex envelope for an OFDM signal with
%N samples per OFDM symbol where N is the number of subcarriers. These
%samples constitute the result of sampling the OFDM complex envelope
% at the Nyquist rate, assuming minimum bandwidth pulse shaping.

y = def_sig_struct

% N is the number of subcarriers
% L = 1; % number of OFDM symbols
% M is the order of per-subcarrier modulation (ex: M=4 ==> QPSK) % this
code works correctly for M = 2 and any M = 2^(e) where e is an even
integer.

symbols = randi(M, N, L); % This generates a random N x L matrix where
             % each element is 1,2, ... M


Es = 1 *(M==2)          ... % Es is the energy per sub-carrier
  + (M-1)*(1/3) *(M~=2);     % sub-carrier symbol
```

```
symbols = qammod(symbols-1, M)/sqrt(Es); % This produces an amplitude-
                    % phase point in signal space
                    % for each sub-carrier symbol.

                    % QAM symbols with unit symbol
                    % energy.

z = sqrt(N)*ifft(symbols);%calculate OFDM symbols (one per column).
            %The scale factor (sqrt(N)) preserves power.

y.sig = (((1/sqrt(L)))*reshape(z,1,N*L)); %convert to single row vector
(i.e. put the
            % ofdm symbols one after another in time.
            % There are N samples per OFDM symbol. The OFDM
            % symbol duration is N*Tsamp
y.Tsamp =  1/B;
n = 0:length(y.sig)-1;
y.t = n*y.Tsamp;
y.duration = max(n)*y.Tsamp;
y.duration = N*y.Tsamp*L;
y.bandwidth =1/y.Tsamp; %1/Ts
y.sigenergy = (1/sqrt(N))*sum(abs(y.sig.^2))*y.Tsamp


function  y = fast_matched_filter(reference_sig, echo_ref,
received_sig, targets)
% This function generates the fast-time matched filtered signal.
y = def_sig_struct();
t = time_samples(targets, reference_sig);
u = u_array(targets);

c=3e8;
y.fourier= received_sig.fourier.*
(conj(echo_ref.fourier)*ones(1,u.u_samples));
y.sig = iftx(y.fourier);

% This plots the SAR signal after fast time matched filtering
G1 = abs(y.sig)';
xg=max(max(G1));
ng=min(min(G1));
cg=255/(xg-ng);
% fast-time array after matched filtering
tm=(2*targets.x_center/c)+t.delta_t*(-t.samples/2:t.samples/2-1);  %
fast-time array after matched filtering

figure(2)
% colormap(gray(256))
image(tm,-u.u_array,255-cg*(G1-ng));

xlabel('Fast-time t, sec', 'Fontsize', 14, 'Fontname', 'Times New
Roman')
ylabel('Synthetic Aperture (Slow-time) U, meters', 'Fontsize', 14,
'Fontname', 'Times New Roman')
```

```
function wn= CR_MF(FMF, targets, reference_sig, wc, lambda_max,
lambda_min )
%The function performs a 2D matched filter in the wavenumber domain.

w = wavelength_parameters(wc, lambda_max, lambda_min, targets,
reference_sig);
u = u_array(targets);

% FFT of u dimension (freq domain)
fs = fty(FMF.fourier);

% Cross Range reference signal
 fs0 = (w.kx_array > 0).*
exp(1i*w.kx_array*targets.x_center+1i*.25*pi...
   -1i*2*w.wavenumber_array(:)*ones(1,u.u_samples)*targets.x_center);


wn.sig = fs.*fs0;

t = time_samples(targets, reference_sig);
n = t.samples;
ny = u.u_samples;
kx = w.kx_array;
ky = w.CR_array;

% Un-Comment to plot kx vs ky
% colormap(gray(256))
% figure(2)
% plot(kx(1:20:n*ny),ky(1:20:n*ny),'.')
% xlabel('Spatial Frequency k_x, rad/m')
% ylabel('Spatial Frequency k_y, rad/m')
% title('Stripmap SAR Spatial Frequency Data Coverage')
% axis image; axis xy
% print P6.6.ps
% pause(1)




function ff= interpolation(FMF, targets, reference_sig, wc, lambda_max,
lambda_min )
%A sinc interpolator is used in this function to correct the spacing of
%the kx samples. The orginal kx samples area unevenly spaced. Refer to
%page 198-200 of SAR textbook
ff= def_sig_struct();
w= CR_MF(FMF, targets, reference_sig, wc, lambda_max, lambda_min );
t = time_samples(targets, reference_sig);
u = u_array(targets);
y = wavelength_parameters(wc, lambda_max, lambda_min, targets,
reference_sig);
% Interpolation
```

```
%
is=8;   % number of neighbors (side lobes)
I=2*is+1;
kxs=is*y.delta_kx; % plus/minus size of interpolation in KX domain%

y.kx_samples=y.kx_samples+2*is+4; %increase number of samples to avoid
        % negative array index during interpolation in kx domain

dkx= y.delta_kx;
KX=y.kxmin+(-is-2:y.kx_samples-is-3)*dkx; %uniformly-spaced kx points
                                          % where interpolation is done
                                % carrier frequency in kx domain
kxc=KX(y.kx_samples/2+1);
KX=KX(:)*ones(1,u.u_samples);

% Initialize F(kx,ky) array for interpolation
F=zeros(y.kx_samples,u.u_samples)
%
for i=1:t.samples;             % for each k loop
 icKX=round((y.kx_array(i,:)-KX(1,1))/dkx)+1; % closest grid point in
 cKX=KX(1,1)+(icKX-1)*dkx;       % KX domain
 ikx=ones(I,1)*icKX+[-is:is]'*ones(1,u.u_samples);
 ikx=ikx+y.kx_samples*ones(I,1)*[0:u.u_samples-1];
 nKX=KX(ikx);
 SINC=sinc((nKX-ones(I,1)*y.kx_array(i,:))/dkx);      interpolating
sinc
 HAM=.54+.46*cos((pi/kxs)*(nKX-ones(I,1)*y.kx_array(i,:))); %Hamming
window
     %%%%  Sinc Convolution (interpolation)
 F(ikx)=F(ikx)+(ones(I,1)*w.sig(i,:)).*(SINC.*HAM);
end


temp = fftshift(ifft(fftshift(F.'))).';
ff.sig = fftshift(ifft(fftshift(temp)));

 ff.nx = y.kx_samples+2*is+4;

 dx = (2*pi)/(y.kx_samples * y.delta_kx); %range sample spacing
 x=dx*(-y.kx_samples/2:y.kx_samples/2-1);

temp = ifft(F.').';



function y = get_echo_sig_2D(reference_sig, targets, wc, lambda_max,
lambda_min)
% This function generates the echoed signal for the 2D SAR.
% The echoed signal is 2 dimensional matrix. txu where t is fast-
% time and corresponds to the speed of the transmitted signal and u is
% slow time that corresponds to the speed on the radar.

c = 3e8;
y = def_sig_struct();
```

```
t = time_samples(targets, reference_sig);
u = u_array(targets);
w = wavelength_parameters(wc, lambda_max, lambda_min, targets,
reference_sig);


tot_wavenumbers = find(w.wavenumber_array >= w.wavenumber_min ...
          & w.wavenumber_array <= w.wavenumber_max);
                  % Finding the total number
                  % of wave numbers between
                  % [kmin kmax] in wavenumber
                  % array.

[temp, num_wavenumber] = size(tot_wavenumbers);
                 % Getting the value of total number of
                 % wavenumbers

wave_array = zeros(1,t.samples); % Creating wavenumber array

%Wavelength Array
wave_array(tot_wavenumbers) = (2*pi) *ones(1,num_wavenumber)./...
                w.wavenumber_array(tot_wavenumbers);

%Divergence angle for planar antenna
phi = asin( wave_array/targets.Diameter);


y.t = t.array(:)*ones(1, u.u_samples); % y.t is a matrix, txu, where
                    % each column contains the time
                    % array.
y.duration = t.duration;
y.Tsamp = t.Tsamp;

y.sig = zeros(ceil(t.samples), u.u_samples);% y.sig is the synthetic
                     % aperture array. It is a TxU
                     % matrix of zeros.

for i=1:targets.num;
% 'delay' is the time it takes the signal to get to the target(s) and
% back to the radar. delay incorporates both the speed of the signal
% and the radar's position.
% fast time, t (column) * slow time, u(row)
% t.array(:)*ones(1, u.u_samples) ------ same time along each column

delay = 2*ones(ceil(t.samples),1)...
  * sqrt((targets.x_center + targets.x_rel(i))^2 + ...
  (targets.y_rel(i) - u.u_array).^2)/c;


term = interpolate_2D_1(reference_sig, y.t, delay);

echo_sig = targets.sigma(i)*term.sig;
```

```
%

echo_sig = echo_sig.*exp(-1i*wc*t.array(:)*ones(1,u.u_samples));


% Beam Pattern is in freq domain.
theta_n= ones(num_wavenumber, 1)*atan((targets.y_rel(i) -
u.u_array)/...
            (targets.x_center+targets.x_rel(i)));
% size_theta_n = size(theta_n)
beam_pattern=zeros(t.samples,u.u_samples);

% Applying Hamming Window
beam_pattern(tot_wavenumbers,:) = (.5+.5*cos((pi*theta_n)./...
            (phi(tot_wavenumbers).'*ones(1,u.u_samples)))).* ...
            (abs(theta_n) <= phi(tot_wavenumbers).'...
            *ones(1,u.u_samples));
% size_beam_pattern=  size(beam_pattern)


y.sig=y.sig+iftx(ftx(echo_sig).*beam_pattern);

end
y.fourier = fftshift(fft(fftshift(y.sig)));



function  ref = get_echo_ref(reference_sig, targets, wc)
% This function generates the echoed signal for the 2D SAR.
% The echoed signal is 2 dimensional matrix. txu where t is the fast
% time and corresponds to the speed of the transmitted signal and u is
% the slow time that corresponds to the speed on the radar.

c = 3e8;
ref = def_sig_struct();
t = time_samples(targets, reference_sig);



ref.t = t.array;          % y.t is a matrix, txu, where all
                % where each column contains the time
                % array.
ref.duration = t.duration;
ref.Tsamp = t.Tsamp;

ref.sig = zeros(ceil(t.array)); %add to echo sig
ref_delay = 2*targets.x_center/c;
% size_of_ref_delay = size(ref_delay); %
term = interpolate_2D(reference_sig, ref.t, reference_sig.Tsamp,
ref_delay);

echo_sig = term.sig;
```

```
ref.sig = echo_sig(:).*exp(-1i*wc*t.array(:));
ref.fourier = ftx(ref.sig);

function  y = fast_matched_filter(reference_sig, echo_ref,
received_sig, targets)
% This function generates the fast-time matched filtered echoed signal.
y = def_sig_struct();
t = time_samples(targets, reference_sig);
u = u_array(targets);

c=3e8;
y.fourier= received_sig.fourier.*
(conj(echo_ref.fourier)*ones(1,u.u_samples));
y.sig = iftx(y.fourier);

% This plots the SAR signal after fast time matched filtering
G1 = abs(y.sig)';
xg=max(max(G1));
ng=min(min(G1));
cg=255/(xg-ng);
% fast-time array after matched filtering
tm=(2*targets.x_center/c)+t.delta_t*(-t.samples/2:t.samples/2-1);  %
fast-time array after matched filtering

figure(2)
% colormap(gray(256))
image(tm,-u.u_array,255-cg*(G1-ng));

xlabel('Fast-time t, sec', 'Fontsize', 14, 'Fontname', 'Times New
Roman')
ylabel('Synthetic Aperture (Slow-time) U, meters', 'Fontsize', 14,
'Fontname', 'Times New Roman')
```

LIST OF REFERENCES

[1] D. L. Mensa, *High Resolution Radar Cross-Section Imaging*. Norwood, MA: Artech House, 1991.

[2] I. G. Cumming and F. H. Wong, *Digital Processing of Synthetic Aperture Radar Data, Algorithms and Implementation*. Norwood, MA: Artech House, Inc, 2005.

[3] W. Stutzman and G. Thiele, *Antenna Theory and Design*, 3rd. ed. New York: Wiley, 2013.

[4] C. Ozdemir, *Inverse Synthetic Aperture Radar with MATLAB Algorithms*. Hoboken, NJ: John Wiley and Sons, 2012.

[5] C. Oliver and S. Quegan, *Understanding Synthetic Aperture Radar Images*. Norwood, MA: Arctech House, 1998.

[6] M. Skolnik, *Introduction to Radar Systems*, 3rd ed., New York: McGraw Hill, 2001.

[7] E. Dahlman, S. Parkvall and J. Skold, *4G LTE/LTE-Advanced for Mobile Broadband*. Burlington, MA: Elsevier Ltd, 2011.

[8] B. J. Fason, "Modeling and simulation of synthetic aperture radars in MATLAB," M.S., Naval Postgraduate School, Monterey, CA, 2013.

[9] A. V. Oppenheim and R. W. Schafer, *Discrete Time Signal Processing*. Upper Saddle River, NJ: Princeton Hall, 1999.

[10] D. G. Manolakis, I. K. Vinay and S. M. Kogon, *Statistical and Adaptive Signal Processing*. Norwood: McGraw-Hill, 2005.

[11] S. Haykin, *An Introduction to Analog and Digital Communication*. New York: John Wiley and Sons, Inc, 1989.

[12] G. Forbes. (July 2010)."Phase demodulation using the Hilbert transform in the frequency domain." [Online]. Available: http://www.varg.unsw.edu.au/Assets/link%20pdfs/phase_demodulation_rev-1.pdf. [Accessed 3 June 2014].

[13] B. R. Mahafza, *Radar Signal Analysis and Processing Using MATLAB*. Boca Raton, FL: CRC Press, 2009.

[14] M. Soumekh, *Synthetic Aperture Radar Signal Processing with MATLAB Algorithms*. New York: Wiley-Interscience, 1999.

[15] B. Wang, *Digital Signal Processing Techniques and Applications in Radar Image Processing*. Haboken, NJ: Wiley and Sons, 2008.

[16] G. Franceschetti and R. Lanari, *Synthetic Aperture Radar Processing*. Boca Raton: CRC Press, 1999.

[17] R. G. Lyons, "Understanding digital signal processing," Addison-Wesley Publishing Company, Reading, MA, 1997.

[18] W. Stallings, *Data and Communications*, 9th ed. Upper Saddle River, NJ: Pearson Education, 2011.

[19] M. Soumekh. (August 2002). "MATLAB central," Mathworks. [Online]. Available: http://www.mathworks.com/matlabcentral/fileexchange/2188-synthetic-aperture-radar-signal-processing-with-matlab-algorithms/content/soumekh/stripmap.m. [Accessed 18 May 2014].

INITIAL DISTRIBUTION LIST

1. Defense Technical Information Center
   Ft. Belvoir, Virginia

2. Dudley Knox Library
   Naval Postgraduate School
   Monterey, California